Grid Integration of Large-Scale PV Plants

PhD. dissertation prepared to

obtain the Doctor degree by

Íñigo de la Parra Laita

Supervisors

Javier Marcos Álvarez

and

Miguel García Solano

Department of Electrical and Electronic Engineering

Pamplona, February 2015

This thesis has been partially financed by the Seventh Framework Programme of the European Commission with the project PVCROPS (Photovoltaic Cost R€duction, Reliability, Operational Performance, Prediction and Simulation – Grant Agreement no: 308468) and by the Spanish Ministry of Economy and Competitiveness under Grant DPI2013-42853-R.

upna Universidad Pública de Navarra Nafarroako Unibertsitate Publikoa

“Los principios y los finales son fluidos, largas cadenas de acontecimientos donde algunos eslabones parecen insignificantes y otros trascendentales, más en realidad todos tienen el mismo peso. Lo que puede parecer un instante dramático y único es tan sólo un vínculo entre lo que había antes y lo que viene después.”

Linda Olsson. *Astrid y Veronika*

upna Universidad Pública de Navarra Nafarroako Unibertsitate Publikoa

CONTENTS

upna Universidad Pública de Navarra Nafarroako Unibertsitate Publikoa

upna Universidad Pública de Navarra Nafarroako Unibertsitate Publikoa

1

INTRODUCTION AND OBJECTIVES

"The most difficult and complicated part of the writing process is the beginning".
A. B. Yehoshua (1936)

Over the last few years the spectacular fall in the cost of PV raw materials (particularly for polysilicon) combined with improved fabrication processes and scale economies have reduced manufacturing costs, and far faster than targeted by the industry, with top Chinese producers approaching costs of 0.50$/Wp in the 2013 PV module prices (REN21, 2014). Furthermore, solar PV was below retail electricity prices in several countries and particularly in a number of islands, such as the Canary Islands, which are deemed to be competitive without subsidies (Eclaeron, 2014). Consequently, in the last years the installed PV power worldwide has continued to grow (Masson et al., 2013). In **Figure 1.1** it is shown the solar PV total global capacity from 2004 to 2013.

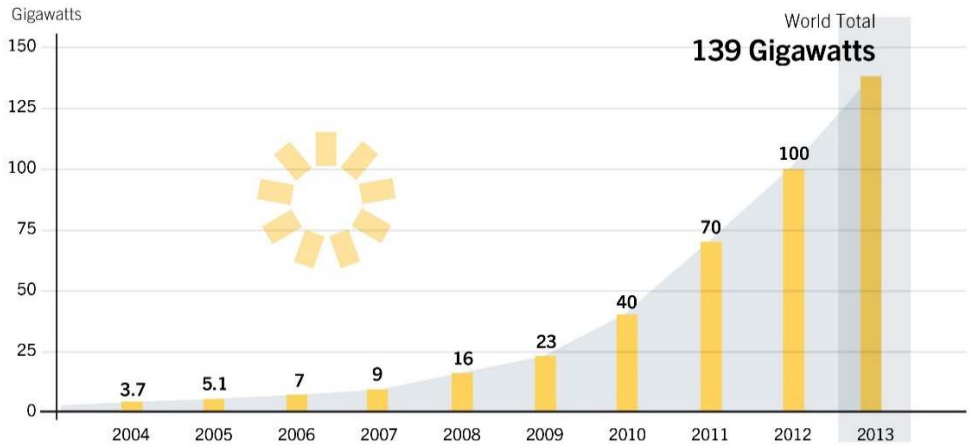

***Figure 1.1**: Solar PV total global capacity, 2004-2013* (REN21, 2014)

upna Universidad Pública de Navarra Nafarroako Unibertsitate Publikoa

More than 39 GW was added in 2013, bringing total capacity to approximately 139 GW (REN21, 2014). The average size of PV installations have also grown. Although historically these installations have been small and distributed, today the number of large-scale PV plants (from ten to several hundreds MWs) is considerably increasing (Shah et al., 2015). It is believed that the integration of large-scale PV to the grid would not be trivial, especially for the high penetration level. Utilities are expected to face some new non-traditional operational problems due to the distinctly different in dynamic characteristics of large-scale PV compared to conventional generators.

The short-term variability of the PV power due to the intermittent nature of the solar resource poses one of the great challenges to those responsible for PV integration into electricity networks with conventional generators. While irradiance fluctuations can produce significant variations in the PV power output in a few seconds, the system operator response capacity is far away from this time scale, being 10 minutes the temporary window presented as the reaction capacity frontier for the grid operator. Therefore, any power fluctuation under this time scale might be a risk for the system stability. This problem alerted such grid operators and promoted research initiatives to study these fluctuations (Marcos et al., 2011a; Perpiñán et al., 2013) finding PV output ramp-rates of the rated capacity with variations from 45-90%/min for multi-MW solar plants (Hansen, 2007; Jolmson et al., 2012; Marcos et al., 2011a; Mills et al., 2011; van Haaren et al., 2014) being values high enough to compromise the grid stability in places with high PV power penetration levels. As a result, some transmission system operators (TSO) have issued new grid codes to address this matter, including new criteria to make it easier for the TSO to react appropriately against harmful power fluctuations, i.e., fluctuations with a time scale of less than 10 minutes (CRE, 2014; NERSA, 2012; PREPA, 2012). Such criteria include setting power variation maximum ramps for the power being fed into the network by intermittent generation plants. This ensures that the power variation of PV power generators does not exceed the dynamics with which conventional plants in the system may increase or reduce power, so that the production and consumption balance is not altered at any time. In order to set these values, potential power variation rates for thermal power plants, between 2.5%-4% of their nominal power per minute, being part of the manageable generation, is usually taken as a reference. In this way, for instance, the target specified in Mexico (CRE, 2014) varies from 1-5%/min. It is thereby ensured that the rest of the system, if provided with sufficient control capacity, may respond to any

upna Universidad Pública de Navarra Nafarroako Unibertsitate Publikoa

rapid power changes in the intermittent power generation plants. Given the fact that PV power fluctuations are greater than the restrictions imposed, some type of energy storage system (ESS) is required in order to comply with the same.

Although the decreasing cost of power electronics devices as well as the breakthrough of new technologies in the field of energy storage (Boicea, 2014; Bradbury et al., 2014; Luo et al., 2014; Zakeri and Syri, 2015) make it possible to incorporate ESS into renewable power systems (Arghandeh et al., 2014; Atwa and El-Saadany, 2010; Bozchalui and Sharma, 2014), the cost per power unit is a strong function of their capacity, and a too high cost is almost prohibitive for industrial and commercial acceptance. It is therefore essential to establish a method for optimizing the size and operation (losses, lifecycle...) of such ESS in order to meet both application constraints and increase the economic viability of the PV system with an ESS incorporated. There are different ways of using the ESS which allows to achieve the two latter objectives depending on the smoothing control strategy implemented. Likewise, it is logical to think that this control strategy selected in order to smooth out fluctuations will be a crucial decision and storage requirements will depend on the strategy chosen.

When establishing the objectives of this thesis, there were only two strategies proposed in the state of the art, the moving average control (Datta et al., 2010; Han et al., 2012; Seo et al., 2010) and the ramp-rate control (Kakimoto et al., 2009; Khanh et al., 2010; Ruifeng and Saha, 2010; Wang and Ying-Hao, 2001). These studies deal with the implementation of these control strategies in small systems (a few kilowatts). However, storage requirements have been scarcely addressed. Power and energy storage capacity have only been derived from some rather simple and intuitive considerations regarding PV output profiles: sudden drops from full power to 0, which is obviously the maximum conceivable fluctuation, were assumed in Kakimoto et al., 2009 in order to determine the size of the required ESS (a double-layer capacitor is proposed in this case). Somewhat more realistically, a drop from full power to 10% in 2 s was assumed in Hund et al., 2010 to conclude that relatively small batteries suffice. In short, there was not any specific engineering rule in order to calculate energy and power storage requirements to smooth out short-term PV output variability implementing these strategies. Likewise, the impact of each strategy on the ESS losses and lifecycle has not been yet evaluated, two key factors that may become decisive in a project viability. From

upna Universidad Pública de Navarra Nafarroako Unibertsitate Publikoa

here arises the first objective of this thesis*:* to propose a method to calculate, for any PV plant size and maximum allowable ramp-rate, the energy storage requirements alike for these two strategies and the effect in the ESS losses and lifecycle. In addition, it is also proposed as a second objective to study the viability of improving these known strategies and try to find out new ones trying to optimize the requirements of the ESS capacity, losses and lifecycle requirements to the utmost. These objectives are dealt with in chapters 3 and 4.

Everything mentioned up to now has dealt with the fluctuations smoothing at a single PV plant level. However, it is well-known that short-term power fluctuations generated by an ensemble of geographical dispersed large PV plants are considerable reduced compared with a single one (A. E. Curtright and Apt, 2008; Hossain and Ali, 2014; Lave et al., 2012, 2011; Marcos et al., 2012; Murata and Otani, 1997; Otani et al., 1997; Perez et al., 2012; Sengupta and Keller, 2011; Wiemken et al., 2001). This phenomenon has raised two new issues that can be taken into account in order to correctly integrate distributed PV generation.

The first one is motivated by the possibility of further optimization of the ESS required to smooth out short-term PV power variability. It now makes sense to consider allocating an ESS in a network node in which a number of PV plants converge, expecting some savings in terms of the ESS capacity required to limit the total ramp-rate fluctuations. This is of particular interest in islands with stand-alone power grids. Therefore, in the same way as it is interesting to dispose a methodology to calculate the minimum energy storage requirements and the maximum power at a single PV plant, another objective of this thesis is to develop a similar methodology for a centralized ESS solution at a PV fleet. The work related to this objective is shown in Chapter 5.

The second issue is motivated from the point of view of both TSO and distribution system operators (DSO). Currently, new grid codes that have motivated the above mentioned objectives, are based on the imposition of a maximum allowable ramp-rate restriction. This restriction is the result of the knowledge of the TSOs of its own grids together with the expected effect of dispersed PV generation. However, up to now there are only tools that enable to simulate the fluctuations at a single PV plant (Marcos et al., 2011b) but not at a PV fleet. The simulated production profiles of a PV fleet could prove

upna Universidad Pública de Navarra Nafarroako Unibertsitate Publikoa

extremely useful for the TSO and DSO, and even more so today when PV technology is gaining strength in distributed generation. It would allow to plan energy reserves, redesign grid codes, plan new PV projects studying its impact in the main electrical grid and even it could be integrated in the grid operator simulation tools. In this way, the development of a model that enables to simulate the power generated by a PV fleet was set as another objective of this thesis. This model is also presented in chapter 5.

All the proposals of this thesis have been validated through high resolution real operational data taken from large PV plants with powers varying 1 to 45 MWp with a total power greater than 60 MWp. It is therefore a database with no comparison in the state of the art which provides an exceptional framework for the grid integration of large-scale PV plants. The database fully description will be the beginning of this document in chapter 2. Finally, the conclusions of this thesis dissertation, the contributions which have given raise and the future lines are dealt in chapter 6.

upna Universidad Pública de Navarra Nafarroako Unibertsitate Publikoa

upna
Universidad Pública de Navarra
Nafarroako Unibertsitate Publikoa

2
THE PV OBSERVATORY

"A few observation and much reasoning lead to error; many observations and a little reasoning to truth."
Alexis Carrel (1873-1944)

2.1 INTRODUCTION

The study of PV power fluctuations demands the proper equipment to be able to monitor the PV power injected into the grid at a MW level. Firstly, a sampling time small enough is necessary to be coherent with the fast occurrence of these fluctuations, i.e., sample periods of at least few seconds. Secondly, as the objective of this study is the grid integration of large-scale PV plants, it is necessary to study this fluctuations as seen by the grid operator, a fact that implies synchronized measurements of this power. This allows to add the PV power generated of different PV plants and study the dynamics of the aggregation of different PV plants. Next sections explain the two databases used in this study.

2.2 MOURA PV PLANT

One of the database used in this work is taken from Moura PV plant, which is located in Amareleja (South Portugal) PV plant. This plant occupies an area of 250 Ha and includes 2520 solar trackers with a rated output of 17.7 to 18.8 kWp, up to a total peak power of 45.6 MWp. The corresponding inverter power, P_n, is 38.5 MW and the ground cover ratio (GCR) is 0.162. The trackers are one-vertical axis models, with the receiving surface tilted 45º from the horizontal. The plant is divided into 70 units, each comprising 36 tracking systems connected to a 550 kW DC/AC inverter. The minimum

upna Universidad Pública de Navarra Nafarroako Unibertsitate Publikoa

and maximum distances between the units, are 220 meters and 2.5 km respectively. Thanks to extensive monitoring, 5 s synchronized records of the output power of all the inverters are available from May 2010. From this work, data was taken not only of the entire PV plant but also of 5 sections with P_n between 0.55 kW and 11.5 MW (**Figure 2.1**), making it possible to study the dependence between the storage requirements and the size of the PV power plant.

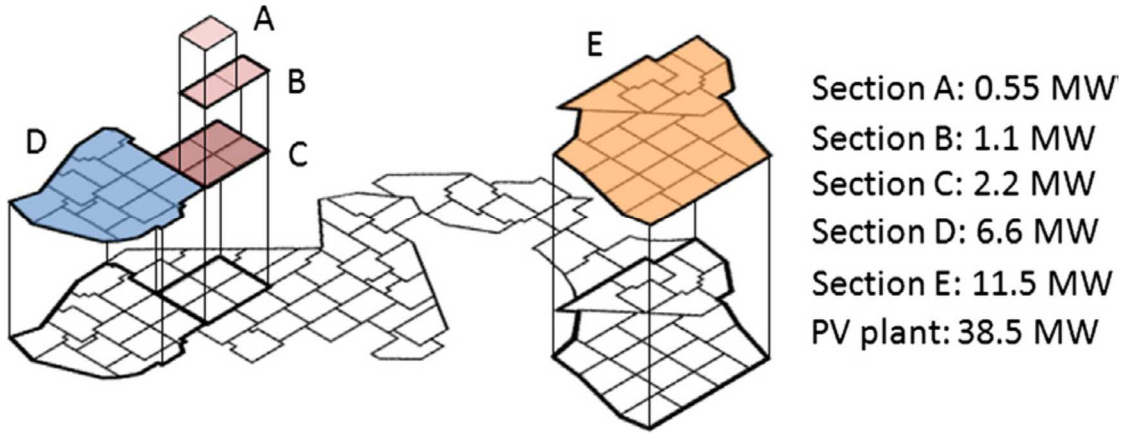

***Figure 2.1**: Field distribution of the Amareleja PV plant sections.*

2.3 RIBERA PV PLANTS

The other experimental data used for this study was taken from six PV plants located in Spain, based on 1 s data recorded since 2009 up to now. The timing was controlled through a GPS, so that it is possible to accurately synchronise the recordings from all the sites. The plant power output ranges from 1 to 9.5 MWp, for a total of 19 MWp. All the PV plants are equipped with vertical-axis trackers (azimuth) paralleling the sun's east–west motion, and each generator is tilted 45°. 1 s power output data are obtained at the point of common coupling by means of a power meter (Allen–Bradley, Power monitor, Milwaukee, WI, USA), and are recorded by a PLC (Allen-Bradley, CompactLogix, Milwaukee, WI, USA). The plants are scattered over a ~1100 km^2 area in the south of Navarra (Spain). **Figure 2.2** details the location of the five sites considered. Distances between them range from 6 to 60 km. **Table 2.1** details the power and surface area of the PV plants.

upna Universidad Pública de Navarra Nafarroako Unibertsitate Publikoa

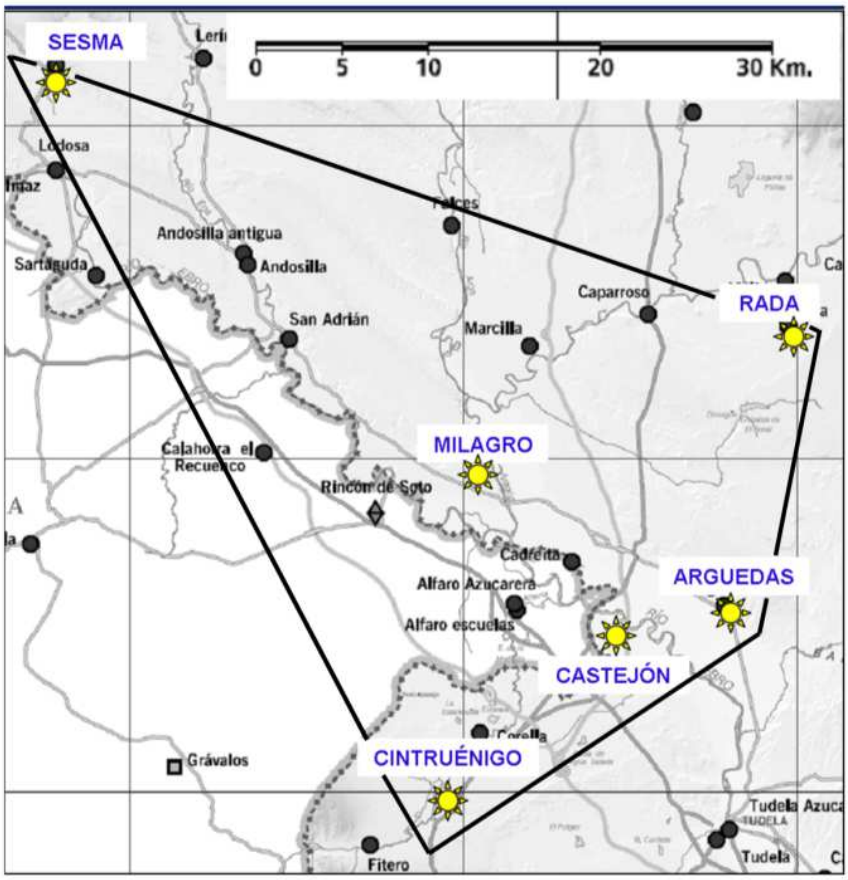

***Figure 2.2**: Geographic distribution of the PV plants under study.*

***Table 2.1**: Characteristics of the PV plants.*

PV plants	Peak Power (kWp)	Transformer Power P_n (kW)	Size S (Ha)	Location (Lat; Lon)
Arguedas	958	775	4.1	**42°10'32" N 1°35'28" W**
Sesma	990	800	4.2	**42°27'43" N 2° 5'31" W**
Cintruénigo	1438	1155	6.4	**42° 3'35" N 1°47'50" W**
Rada	1780	1400	8.7	**42°19'3.25" N 1°34'10" W**
Castejón	2640	2000	11.8	**42° 9'7"N 1°39'36" W**
Milagro	9500	7243	52	**42°15'28.24"N 1°46'30" W**
Total	**17306**	**13375**	-	-

upna Universidad Pública de Navarra Nafarroako Unibertsitate Publikoa

3

POWER FLUCTUATIONS SMOOTHING OF LARGE PV PLANTS WITH ENERGY STORAGE SYSTEMS

"Gray skies are just clouds passing over."
Duke Ellington (1899-1974)

3.1 INTRODUCTION

Concerns about the potential of PV output fluctuations caused by transient clouds were expressed more than 25 years ago (Jewell and Ramakumar, 1987; Jewell and Unruh, 1990) and are now attracting widespread interest and attention, as a result of growing PV penetration rates. As the PV power share in the grid increases, such fluctuations may adversely affect power quality and reliability (Marcos et al., 2011b). In particular, power fluctuations of less than 10 minutes are typically absorbed by the grid as frequency fluctuations. This issue is of special importance in relatively small grids, such as islands, with high penetration rates, because the smoothing effect from the aggregation of geographically dispersed PV plants is intrinsically limited (Marcos et al., 2012; Perpiñán et al., 2013). It was precisely an island grid operator, The Puerto Rico Electric Power Authority, that recently opened the door for PV power variability regulations, by imposing a 10% per minute rate (based on nameplate capacity) limitation on the PV plants being connected to its grid (PREPA, 2012). In addition, in other countries such as Mexico, the regulations target greater restrictions, of around 1 - 5% per minute (CRE, 2014).

upna Universidad Pública de Navarra Nafarroako Unibertsitate Publikoa

Standard (without storage) PV plants exhibit power variations far beyond this limitation. For example, a PV output ramp-rate as high as 63% of the rated capacity/minute was revealed at the 1.2 MW La Ola island power plant (Jolmson et al., 2012), whilst power variations of up to 90% to 70 % per minute were recorded, respectively, at 1 MW and 10 MW PV plants (Marcos et al., 2011a), and variations of 70% per minute were found at a 5MW PV plant (van Haaren et al., 2014). Other multi-megawatt PV plants showed ramp-rates per minute of up to 50% for a 4.6 MW (Hansen, 2007) system and 45% for a 13.2 MW PV plant (Mills et al., 2011). Hence, compliance with such regulations requires combining the PV generator with some form of energy storage technology, to either add or subtract power to or from the PV output in order to smooth out the high frequency components of the PV power. Fuel cells (Rahman and Tam, 1988), electric-double layer capacitors (Kakimoto et al., 2009) and, mainly, batteries (Byrne et al., 2012; Ellis and Schoenwald, 2012; Hund et al., 2010; Leitermann, 2012; Li et al., 2013) have been proposed. Smoothing algorithms can be found (Beltran et al., 2011; Hund et al., 2010; Kakimoto et al., 2009; Khanh et al., 2010; Li et al., 2013). However, storage requirements have been scarcely addressed. Power and energy storage capacity have only been derived from some rather simple and intuitive considerations regarding PV output profiles: sudden drops from full power to 0, which is obviously the maximum conceivable fluctuation, were assumed in Kakimoto et al., 2009 in order to determine the size of the required ESS. Somewhat more realistically, a drop from full power to 10% in 2 seconds was assumed in Hund et al., 2010 to conclude that relatively small batteries suffice. Although detailed observations and studies on irradiance fluctuation are also available (Kuszamaul et al., 2010; Lave et al., 2012; Mills and Wiser, 2010; Mills et al., 2010; Perez et al., 2012), these have not yet led to specific engineering rules in order to determine the storage system size to PV output smoothing.

Indeed, the installation of an ESS has a major impact on the energy/economic balance of the PV system, playing a key role in the viability of the future PV systems due to their high costs and reduced shelf life. As a result, parameters such as energy capacity, losses and the cycling degradation of the ESS, take on particular importance. Any reduction in both the ESS required capacity and charge/discharge cycles will have a positive impact on reducing the investment required to install and maintain the ESS. Consequently, the control strategy selected in order to smooth power fluctuations will be

upna Universidad Pública de Navarra Nafarroako Unibertsitate Publikoa

a crucial decision. At present, given the maximum fluctuation limitation, there is a range of control strategies to reduce the fluctuations below this limit. Among them, the two most often proposed ones in the literature are ramp-rate control (Alam et al., 2014; Kakimoto et al., 2009; Khanh et al., 2010; Li et al., 2013; Ruifeng and Saha, 2010; Wang and Ying-Hao, 2001) and the moving-average (MA) (Chanhom et al., 2013; Datta et al., 2010; Han et al., 2012; Seo et al., 2010). Considering the converter and ESS as ideal elements, the main advantage of MA is that, by definition of the mean value, the value of the energy in the ESS at the beginning and end of any given day is the same. In real practice, however, the battery is discharged at the end of the day to a value equal to the energy lost in the charging/discharging processes. On the other hand, the key point of the ramp-rate control is that only acts when the fluctuation exceeds the maximum allowable ramp-rate value (*i.e.*, lower degradation). There are also other strategies available such as the constant production strategy (Beltran et al., 2013; Darras et al., 2012). However, this technique goes beyond smoothing out the fluctuations in short periods of time and thus requires a much larger ESS. Even so, no individual analysis is made for each of these two strategies as to the impact of them on the actual ESS requirements: energy capacity, charge/discharge cycles, cycling degradation, losses in the power electronic converter (PEC), losses in the ESS, *etc.* Accordingly, few comparisons have been made between the performance of the strategies ramp-rate control and the moving average working in the same PV plant-ESS system. The studies conducted are primarily focused on programming, monitoring and implementing the strategy (Beltran et al., 2011; Cheng et al., 2012; Datta et al., 2010; Nuhic et al., 2013).

In this chapter, the necessity of the installation of an ESS in order to comply with the ramp-rate limitations imposed by the new grid codes is firstly ratified. The model used to simulate a generic strategy to smooth out fluctuations is then shown. Next, both the well-known ramp-rate control and moving-average control are studied in terms of both capacity and power necessities. Thanks to this analysis, a new strategy is proposed, named the step-control strategy, which improves the results in relation to the previous ones. In addition, for the three strategies under study, it is proposed a method to calculate, for any PV plant size and maximum allowable ramp-rate, the maximum power and the minimum energy storage requirements alike. Finally, a comparison of the three strategies in order to fit the grid quality demands is also made. Each control method is

upna Universidad Pública de Navarra Nafarroako Unibertsitate Publikoa

evaluated regarding the quality of the produced signal and the ESS demand. All the simulations were based on actual PV production data, taken every 5 s in the course of one year (2012) from different section of Moura PV plant (see section 2.2), with power outputs ranging from 550 kW to 40 MW. The experimental ESS comprised a lithium-ion battery connected at the AC side through a two-way DC/AC PEC. The presented results can be used as a guide to select the best control strategy, and the optimum design and selection of the ESS, making it possible to assess the impact of the ESS on the PV plant energy/economic balance.

3.2 POWER FLUCTUATIONS WITHOUT STORAGE

Given a power time series *P(t)*, recorded with a certain sampling period, *Δt*, power fluctuation at time *t*, $\Delta P_{\Delta t}(t)$ is defined as the difference between two consecutive samples of power, normalized to the inverter power P_n. That is Eq.(3.1):

$$\Delta P_{\Delta t}(t) = \frac{\left[P(t) - P(t-\Delta t)\right]}{P_n} \times 100 \ [\%] \qquad \textbf{(3.1)}$$

It is then possible to compare the time series of $\Delta P_{\Delta t}(t)$ with a given ramp value, *r*, and count the time the fluctuations exceed the ramp (*abs* $[\Delta P_{\Delta t}(t)] > r$). Figure 3.1 shows the results for a full year (2012) and for the different Amareleja PV sections described in section 2.2. As expected, the occurrence of fluctuations decreases with *r* and with P_n. For *r* = 1%/min and P_n = 550 kW, power fluctuation exceed the ramp for 40% of the time. For the same ramp, increasing the PV size to P_n = 38.5 MW reduces the time the ramp is exceeded to 23%, whilst for a much less stringent ramp, *r* = 30%/min, these values drop to 3% and 0.1%, respectively. These examples show that imposing power ramp limits (typically around 10%/min) makes it necessary to resort to an ESS even when large PV plants are concerned.

upna Universidad Pública de Navarra Nafarroako Unibertsitate Publikoa

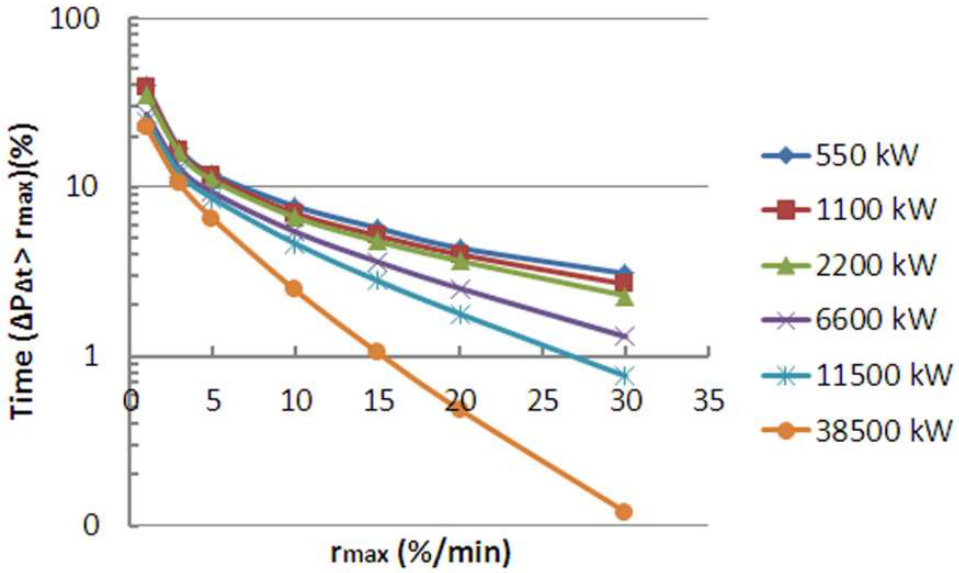

***Figure 3.1**: Frequency over one year (2012) of PV power fluctuations calculated in 1-min time window, ΔP1min(t), are superior to a given ramp r (%/min). The frequency value is given in relative terms to the total production time (4380 h).*

3.3 A GENERIC STRATEGY FOR SMOOTHING FLUCTUATIONS THROUGH ENERGY STORAGE

For the simulations, a lithium ion battery-based storage system was selected. Logically, the methodology put forward is equally valid for any other type of storage system (such as supercapacitors, flow batteries, fly wheels, *etc.*). **Figure 3.2** shows the model used to simulate a generic strategy to smooth out fluctuations. For each sampling period, the algorithm reduces the fluctuations of $P_{PV}(t)$ to the maximum permitted level r_{max} and the result is the power injected into the grid, $P_G(t)$. The difference between $P_G(t)$ and $P_{PV}(t)$ is the power setpoint to either be provided by ($P_{ESS} > 0$) or to be absorbed by the ESS ($P_{ESS} < 0$). The next step is to apply the PEC efficiency, η_{PEC}, and that of the lithium ion battery, η_{BAT}, in order to obtain the required battery power, P_{BAT}.

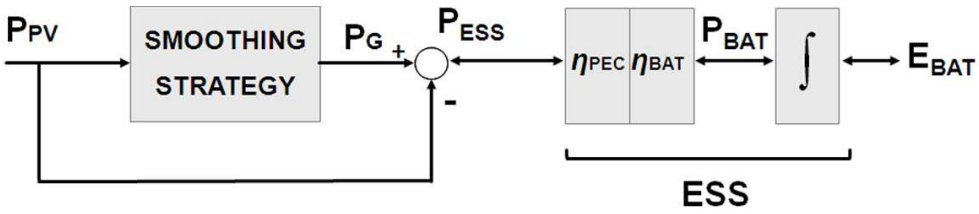

***Figure 3.2**: Generic model for the evaluation of the fluctuation smoothing strategies at a PV plant with energy storage. As can be seen, the performance of the energy storage system (ESS) has been divided*

upna Universidad Pública de Navarra Nafarroako Unibertsitate Publikoa

into two: on the one hand, the performance of the power converter (η_{PEC}) and, on the other hand, that of the lithium ion battery (η_{BAT}).

To calculate the PEC losses, a real curve obtained from the Ingecon Sun Powermax® 1 MW (INGETEAM, 2014) commercial converter was used (**Figure 3.3**). This same converter is connected to a 1 MW transformer on the AC side, whose efficiency curve is also shown in **Figure 3.3**, together with the total for the PEC (Ingecon Sun + Transformer). With regard to the lithium ion battery losses, data was used from the manufacturer's catalogue, specifically the 1 MW/560 kW·h Intensium® Max battery made by SAFT (Bagnolet, France), whose round-trip efficiency can be considered constant and equal to 95% (SAFT SA, 2008). The integral of P_{BAT} is the energy E_{BAT} to be provided by the battery in order to smooth the fluctuations. It must be noted that this study does not seek to achieve an accurate modelling of the ESS efficiency, but rather to make a comparison of different strategies.

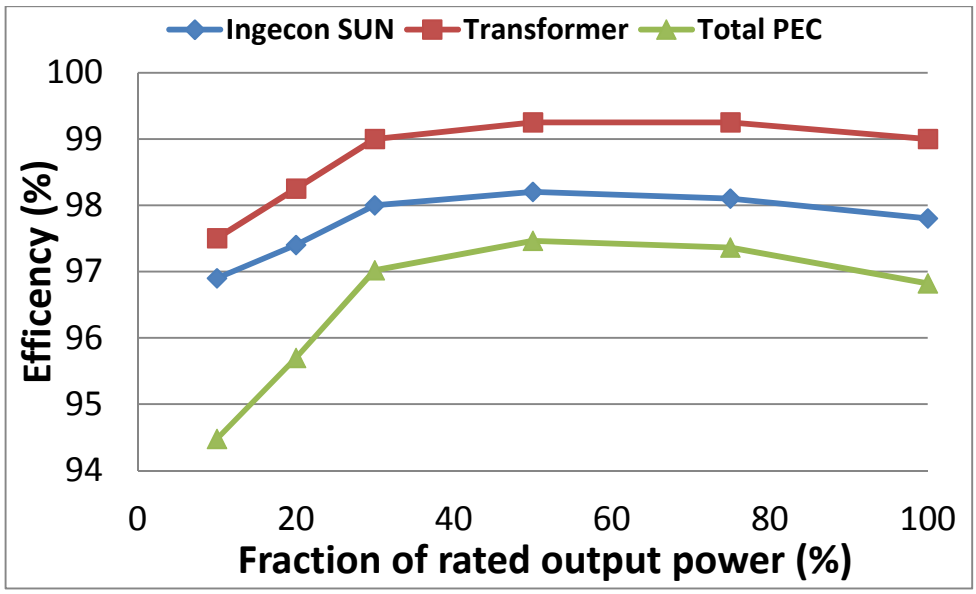

***Figure 3.3**: Power electronic converter (PEC) efficiency curve (reversible DC/AC converter, corresponding to the commercial converter INGECON SUN POWERMAX® 1 MW plus 1 MW transformer).*

3.4 RAMP-RATE CONTROL

3.4.1 Control strategy

Let us consider a maximum permissible ramp rate value of the power injected into the grid, r_{MAX} [%/min]. **Figure 3.4** shows a basic model of the corresponding ramp-rate control. $P_{PV}(t)$, $P_G(t)$ and $P_{BAT}(t)$ are, respectively, the power provided by the PV inverter, the power injected into the grid and the power provided by the battery. Obviously:

$$P_{BAT}(t) = P_G(t) - P_{PV}(t) \qquad \textbf{(3.2)}$$

Initially, the inverter tries to inject all its power into the grid, $P_G(t) = P_{PV}(t)$. The control is activated when the maximum allowable ramp condition is broken. That is, if:

$$\frac{\left|\Delta P_{PV,1\min}(t)\right|}{P_n} \cdot 100 > r_{MAX} \qquad \textbf{(3.3)}$$

Then, the corresponding power excess or shortage is either taken from ($P_{BAT}(t) > 0$) or stored into ($P_{BAT}(t) < 0$) the battery. The energy stored at the battery, $E_{BAT}(t)$, is given by the integral of $P_{BAT}(t)$ over time. In this way, the behaviour of the whole system can be easily simulated for any time series of $P_{PV}(t)$.

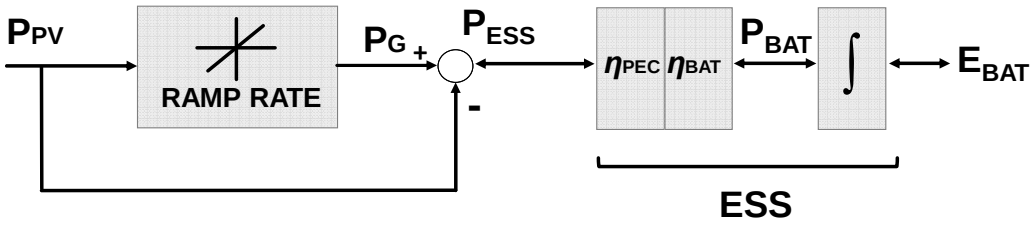

***Figure 3.4**: Ramp-rate control model modified with additional SOC control. Notice that the SOC control action is also smoothed by the ramp-limiter in order to guarantee that power fluctuations are always below r_{MAX}.*

As a representative example, **Figure 3.5** shows, for r_{MAX} = 10%/min, the 1.1 MW Amareleja PV section on an extremely fluctuating day (31th October, 2012), the resulting evolution of $P_{PV}(t)$ and $P_G(t)$ (**Figure 3.5 (a)**), $P_{BAT}(t)$ (**Figure 3.5 (b)**) and $E_{BAT}(t)$ (**Figure**

upna Universidad Pública de Navarra Nafarroako Unibertsitate Publikoa

3.5 (c)). Battery requirements for this day derive from the corresponding maximum power and energy values. In this example, the required battery power is $P_{BAT,MAX}$ = 873 kW (or $P_{BAT,MAX}$ = 0.79 P_n) and the required battery capacity is C_{BAT} = $E_{BAT,MAX}$ - $E_{BAT,MIN}$ = 175 kWh (or 10 min of capacity, equivalent to 0.16 hours of PV plant production at P_n). It is worth mentioning that the daily battery energy balance is negative (- 20 kWh). At first glance, this may appear counter-intuitive, because the PV power fluctuation distribution is essentially symmetrical (clouds reaching and leaving the PV field). However, this can be understood by carefully observing the battery charge and discharge dynamic. Note that the area of upper regions (charging) is larger than the area of lower ones (discharging).

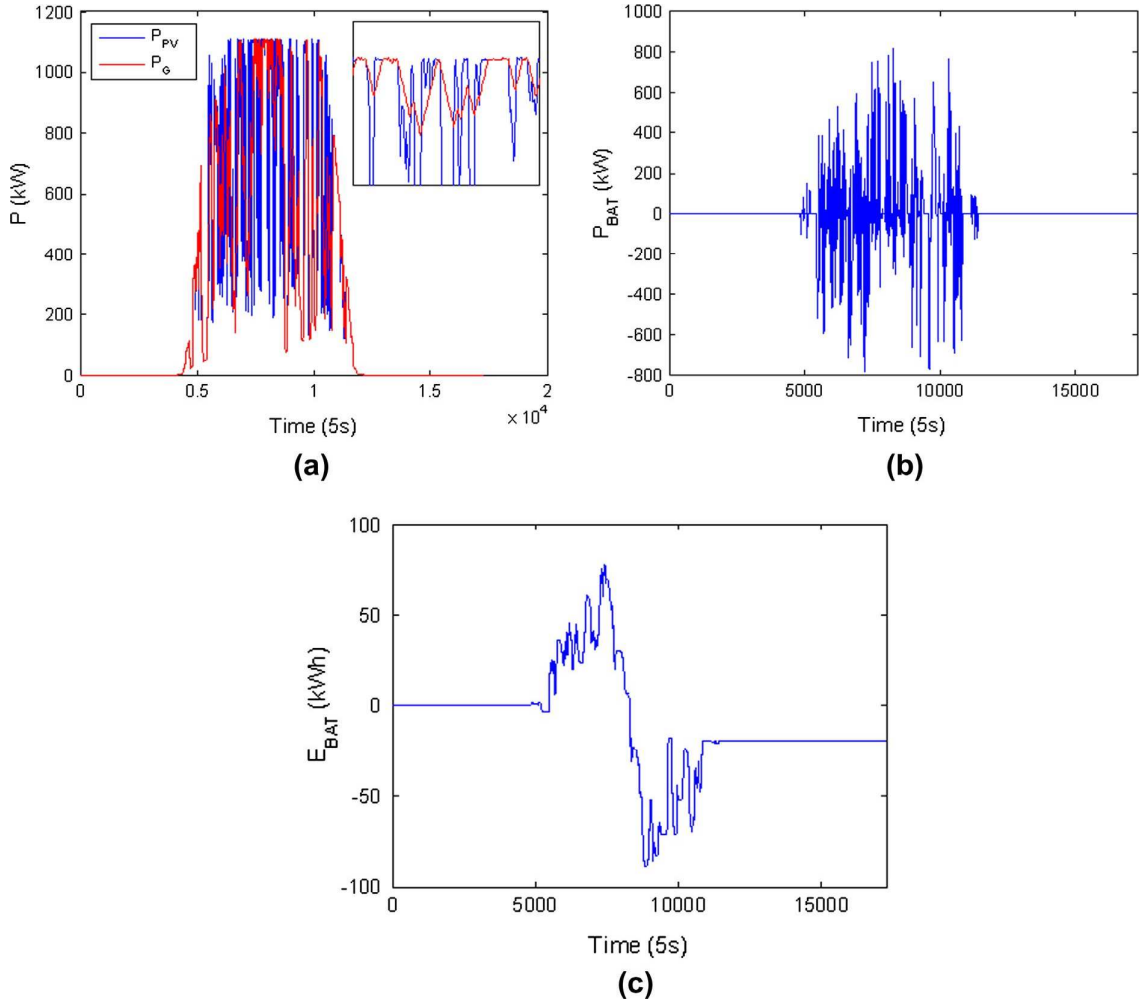

***Figure 3.5**: (a). Evolution of the generated power, P_{PV} (t) by Section B (1.1 MW) on 31th October 2012 and the simulated power which would be injected to the grid P_G (t) in the case of disposing a battery which limits fluctuations to r_{MAX} of 10%/min (0.833%/5s). (b) Battery power, P_{BAT}. (c) Battery energy, E_{BAT}.*

Figure 3.6 shows the result of extending the simulation exercise to an entire year (2012), to all the Amareleja PV sections, and for r_{MAX} = 10%/min. The State of Charge (SOC) of the battery at the end of a day has been concatenated with the SOC at the beginning of the next day. As the example shown in **Figure 3.5**, the tendency of the battery to continuously discharge affects the entire one year period. An important initial conclusion can be drawn: instead of distributing the storage systems for single power plants or sections within a power plant, it seems wiser to add multiple sections or power plants to a single storage system. On the other hand, the battery discharging tendency leads to excessive battery capacity requirements, in the order of some hours. More practical alternatives are obtained when adding charge to the battery at different times throughout the year, as will be seen below. Nevertheless, an important conclusion can be reached from **Figure 3.6**: the energy that must be managed through the storage systems is very low, only about 0.3% of the total energy production for limiting the power ramps of a 0.5 MW plant at a maximum of 10%/min (for this case, as Figure 3.1 showed, the battery time of use is equal to 8%).

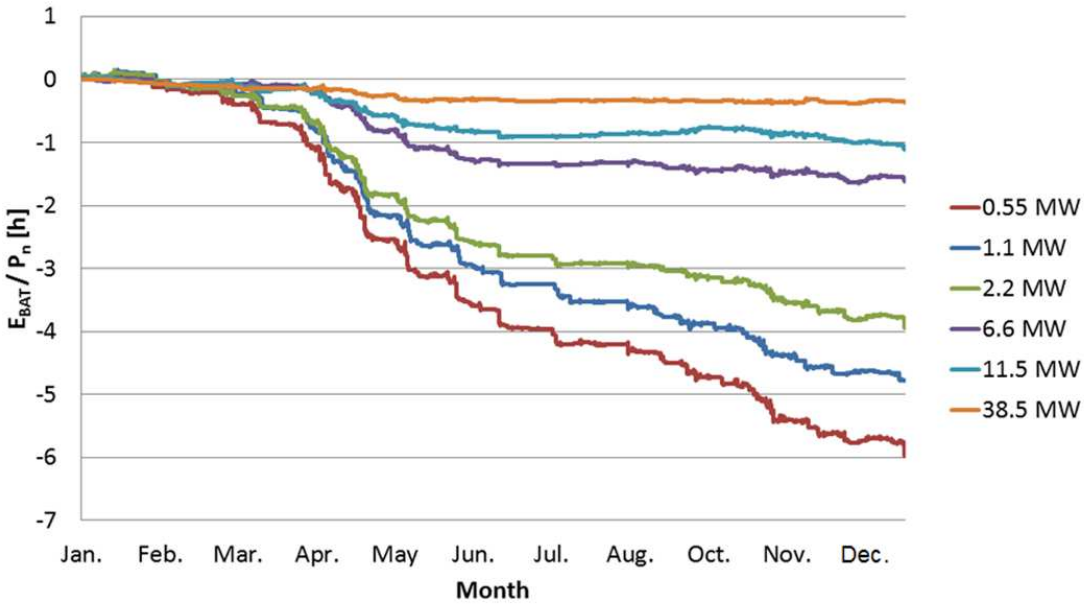

***Figure 3.6**: Evolution of storage time, E_{BAT}/ P_n [h], in the battery during one year (2012), limiting the ramps to a maximum of 10%/min in different PV systems.*

3.4.1.1 Overnight battery recharging

Overnight battery recharging from the grid makes sense because electricity demand usually drops at night. **Figure 3.7** presents the results of a simulation exercise similar to **Figure 3.6**, except that this time, if required, energy at the battery is restored each night. That is:

$$E_{BAT,end\ day_{i-1}} < 0 \Rightarrow E_{BAT,beginning\ day_i} = 0 \qquad \textbf{(3.4)}$$

In this way the tendency of the battery to discharge continuously does not affect the entire period of one year, but is limited to one day and therefore significantly reduces the required battery size, which is now in the order of some minutes. For example, battery requirements for r_{MAX} = 10%/min in the 1.1 MW Amareleja PV section are now $P_{BAT,MAX}$ = 890 kW (or $P_{BAT,MAX} = 0.81 \cdot P_n$) and $E_{BAT,MAX}$ = 451 kWh (or 25 min of capacity, equivalent to 0.41 h of PV plant production at P_n). The comparison of these figures with the above mentioned results for 31th October 2012, reveals that power battery requirements, which are obviously imposed by the worst individual fluctuation, tend to be constant throughout the analysis period. However, the same is not true for the battery energy requirements, which are imposed by the fluctuation distribution throughout the worst day.

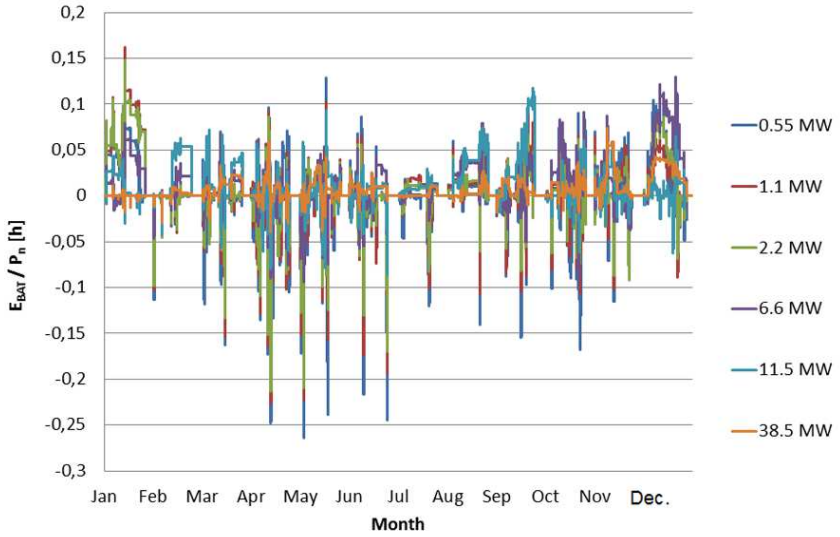

***Figure 3.7**: Evolution of storage time, E_{BAT}/ P_n [h], in the battery during one year (2012), limiting the ramps to a maximum of 10%/min in different PV systems with overnight recharge.*

upna Universidad Pública de Navarra Nafarroako Unibertsitate Publikoa

3.4.1.2 Daytime battery recharging controlled by State of Charge

Another interesting battery recharging possibility, not requiring energy to be supplied from the grid, consists in establishing a reference value for the energy stored in the battery, $E_{BAT,REF}$ and in implementing a control loop that continuously tries to return $E_{BAT}(t)$ to this reference, providing the ramp-rate limit is observed and energy is never taken from the grid (night-time charging forbidden). **Figure 3.8** presents the corresponding model. The control will be faster or slower depending on the value of K. For example, a value of K = 1 means that if $E_{BAT}(t)$ - $E_{BAT,REF}$ = 1 kWh the control would request 1 kW from the battery. Obviously, once the battery capacity is defined, E_{BAT} control is equivalent to SOC control.

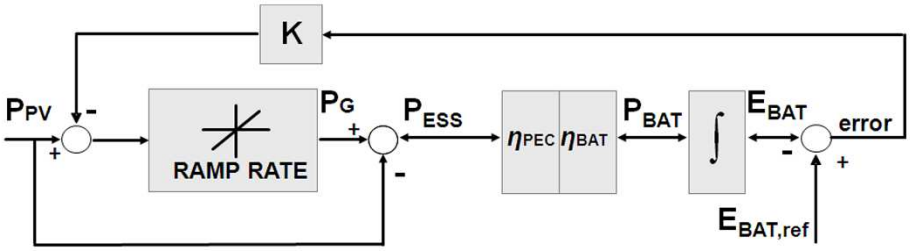

***Figure 3.8**: Ramp-rate control model modified with additional SOC control. Notice that the SOC control action is also smoothed by the ramp-limiter in order to guarantee that power fluctuations are always below r_{MAX}.*

In this way the battery tendency to continuously discharge has no effect on the entire one year period or on the entire one day period, but only on the short period the control requires to restore $E_{BAT,REF}$. This therefore further reduces the required battery size. **Figure 3.9** shows the results of a simulation exercise again for the 1.1 MW Amareleja PV section and for a one year period (2012). $E_{BAT,REF}$ and K have been set to 175 kWh and 6, respectively, which allows for a good compromise between system stability and fast battery recharging. In this case, corresponding battery requirements are $P_{BAT,MAX}$ = 890 kW (or $P_{BAT,MAX}$ = 0.81· P_n) and C_{BAT} = $E_{BAT,MAX}$ - $E_{BAT,MIN}$ = 124 kWh (or 6.7 min of capacity, equivalent to 0.11 hours of PV plant production at P_n). Thus, the required battery capacity is significantly lower than that corresponding to night-time recharging. In fact, this K value is large enough to almost restore $E_{BAT,REF}$ just after each fluctuation. Thus the impacts of successive fluctuations become independent of each

upna Universidad Pública de Navarra Nafarroako Unibertsitate Publikoa

other and battery requirements become essentially linked to the “worst fluctuation”, i.e. the individual fluctuation requiring the highest energy demand.

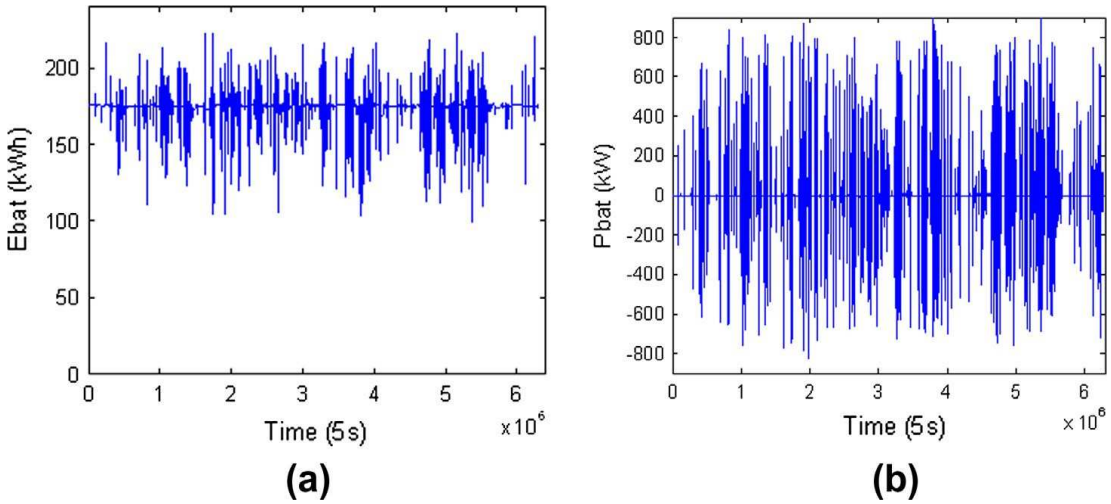

***Figure 3.9**: Evolution along the year 2012 of E_{BAT} (a) and P_{BAT} (b) for section B (1.1 MW), a r_{MAX} of 10%/min and with SOC control. $E_{BAT,REF}$ and K have been arbitrarily set to 175 kWh and 6, respectively.*

3.4.2 Energy storage requirements: the worst fluctuation model

Careful study of real worst fluctuations observed at Amareleja lead to postulate that the worst fluctuation is properly described (**Figure 3.10**) by a power exponential decay from P_n to 0.1 P_n (or an exponential rise from 0.1 P_n to P_n) with a time constant, τ [s], which is empirically correlated (**Figure 3.11**) with the shortest dimension of the perimeter of the PV plant, l [m], by an expression such as:

$$\tau = a \cdot l + b \qquad \textbf{(3.5)}$$

where a = 0.042 [s/m] and b = -0.5 s. **Table 3.1** presents the real τ values observed at the different PV Amareleja sections and **Figure 3.11** shows that they are in good agreement with Eq.(3.5).

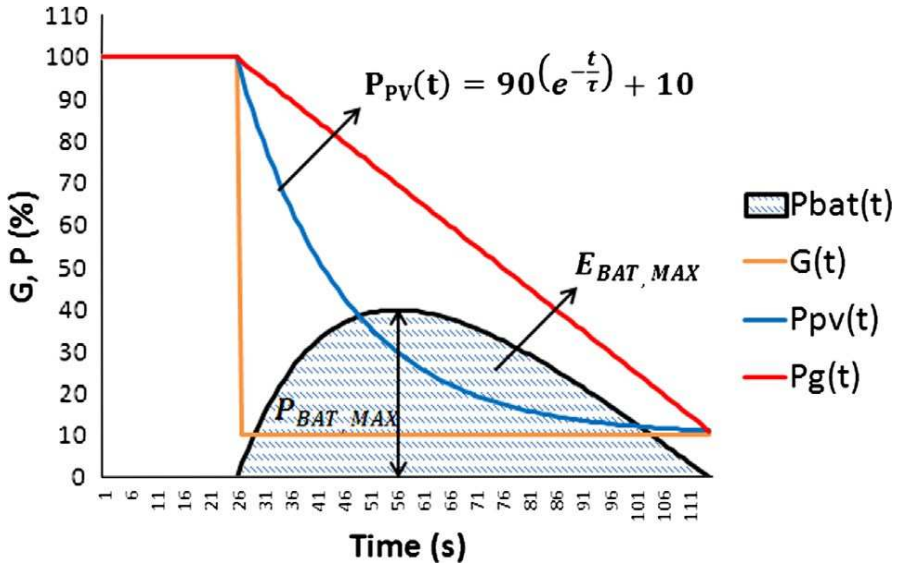

***Figure 3.10**: Worst fluctuation model. The blue line represents the P_{PV} (t) response to an irradiance fluctuation (yellow line) and the red one is the power injected to the grid P_G with a ramp-rate control. The difference between P_G and P_{PV} is P_{BAT}, the maximum difference corresponds to $P_{BAT,MAX}$ and the defined integral of P_{BAT} corresponds to $E_{BAT,MAX}$.*

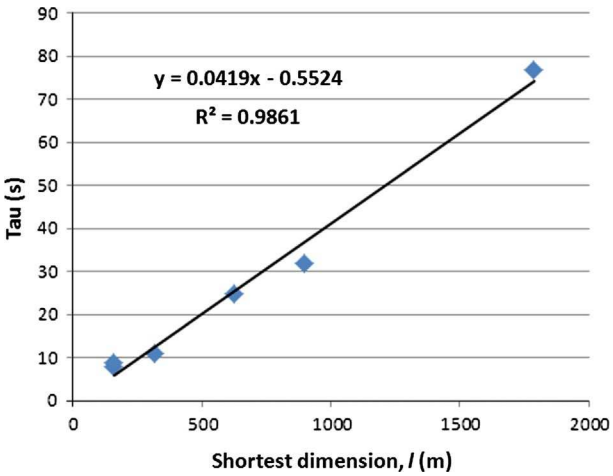

***Figure 3.11**: Adjustment of observed time constant values τ vs. shortest perimeter dimension l, Eq.(3.5). The general expression of this equation is y = mx+n, where m gives the coherency to the units. In this case, m = 0.042 [s/m].*

***Table 3.1**: Characteristic power P_n, shortest perimeter dimension l and time constant τ of all of the observed worst fluctuation at the different Amareleja PV sections.*

Power P_n (MW)	Short dimension l (m)	Tau τ (s)
0.55	158	8
1.1	158	9
2.2	318	11
6.6	626	25
11.5	896	32
38.5	1786	77

Battery requirements for ramp-rate limitation are easily derived from the model showed in **Figure 3.10**. In this figure, the response of $P_{PV}(t)$ and $P_G(t)$ to a negative irradiance $G(t)$ fluctuation can be seen. $P_{PV}(t)$ evolution corresponds to a first order system with a time constant τ, while P_G decreases with a rhythm being set by r_{MAX}. The power demanded to the battery $P_{BAT}(t)$ corresponds with the difference between $P_G(t)$ and $P_{PV}(t)$, Eq.(3.2). Therefore, $P_{BAT}(t)$ along the worst fluctuation time is given by:

$$P_{BAT}(t) = \frac{P_n}{100}\left[90\,(1-\exp(-t/\tau)) - t \cdot r_{\max}\right] \qquad \textbf{(3.6)}$$

where r_{MAX} is expressed as % per time. This expression gets a maximum for

$$t_{P_{BAT,MAX}} = \tau \cdot \ln\frac{90}{\tau \cdot r_{MAX}} \qquad \textbf{(3.7)}$$

Thus, the required battery power is given by:

$$P_{BAT,ramp}(t) = \frac{P_n}{100}\left[90 - \tau \cdot r_{MAX}\,(1+\ln\frac{90}{\tau \cdot r_{MAX}})\right] \qquad \textbf{(3.8)}$$

where P_n, $P_{BAT,ramp}$ is expressed in [kW], r_{MAX} in [%/s] and τ in [s]. On the other hand, the battery discharging process lasts until the time the power ramp reaches 0.1 P_n. Corresponding time span, T_R, is:

$$T_R = \frac{90}{r_{MAX}} \qquad \textbf{(3.9)}$$

Thus, the required battery energy is given by:

upna Universidad Pública de Navarra Nafarroako Unibertsitate Publikoa

$$E_{BAT,ramp} = \int_0^{T_R} P_{BAT}(t)\,dt = \frac{0.9P_n}{3600}\left[\frac{90}{2\cdot r_{MAX}} - \tau\cdot\left(1-\exp\left(-\frac{90}{\tau\cdot r_{MAX}}\right)\right)\right] \approx \frac{0.9P_n}{3600}\left[\frac{90}{2\cdot r_{MAX}} - \tau\right] \quad \textbf{(3.10)}$$

where P_n is expressed in [kW], r_{MAX} in [%/s], τ in [s] and $E_{BAT,MAX}$ in [kWh]. As the sign of the first fluctuation is unknown, a double capacity battery is required to absorb both the upwards and downwards fluctuation:

$$C_{BAT,ramp} = 2\cdot E_{BAT,ramp} = \frac{1.8P_n}{3600}\left[\frac{90}{2\cdot r_{MAX}} - \tau\right] \quad \textbf{(3.11)}$$

For example, for P_n =1.1 MW and l = 158 m, Eq.(3.5) leads to τ = 6.14 s, and battery requirements for limiting the ramp-rate to r_{MAX} = 10%/min are, from Eq.(3.8), $P_{BAT,ramp}$ = 0.84·P_n = 928 kW and, from Eq.(3.11), C_{BAT} = P_n·0.132h = 145 kWh. For P_n = 38.5 MW and l = 1786 m, corresponding results are τ = 74.51s, $P_{BAT,ramp}$ = 0.53·P_n = 20.4 MW and $C_{BAT,ramp}$ = P_n·0.098h = 3773 kWh.

Figure 3.12 compares the battery requirements for the different PV Amareleja sections and for different ramp-rate limits, as deduced from simulation based on a year of observed 5 s data and as given by Eq.(3.8) and (3.11). Good agreement is clearly observed. Furthermore, in order to check the general validity of the worst fluctuation model, it is performed a similar exercise for two different PV plants located at a distance of about 660 km from Amareleja, at Rada (P_n = 1.4 MW; l = 260 m; τ = 10 s) and Castejón (P_n = 2 MW; l = 310 m; τ = 12 s), both in the South of Navarra (Spain).

upna Universidad Pública de Navarra Nafarroako Unibertsitate Publikoa

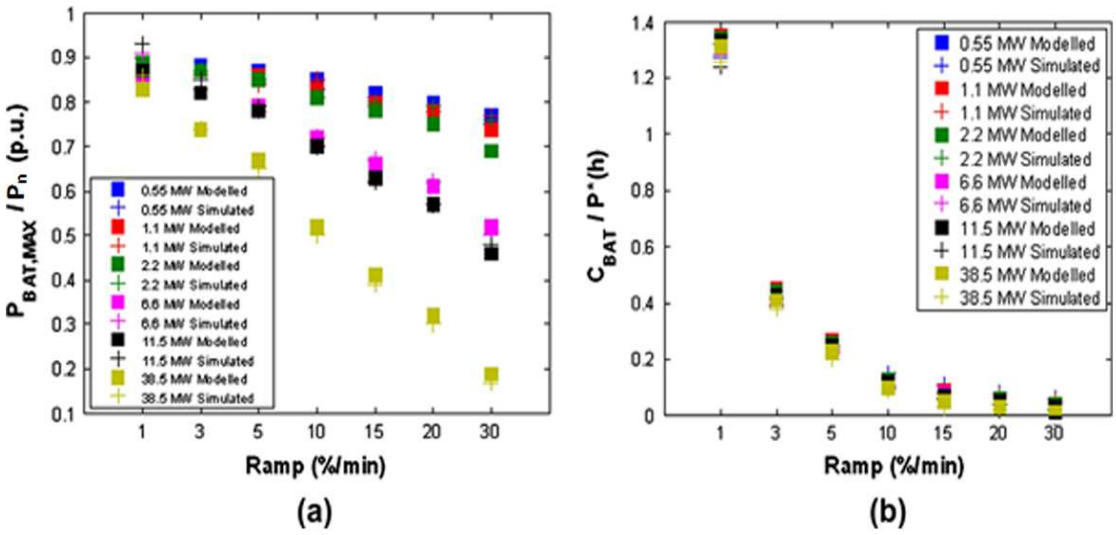

***Figure 3.12**: Storage requirements for ramp-rate control: (a) Battery power $P_{BAT,MAX}$, normalized to inverter power P_n and (b) Storage time C_{BAT}/ P_n, in hours. Results derived from the worst fluctuation model show good agreement with the ones derived from detailed simulation based on 5 s real data recorded at different Amareleja PV sections.*

Figure 3.13 presents the corresponding results which, again, show very good agreement between modelled and simulation-derived data.

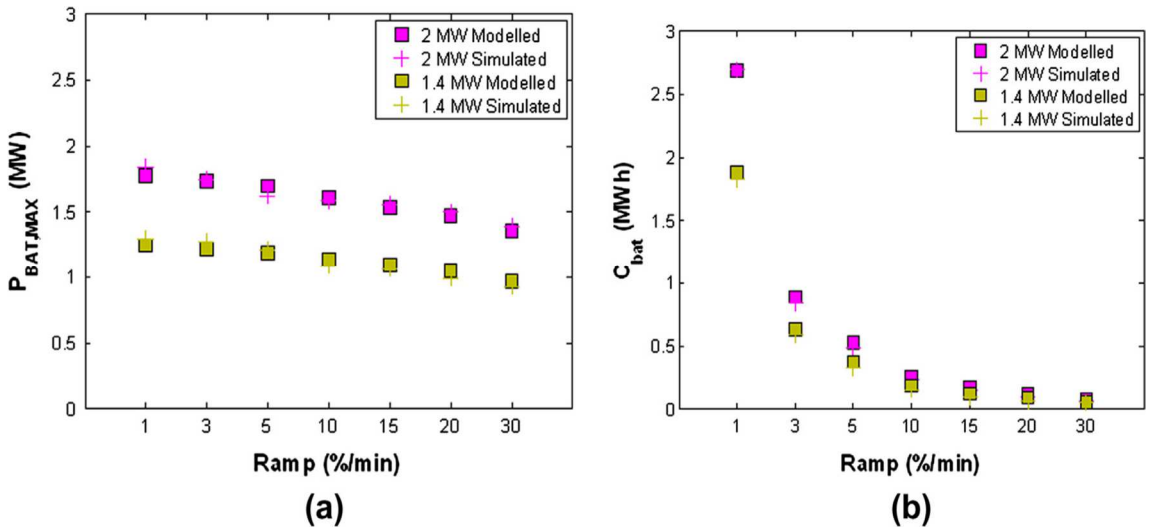

***Figure 3.13**: Worst fluctuation model validation compared to data from two other PV plants, at a distance of 660 km from Amareleja PV plant: (a) Battery power $P_{BAT,MAX}$ in MW and (b) Battery capacity C_{BAT}, in MWh.*

3.5 MOVING-AVERAGE STRATEGY

Given a power time series $P_{PV}(t)$ as recorded in this study, the power smoothed to be injected into the grid $P_G(t)$ is calculated as the mean production value in a time window with a duration of T, in other words, **(3.12**):

$$P_G(t) = \frac{1}{T}\int_{t-T}^{t} P_{PV}(t)\mathrm{d}t \qquad \textbf{(3.12)}$$

The greater the time for window T, the greater the smoothing of the fluctuations at $P_G(t)$. The key advantage of this strategy is that, if the system is equipped with an ideal converter and battery ($\eta_{BAT} = \eta_{PEC} = 1$), by definition of the mean value, the value of E_{BAT} at the beginning and end of any given day should be the same. Therefore, there is no need for any type of SOC control to prevent the continuous battery discharge. However, since η_{BAT} and η_{PEC} <1, this advantage disappears and, at the end of the day, the battery is discharged to a value equal to the energy lost in the charging/discharging processes in the ESS. This same phenomenon was already observed in Hund et al., 2010. This paper proposes a simple solution to this problem, consisting in offsetting the mean value of the losses, also for a time window T (**Figure 3.14**).

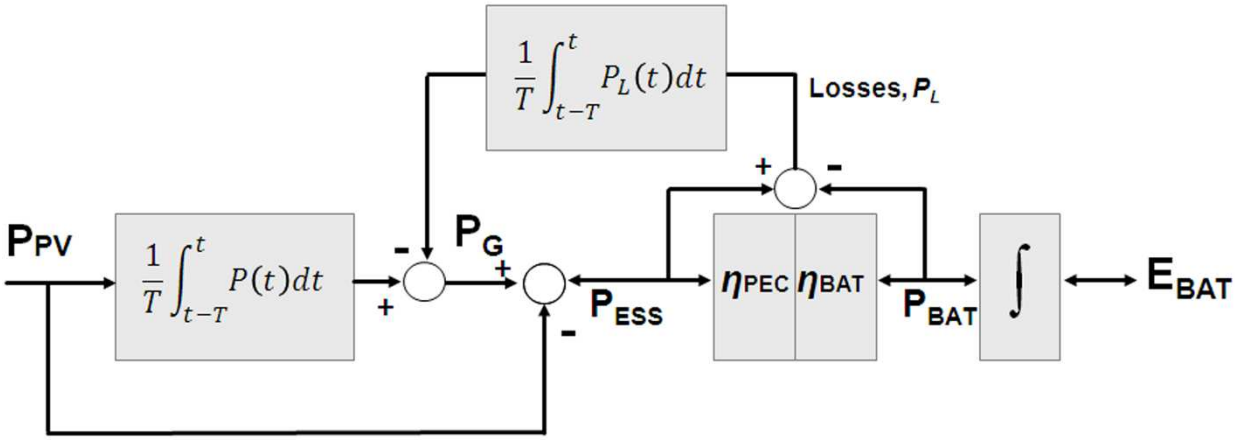

***Figure 3.14**: Model of the moving-average strategy, offsetting the ESS losses.*

In the same manner as was done in ramp-rate control strategy, it would be important to obtain a general expression to determine the storage capacity needed by

the MA strategy. **Figure 3.10** yet again resolves this problem. The analytical expression of function $P_{G,MA}$ is equal to Eq.(3.13):

$$P_{G,MA}(t) = \frac{1}{T}\int_{t-T}^{t} P_{PV}(t)dt = \frac{1}{T}\int_{t-T}^{t} \left[90\left(e^{-t/\tau}\right)+10\right]dt \qquad \textbf{(3.13)}$$

Substituting $T = 5400/r$ and resolving Eq.(3.13), the general expression of $P_{G,MA}$ is obtained, Eq.(3.14):

$$P_{G,MA}(t) = 100 - \frac{90}{5400}\left[t\,r - \tau\left(\frac{1}{e^{t/\tau}} - 1\right)\right] \qquad \textbf{(3.14)}$$

The final term of this expression is responsible for the phase lag existing between $P_{G,MA}$ and $P_{G,ramp}$ which can be seen in **Figure 3.15**. The area between both curves $A_{MA,ramp}$ can approximately be calculated by Eq.(3.15):

$$A_{MA,ramp} = \frac{1.5P^*}{6000}\tau\sqrt{r^2+1}\,\mathrm{sen}[90^o - tg^{-1}(r)] \qquad \textbf{(3.15)}$$

where P_n is expressed in (kW), r_{max} in (%/min), τ in (s), and $A_{MA,ramp}$ in (kW·h). Therefore, the MA strategy requires a battery equal to Eq.(3.16):

$$C_{BAT,MA} = E_{BAT,ramp} + A_{MA,ramp} \qquad \textbf{(3.16)}$$

upna Universidad Pública de Navarra Nafarroako Unibertsitate Publikoa

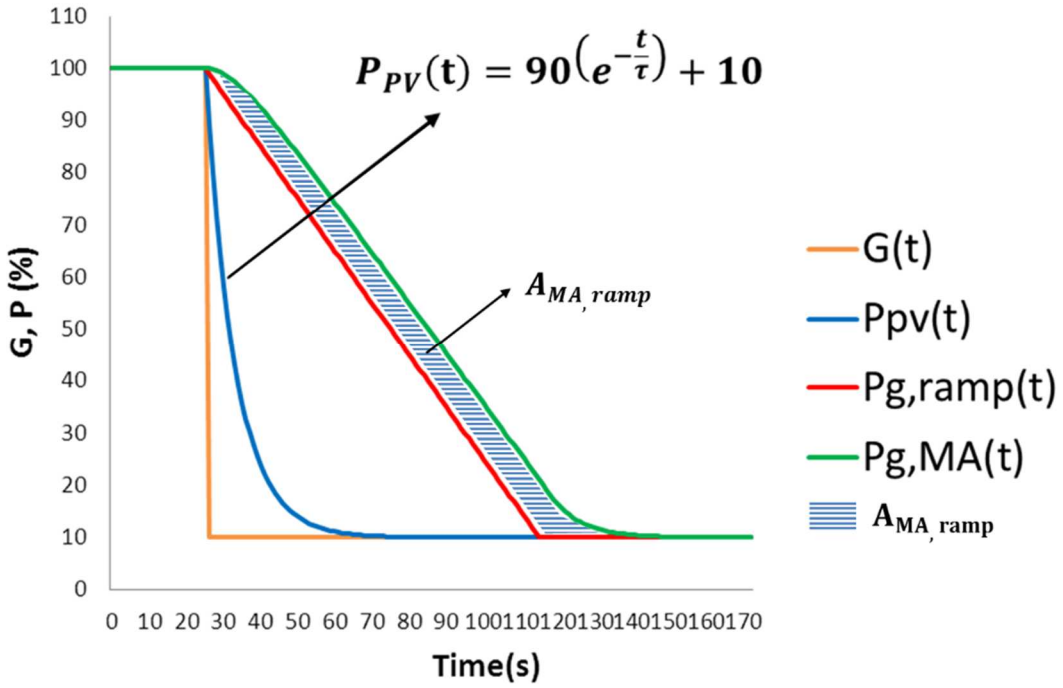

***Figure 3.15**: Model to calculate the storage capacity needed $C_{BAT,MA}$ for the MA strategy.*

For example, for P_n = 1.1 MW (τ = 6.14 s) and r_{max} = 2%/min, Eq.(3.10) provides $E_{BAT,ramp}$ = 370 kW·h and $A_{MA,ramp}$ = 1.8 kW·h, then $C_{BAT,MA}$ = 371 kW·h, equivalent to 0.35 h of PV plant production at P_n. For the same ramp restriction and P_n = 38.5 MW (τ = 75 s), Eq.(3.10) gives $E_{BAT,ramp}$ = 12,995 kW·h and $A_{MA,ramp}$ = 715 kW·h , then $C_{BAT,MA}$ = 13,710 kW·h, equivalent to 0.36 h of PV plant production at P_n.

Figure 3.16 shows the example of applying this strategy once again for 15 February 2012, and with T = 2700 s. For this time window T, the maximum daily fluctuation in 1 min is reduced to 1.95%/min. For this strategy, the required battery power is $P_{BAT,MAX}$ = 919 kW (or $P_{BAT,MAX}$ = 0.83· P_n) and the required effective battery capacity is C_{BAT} = $E_{BAT,MAX}$ − $E_{BAT,MIN}$ = 378 kWh (or 20 min of capacity, equivalent to 0.34 h of PV plant production at P_n). It must be noted that the SOC control tends to return the battery power to its original state, thanks to the offsetting of losses. Likewise, although P_G is slightly smoother than in the case of ramp-rate control, the ESS endures a few more cycles.

upna Universidad Pública de Navarra Nafarroako Unibertsitate Publikoa

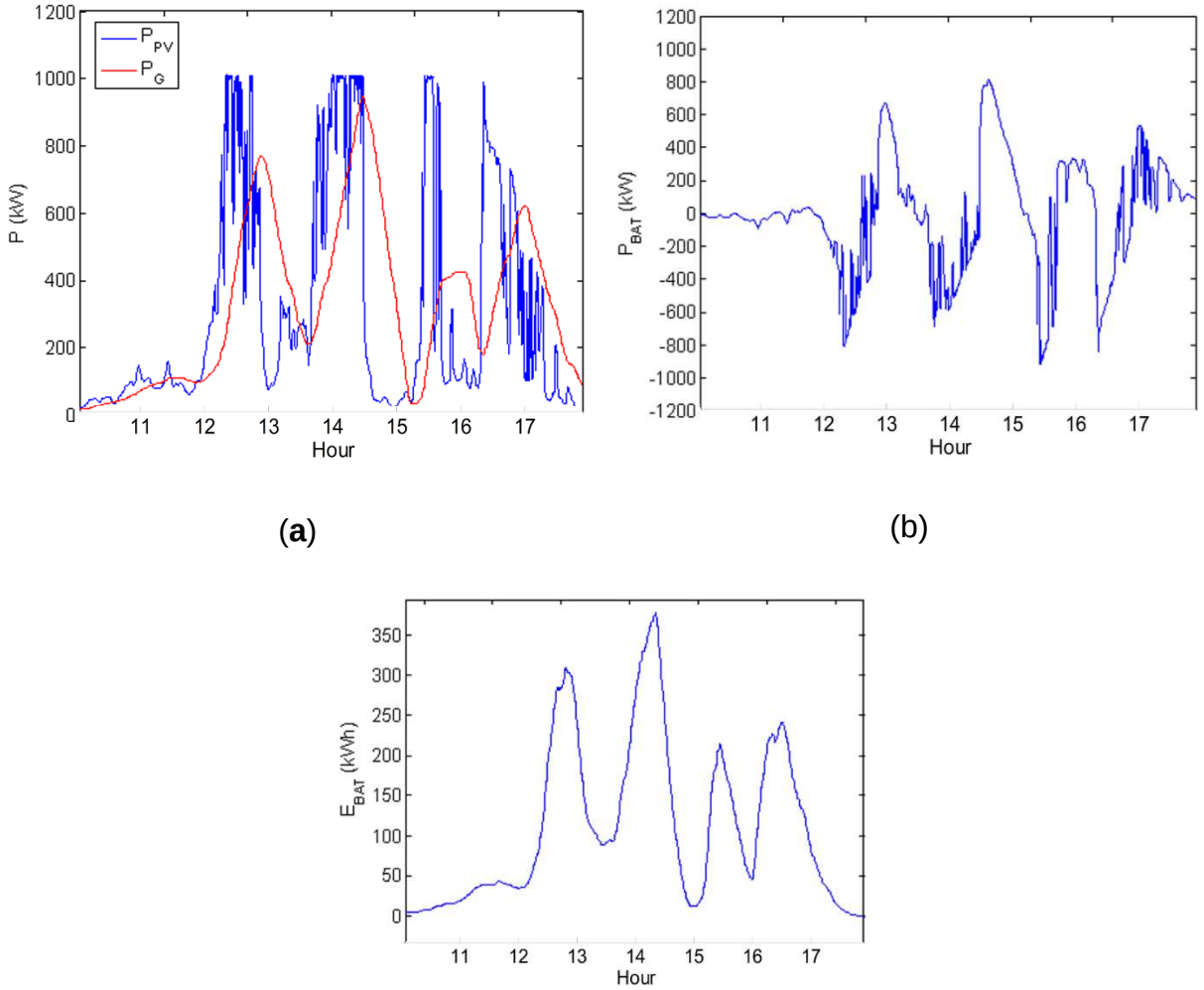

***Figure 3.16**: (**a**) Evolution of the generated power, $P_{PV}(t)$ on 15 February 2012 by Section B (1.1 MW) and the simulated power which would be injected to the grid $P_G(t)$ under the moving average strategy (T = 2700 s); (**b**) battery power, P_{BAT}; and (**c**) battery energy, E_{BAT}. The simulation has been made based on the model shown in **Figure 3.14**.*

It is worth emphasize that this strategy must be operative even on clear days, because the reduction in fluctuations must be ensured in all cases. As will be shown later, this will cause an excessive cycling in the ESS. **Figure 3.17** shows the example of applying this strategy during a clear day. In the absence of methods of predicting fluctuations, the MA must be applied since sunrise, preparing for a potential fluctuation that does not happen. As a result, the ESS suffered one charge-discharge cycle unnecessarily (**Figure 3.17 (c)**).

upna Universidad Pública de Navarra Nafarroako Unibertsitate Publikoa

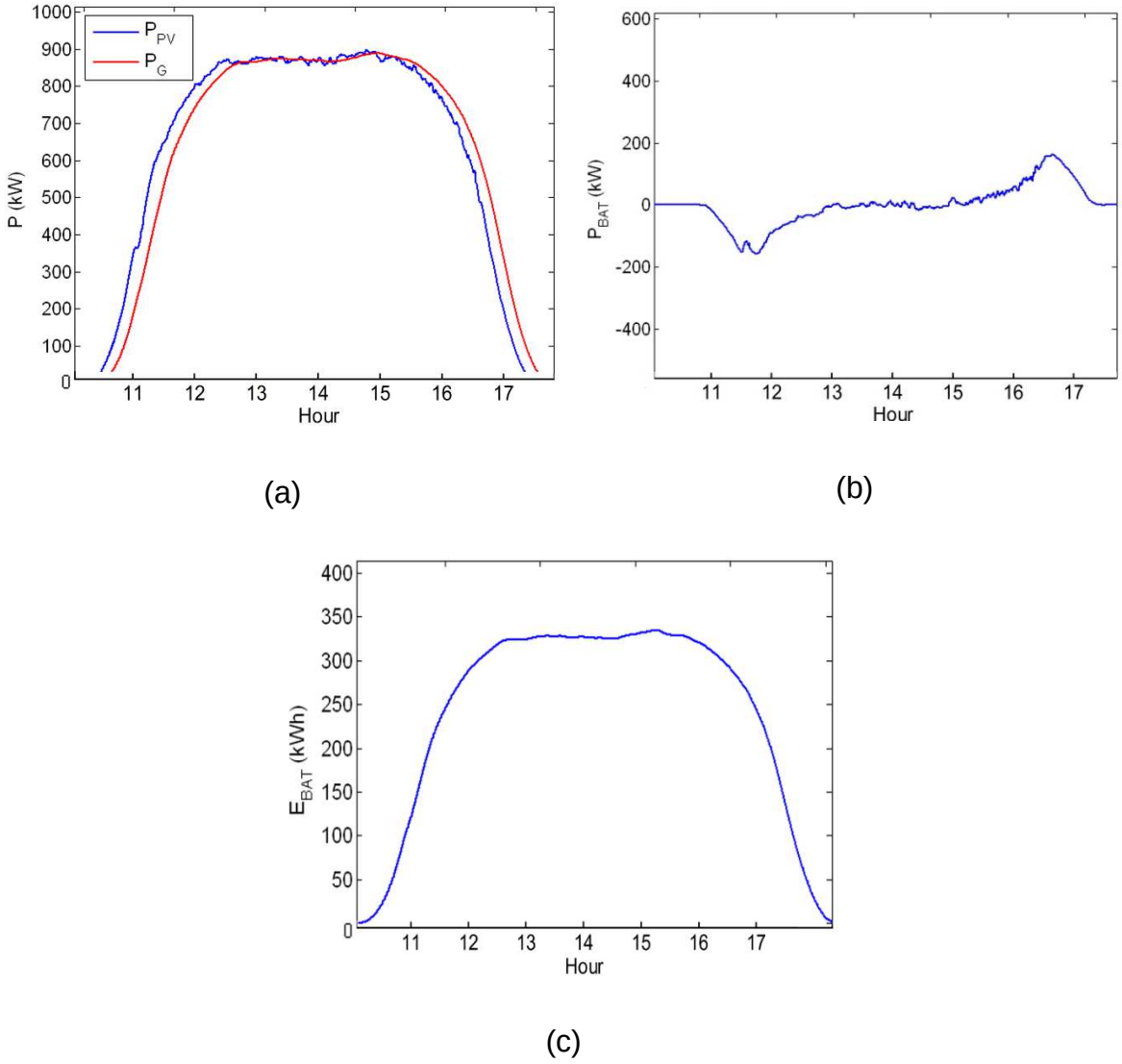

***Figure 3.17**: (a) Evolution of the generated power, $P_{PV}(t)$ during a clear sky day, 10 August 2011 by Section B (1.1 MW) and the simulated power which would be injected to the grid $P_G(t)$ under the moving average strategy (T = 2700 s); (b) battery power, P_{BAT}; and (**c**) battery energy, E_{BAT}.*

➢ Selection of Time Window T for the Moving-Average Strategy

Up to now, the *T* value required to limit the fluctuations to below the r_{max} limit is not known. This chapter provides an answer to this question. To do so, this strategy has been simulated for all the 5 s data over one year (2012) and for all the Moura PV plant sections (0.55–38.5 MW). For a given value of r_{max} successive iterations were made, increasing the duration of *T* (with a 60 s interval) until the condition $|\Delta P_{\Delta t}(t)| < r_{max}$ was met. **Figure 3.18** shows the relationship between the resulting time window *T* and the maximum allowable ramp r_{max}, with the PV plant power output as a parameter. As can

be seen, time window T is solely dependent on $r_{max,}$ and not on the size of the PV plant, P_n which is the reason why in **Figure 3.18** all the curves are superimposed. The evolution of these values, calls for making a fit based on function $T = m \cdot r_{max}^{-1}$, resulting in Eq.(3.17):

$$T = \frac{5400}{r_{\max}} \ (s) \qquad \textbf{(3.17)}$$

where r_{max} is given in (%/min), and m = 5400 (s·%/min). The goodness of fit (R^2 = 0.99) confirms the validity of the Eq.(3.17).

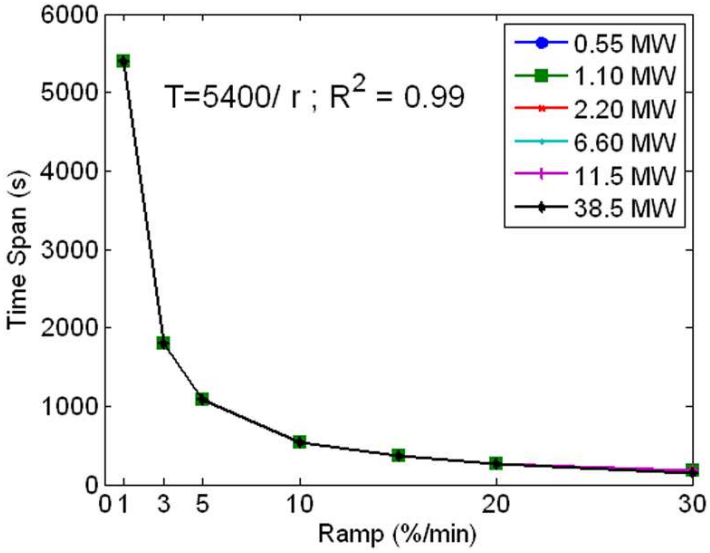

***Figure 3.18**: Relationship between the size of the power plant P_n, the maximum allowable ramp, r_{max} and window T, Eq.(3.17)).*

3.6 STEP-RATE CONTROL STRATEGY

Logically, the specifications required for the ESS are the direct consequence of the standards and regulations to be applied. For example, the reference PREPA, 2012 requires the smoothing of fluctuations of a very short duration, exceeding 10%/min. Translated to another time scale, variations of 100% in 10 min are permitted, being the typical fluctuations of a PV system with no energy storage provisions (for ranges of 1–40 MW) as seen in section 3.2. For this reason, as has been shown in previous sections, very small storage times are required, of around 6 min. For other scenarios, such as

upna Universidad Pública de Navarra Nafarroako Unibertsitate Publikoa

CRE, 2014, storage becomes more important: for a maximum ramp of 2%/min (in other words 20% in 10 min) the required storage time is increased by up to 45 min (section 3.4.2). For these more severe constraints, it makes sense to seek strategies that optimize the ESS system. In this context, an innovative step-rate control strategy based on strict compliance with the maximum ramp constraint r_{max} for the defined time window (for example 10 min) is proposed here.The proposed strategy attenuates the fluctuations in that particular time window and higher. Below that magnitude (high frequencies) it can be taken advantage of the geographical dispersion of a group of PV plants which strongly smoothens the fastest fluctuations. Previous studies (Hoff and Perez, 2010; Lave et al., 2012; Marcos et al., 2012) have well proved that *N* PV plants dispersed and separated at least by a few kilometres (6 km is enough) smoothens out the high frequencies (below 10 min) proportionally with $\sqrt{N}$. *N* is understood to be sufficiently large to produce the necessary smoothing effect in order to mitigate the effect of these steps. Therefore, the step-control strategy is coherent in a scenario with a number *N* of dispersed multi-MW PV-ESS plants, in which the step-control is implemented in each one, in the knowledge the TSO will see a reduction in the step effect simply due to geographical dispersion. Therefore, step control makes sense provided that the TSO permits strict compliance with r_{max} in the given time window. A detailed example of how this strategy works is shown in **Figure 3.19**, and it will be explained below.

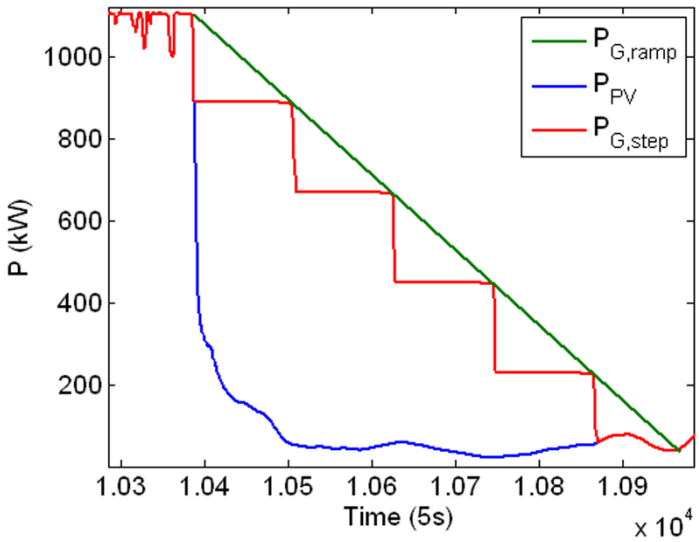

***Figure 3.19**: Evolution of the generated power, $P_{PV}(t)$ on 15 February 2012 by Section B (1.1 MW), the simulated power which would be injected to the grid $P_G(t)$ in the case of the availability of a battery which limits fluctuations to r_{max} of 20%/10min using the step-control strategy ($n = 120$, $n \cdot \Delta t = 600$ s) and the ramp rate control. The reduction of the storage required compared to the ramp control is evident and corresponds to the area between $P_{G,ramp}$ and $P_{G,step}$.*

The algorithm of this strategy is as follows (**Figure 3.20**): the first step is to decide whether the present evolution of the PV generation is positive or negative. Then, a check is made to determine whether the ramp condition is met in a previous time window with a duration of n times the sampling time Δt (5 s in this case). This entails strict compliance with the ramp condition for times that are equal to or higher than $n \cdot \Delta t$, but not below this value.

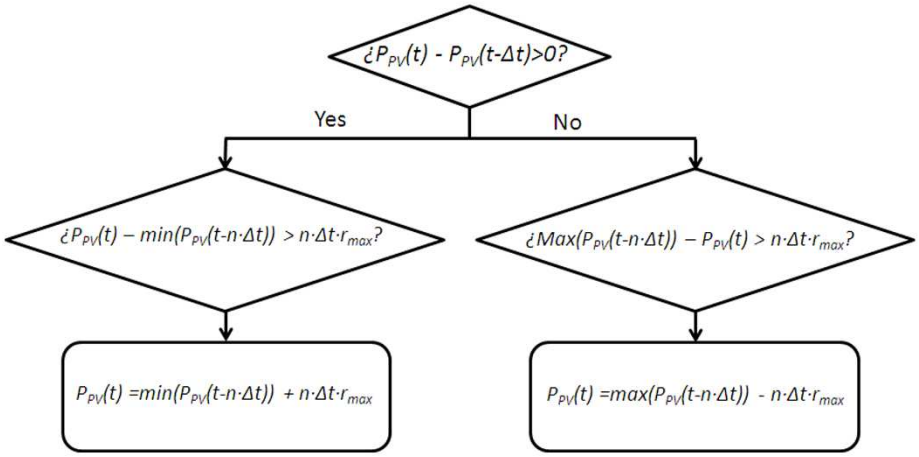

***Figure 3.20**: Flowchart of the step-rate control.*

For example, for grid regulations evaluating the fluctuations every 10 min, this would mean that the fluctuations would need to be below r_{max} = 20%/10 min. For this case, it would be necessary to choose $n \cdot \Delta t$ = 10 min (n = 120 as Δt is equal to 5 s). **Figure 3.19** shows the ramp control response $P_{G,ramp}$ and that of the step-rate $P_{G,step}$ for a negative fluctuation recorded on 15 February 2012 at 14:25:10 am. Before the significant negative fluctuation (during the first instant in **Figure 3.19**), short and small fluctuations (high-frequency) can be seen. These fluctuations are lower than r_{max} (2%/min) evaluated in 10 min (20%), so step-control does not act. However, when a negative fluctuation of around 90% takes place in P_{PV}, step-control acts smoothing this fluctuation in P_G up to a 20% value. From an energetic point of view, thanks to the ESS, the power injected by the PV plant $P_{G,step}$ evolved from 100% to 10% in 40 min, similarly to ramp-rate control, $P_{G,ramp}$. The only difference between $P_{G,ramp}$ and $P_{G,step}$ are the steps, fast fluctuations below 10 min. This high frequency will be strongly smoothed by geographical dispersion as it has been well proved in Hoff and Perez, 2010; Lave et al., 2012; Marcos et al., 2012, and then, going unnoticed for the TSO.

upna Universidad Pública de Navarra Nafarroako Unibertsitate Publikoa

The area within $P_{G,ramp}$ and $P_{G,step}$ corresponds to the necessary battery reduction. Logically, the higher the $n \cdot \Delta t$ value, the less battery required. To prevent the constant battery discharge, this strategy also requires the same SOC control proposed for the ramp strategy (**Figure 3.8**).

Once more, determining the capacity needed by this strategy can be easy solved thanks to the worst fluctuation model (**Figure 3.21**). The energy saving for a power plant P_n using the step-rate strategy instead of the ramp-rate, $E_{step\text{-}ramp}$, (kW·h) is the integral of the difference between $P_{G,ramp}(t)$ and $P_{G,step}(t)$, or, in other words, the total area of each of the triangles N_{tri} of **Figure 3.21**, in other words, Eq.(3.18):

$$E_{step-ramp} = \frac{1}{3600}\left[N_{tri} \cdot A_{tri}\right] = \frac{1}{3600}\left[\frac{90}{r_{max}} \cdot \frac{1}{2}(n \cdot \Delta t)\frac{P_n r_{max}}{100}\right] = \frac{0.45 P_n}{3600}(n \cdot \Delta t) \qquad \textbf{(3.18)}$$

where P_n is expressed in (kW), and $n \cdot \Delta t$ in (s). For example, for P_n = 1.1 MW (τ = 6.14 s) and r_{max} = 20%/10 min, Eq. (3.10) gives $E_{BAT,ramp}$ = 373 kW·h. From Eq. (3.18), with $n \cdot \Delta t$ = 600 s the saving $E_{step\text{-}ramp}$ is equal to 82.5 kW·h, that is 22%. As can be observed, this percentage is independent of r_{max} and the PV plant size (or, in other words, τ).

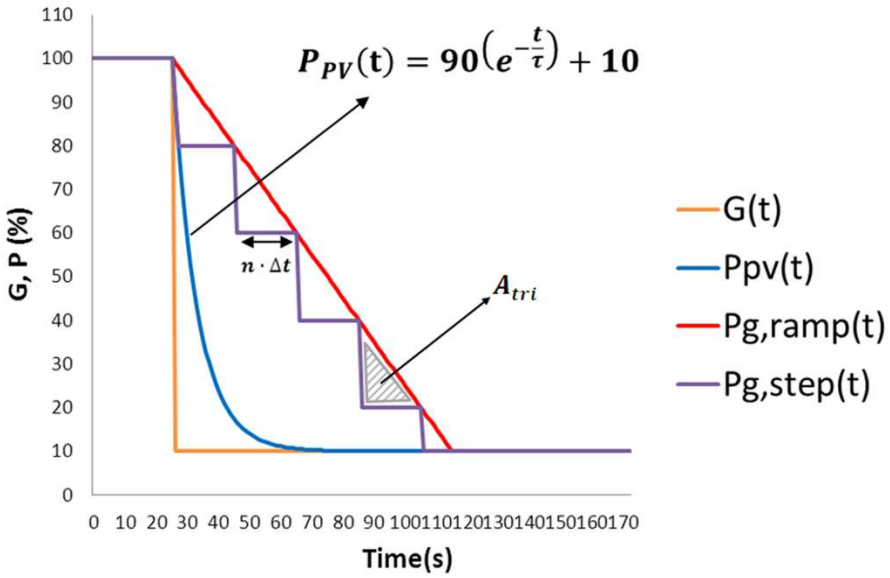

***Figure 3.21**: Model to calculate the storage capacity required for the worst fluctuation and step-rate strategy via $E_{BAT,ramp}$.*

By way of example, **Figure 3.22** again shows the results of simulating this strategy for 15 February and with r_{max} = 20%/10 min (2%/min). For this strategy and according to Eq. (3.18), C_{BAT} needed to smooth the worst fluctuation is equal to 582 kW·h, so $E_{BAT,ref}$ = 291 kW·h. For that given day, the required battery power is $P_{BAT,MAX}$ = 879 kW (or $P_{BAT,MAX}$ = 0.79 P_n) and the required effective battery capacity is C_{BAT} = $E_{BAT,MAX}$ − $E_{BAT,MIN}$ = 312 kWh (or 17 min of storage equivalent to 0.28 h). Obviously, P_G is more fluctuating than in the case of step-rate control, but the stress in the ESS and capacity needed are lower. The steps produced in P_G by this strategy can be better seen in **Figure 3.19**, which is precisely an enlarged version of **Figure 3.22 (a)**.

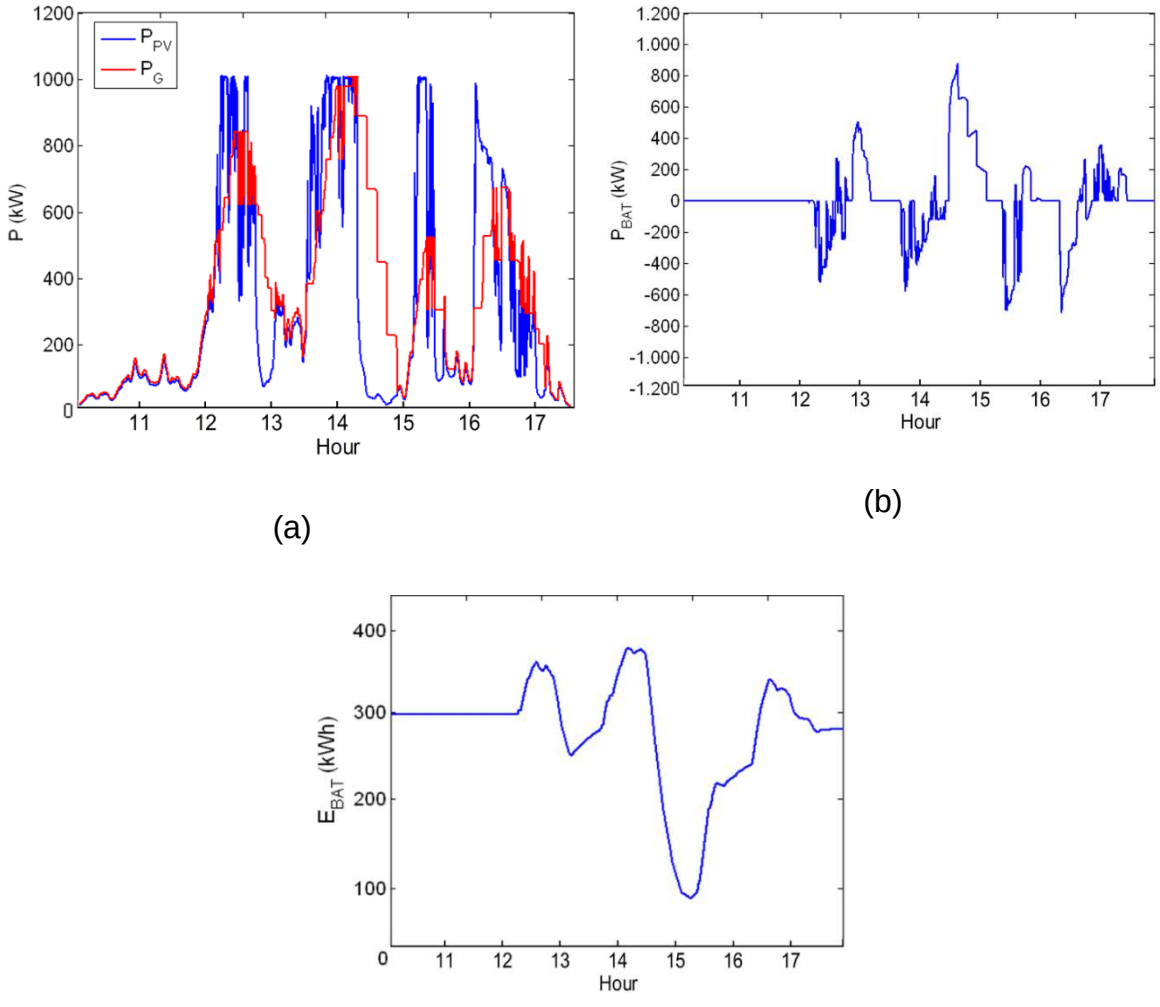

***Figure 3.22**: (**a**) Evolution of the generated power, $P_{PV}(t)$ on 15 February 2012 and the simulated power which would be injected to the grid $P_G(t)$ under the step-rate strategy (n = 120, n·Δt = 600 s), limiting fluctuations to r_{max} of 20%/10 min; (**b**) battery power, P_{BAT}; and (**c**) battery energy, E_{BAT}. The simulation has been made based on the model shown in **Figure 3.8**.*

3.7 A COMPARISON OF THE SMOOTHING STRATEGIES

These three strategies were simulated for 5 s data for one year (2012) and for all the Amareleja PV plant sections (from 0.55 MW to 38.5 MW), with a ramp restriction of r_{MAX} = 2%/min (20%/10 min for the step-control), a similar restriction imposed by CRE, 2014. For the average moving strategy, this restriction requires a minimum T of 2700 s, according to Eq. (3.17 **)**. For the step-rate control, n = 120 (120 × 5 s = 10 min). It should be pointed out that the SOC was calculated on the effective storage capacity C_{BAT}, thereby allowing 100% variations in the SOC (effective SOC). As a result of this, in the case of the ramp control and the step rate control, the reference SOC is 50% whilst, for the moving average, the battery starts and ends each day fully discharged (SOC = 0%). The indices of merit selected to compare the strategies are the effective storage time t_{bat}, the storage system losses, the degradation due to cycling and the quality of the wave injected into the grid.

3.7.1 Effective Storage Time, t_{bat}

As shown above, the difference in the storage capacity required for the different strategies depends on the following factors: rated power output of the PV plant P_n and maximum allowable ramp r_{max}.. **Figure 3.23** shows the storage time required, t_{BAT}, for each strategy, based on the size of the PV plant. This parameter was calculated after annual simulation, as the difference between the maximum and minimum annual energy value in the battery, $E_{BAT,MAX} - E_{BAT,MIN}$ divided between the rated power output P_n of the PV system.

upna Universidad Pública de Navarra Nafarroako Unibertsitate Publikoa

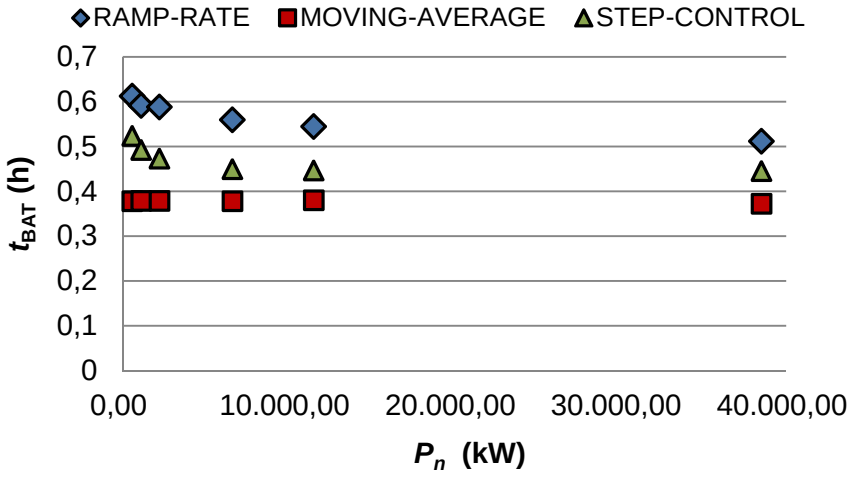

***Figure 3.23**: Storage time required, t_{BAT}, for each strategy, based on the size of the PV plant with a ramp restriction of r_{max} = 2%/min.*

The step-rate control requires an average 20% less storage than the ramp-rate control (the greater the value of parameter $n \cdot \Delta t$, the less battery required). Clearly, the MA strategy requires the smallest battery capacity. However, this strategy does not benefit from the fluctuation smoothing due to the size of the PV plant, as shown in Eq.(3.10), unlike the ramp-rate and step-rate control strategies (section 3.4). The best way to demonstrate this is **Figure 3.24**. It shows the relationship $C_{BAT,ramp}/C_{BAT,MA}$, constructed from Eq.(3.11) and (3.16) for different values of r_{max} and P_n. As r_{max} and P_n increases, $C_{BAT,ramp}/C_{BAT,MA}$ decreases. In any case, for restrictions around 2%/min, approximately half an hour of storage is sufficient to smooth the fluctuations.

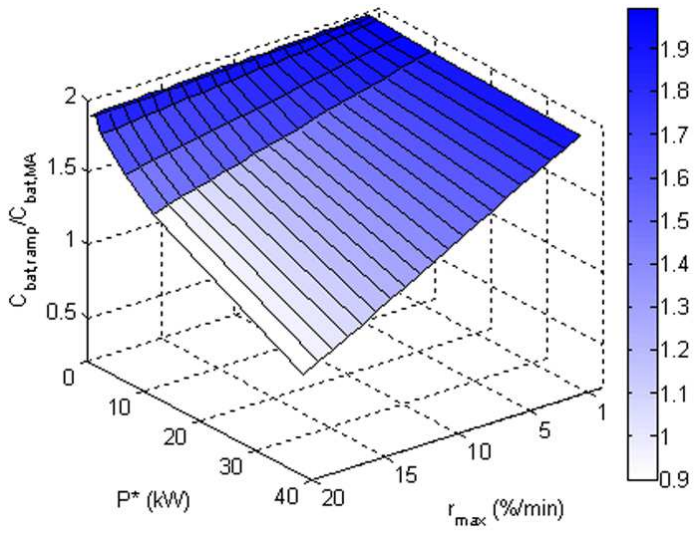

***Figure 3.24**: Relation $C_{BAT,ramp}/C_{BAT,MA}$ based on the PV plant size P_n and the maximum permitted ramp r_{max}.*

upna Universidad Pública de Navarra Nafarroako Unibertsitate Publikoa

3.7.2 Losses in the Storage System

Figure 3.25 shows the total energy loss in the ESS (PEC and battery) for r_{max} = 2%/min, expressed as a fraction of the annual production, based on the PV plant size. As can be seen, the losses for the moving average strategy are considerably higher than those for the other two strategies (2–3 times more). The reason lies in the fact that this strategy must act every day, regardless of whether there are any fluctuations or not, whilst the rate control strategies only act in the event of fluctuations greater than r_{max}. Moving average losses are considerably higher than for ramp-rate control. Note that in this new perspective, step-control would not proceed, because it allows fluctuations of 100%/10 min. In any case, it should be highlighted that the losses are small for all strategies (<1.4% in the worst case).

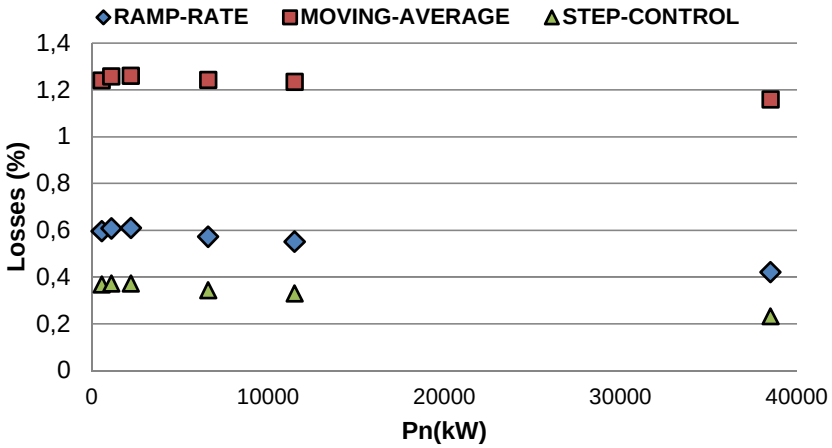

***Figure 3.25**: Losses at the PEC and battery, based on the size of the PV plant considered and the fluctuation smoothing strategy, with a ramp restriction of r_{max} = 2%/min.*

3.7.3 Stress in the Storage System

Figure 3.26 shows the histogram for the annual effective SOC of the storage system for each of the strategies simulated in Section B (1.1 MW, **Figure 2.1**). As can be seen, the SOC distribution for the ramp-rate and step-rate strategies is very similar, being derived from the same algorithm: the control guarantees at all times that the effective SOC is maintained at around 50%, only moving away from this reference value when significant fluctuations occur (charges and discharges to 50%). These situations are extremely rare, consistent with the annual distribution of fluctuations already seen in

upna Universidad Pública de Navarra Nafarroako Unibertsitate Publikoa

Marcos et al., 2011a. However, the SOC distribution for the MA is clearly bimodal, and is quite different from the rate-control strategies. Each day the battery undergoes a complete charge-discharge cycle (100% charge and discharge) with the maximum battery energy achieved at around midday, with full discharge at the end of the day, remaining in this state for the entire night. This explains the frequent SOC values close to 0% and 100%.

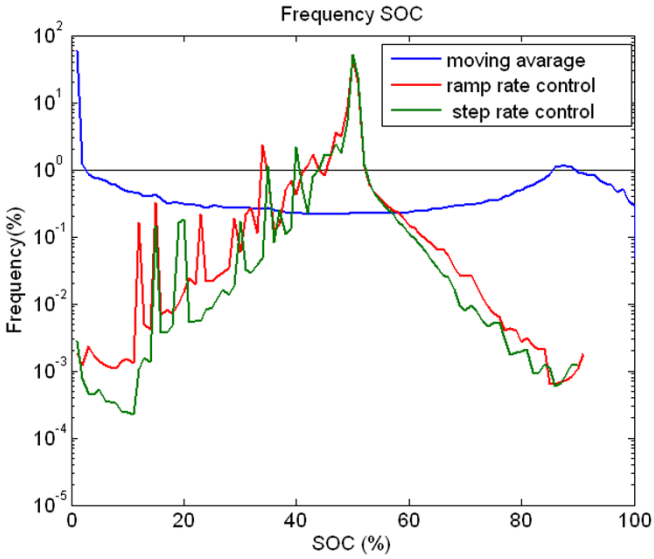

***Figure 3.26**: Histogram for the effective SOC in the storage system resulting from the simulation of the ramp-rate, MA and step-rate strategies for r_{max} = 2%/min. Note that the y-axis is logarithmically scaled.*

However, **Figure 3.26** is insufficient to determine the extent of the storage system degradation due to cycling. This is largely dependent on the number of N_{cicl} cycles and the depth of discharge (*DOD*). However, considering an annual effective SOC profile, such as those obtained in these simulations, there are methods to determine both parameters. One of the most-used algorithms and which provides the best results is Rainflow-counting (Matsuishi, M. & Endo, 1968). Initially developed to calculate mechanical fatigue (Hund et al., 2010), this method has also proved to be equally valid for calculating the ESS ageing due to cycling (Datta et al., 2011; Dufo-López et al., 2014, 2007; Gee et al., 2013; Schaltz et al., 2009). In this way, any complex charging and discharging series can be broken down into a series of simple sub-cycles with a given *DOD*. The methodology followed in this document is similar to that shown in Dufo-López et al., 2014.

upna Universidad Pública de Navarra Nafarroako Unibertsitate Publikoa

Figure 3.27 shows the result of applying the Rainflow-counting algorithm to the annual effective SOC for the various strategies and Section B (1.1 MW, **Figure 2.1**), for r_{max} = 2%/min and 10%/min. The figure shows the number of cycles N_{cicl} occurring (*y* axis) and the *DOD* (*x* axis). For the moving average strategy the ESS performs more cycles and with depths of discharge which are practically double those of the other strategies.

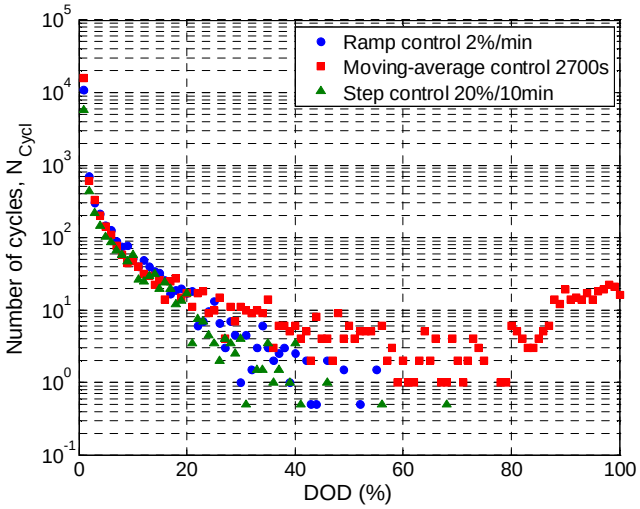

***Figure 3.27**: The number of observed cycles at a given depth of discharge (DOD) for the strategies presented in this study, for a maximum ramp limitation of r_{max} = 2%/min in Section B (1.1 MW). Note that the y axis is logarithmically scaled.*

Once these curves have been obtained, the calculation of the annual degradation due to cycling is immediate. Assuming again that the ESS under study is a lithium ion battery, with a life cycle curve similar to that shown in **Figure 3.28** (SAFT SA, 2008). This shows the number of maximum cycles N_{max} for a given *DOD*. It is possible to calculate the annual degradation due to cycling $C_{BAT,loss}$ as the sum of each individual degradation to a given *DOD*, in other words the relationship between the number of annual cycles observed N_{cycl}, and the number of maximum possible cycles $N_{cycl,max}$, is given in Eq.(3.19 **)**:

$$C_{\mathrm{BAT,loss}} = \sum_{DOD=1}^{100} \frac{N_{\mathrm{cycl},i}}{N_{\mathrm{max},i}} \cdot 100 \quad (\%) \qquad \textbf{(3.19)}$$

upna Universidad Pública de Navarra Nafarroako Unibertsitate Publikoa

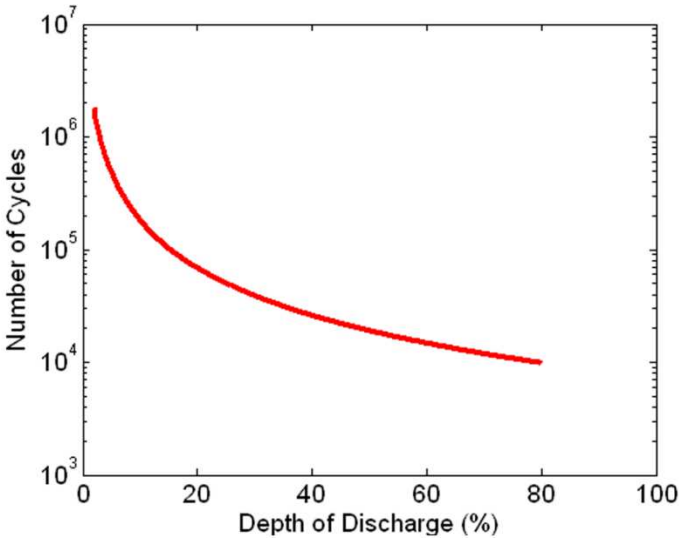

***Figure 3.28**: Life cycle curve at 25 °C, N_{max} vs. DOD, for a lithium ion battery made by SAFT. Reproduced with permission from [34]. Copyright © SAFT 2014.*

The results obtained by Eq.(3.19 **)** show the degradation solely due to the effect of the ESS cycling. However, additional effects exist which are not going to be taken into account and which affect service life, such as operating temperature. The method applied here for lithium batteries is also valid for any other storage technology, simply by knowing the ESS life cycle curve (**Figure 3.29**). The results of applying Eq.(3.19 **)** to the values of applying Eq.(3.19 **)** to the values of **Figure 3.27** are equal to 1%, 11.09% and 0.6% for ramp-rate, MA and step-rate respectively. Given the fact that the manufacturer does not permit *DOD* values greater than 80%, the data in **Figure 3.27 (a)** have been re-scaled to correspond to a *DOD* of between 0% and 80%.

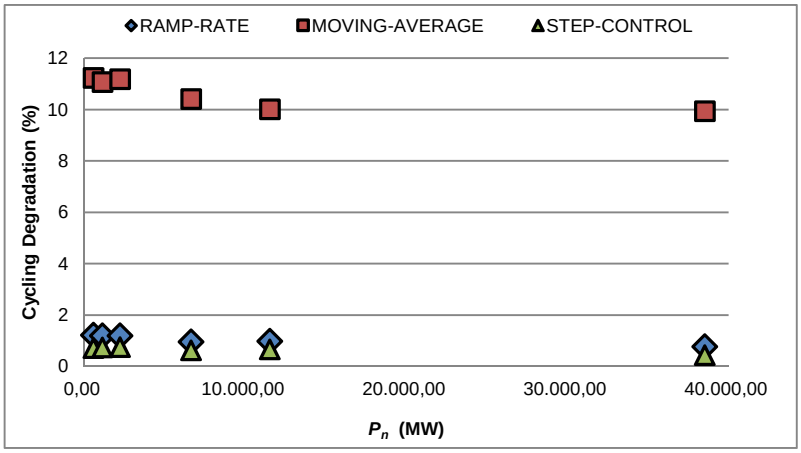

***Figure 3.29**: Annual degradation of the ESS due to cycling for r_{max} = 2%/min for all strategies and based on the PV plant size.*

This calculation methodology can be repeated for all the sections of the Amareleja plant observing the cycling degradation based on P_n and the strategy considered (**Figure 3.29**). The ramp-rate and step-rate control strategies show a very low cycling degradation (0.5%–2%) which hardly affects the useful life of the battery, unlike the moving average strategy with a degradation of around 10 times greater. As can be seen, the step-control cycling degradation is in any case lower than that of the ramp-rate.

Recently, in order to avoid the daily MA cycling Perez and Hoff, 2013 proposed to base the MA on the daily clear sky output ratio. Even so, it needs to resolve practical points such as control of the SOC (for example, how a midday negative fluctuation would be covered if the battery is discharged) or how to avoid constant discharge due to losses in the conversion elements. Likewise, it points out how forecasts can, to a large extent, help anticipate fluctuations and optimize the storage required and, in fact, the reference Perez and Hoff, 2013 discussed the improvement obtained with a perfect forecast, although how to face a situation in which the forecast fails has not been properly resolved.

3.7.4 Quality of the Signal Injected into the Grid

Figure 3.30 shows P_G frequency spectrum for all the data for one year for Section B (1.1 MW) (**Figure 2.1**) and for each of the strategies proposed in this chapter. The methodology followed is identical to that presented in Apt, 2007; Marcos et al., 2011b. Basically, the method consists in applying the discrete Fourier transform (DFT) to variable P_G over an entire year, previously normalized (using P_n), computed by a fast Fourier transform (FFT) algorithm. As can be observed, the three strategies analysed offer a similar cut-off filtering frequency of around 0.2 mHz (1.4 h), smoothing higher dynamics, particularly the MA strategy. However, it can be observed how the effect of the step-rate control filtering is reduced after frequencies close to 10 min (1.2 mHz), allowing faster dynamics to pass through and, therefore, injecting poorer quality power into the grid. However, this faster dynamics are easily reduced when taking into account the production of a PV fleet geographically dispersed, as it was demonstrated in Hoff and Perez, 2010; Marcos et al., 2012; Otani et al., 1997.

upna Universidad Pública de Navarra Nafarroako Unibertsitate Publikoa

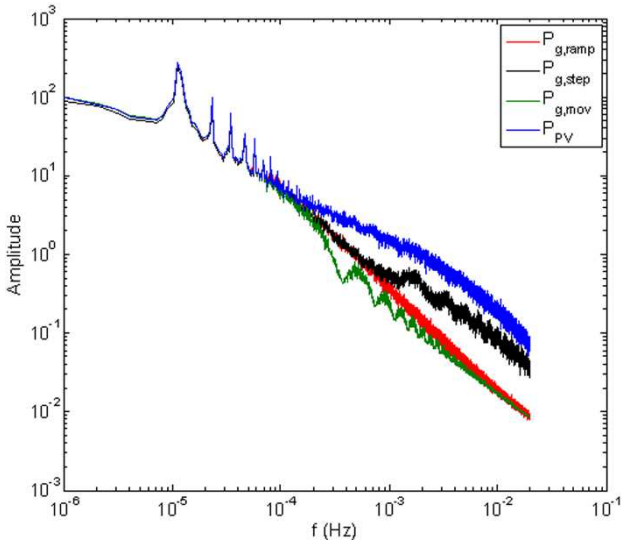

***Figure 3.30**: Spectrum for annual P_G resulting from the simulation of the three control strategies for the data for P_{PV} of Section B (P_n = 1.1 MW).*

3.8 CONCLUSIONS

In this chapter, the storage requirements needed to smooth short-term PV power fluctuations based on different control strategies and for a wide range of PV system power outputs has been quantified. The one-year simulation of the strategies has demonstrated that the MA strategy requires the least storage capacity. However, it is necessary to analyse for each particular case whether, firstly, this saving in size offsets the considerable increase in losses (2–3 times more) and, secondly, whether the storage technology is compatible with greater cycling (about 10 times more) and with SOC values close to zero for long periods of time. For example, for the case of lithium ion batteries, this strategy would have an extremely negative impact on the battery useful life, although this impact may be lower for ultra-capacitors or flow batteries (Luo et al., 2014). The new proposed strategy, namely the step-rate control, provides the most efficient use and with less ESS cycling in situations with several PV plants geographically dispersed and exigent ramp restrictions. Under less restrictive conditions, the ramp-rate control would be preferable against MA. Likewise, for a given grid restriction, an empirical expression is put forward to make it possible to determine the energy capacity required for each strategy.

It would be highlighted the lower losses achieved for the proposed system, particularly for the rate-control strategies (ageing due to cycling of around 1%/year–2%/year). This

upna Universidad Pública de Navarra Nafarroako Unibertsitate Publikoa

result draws attention to the potential use of the ESS for ancillary services (frequency regulation or time shifting), in an endeavour to maximize the value of its installation. To do so, a fluctuation prediction tool would be necessary, and this would need to be accurate enough to determine the critical times, in order to ensure the smart management of the energy stored.

upna Universidad Pública de Navarra Nafarroako Unibertsitate Publikoa

upna Universidad Pública de Navarra Nafarroako Unibertsitate Publikoa

4

ADVANCED CONTROL STRATEGIES TO USE THE MINIMUM ENERGY STORAGE REQUIREMENT FOR PV POWER RAMP-RATE CONTROL

"Look deep into nature, and then you will understand everything better."
Albert Einstein (1879-1955)

4.1 INTRODUCTION

As it has been commented in the previous chapter, one of the advantages of the moving-average control is the use of less ESS capacity at the expense of an energy increase through the ESS which implies higher losses and cycling degradation. On the other hand, the great advantage of the ramp-rate control is that only acts when the fluctuation exceeds the maximum allowable ramp-rate value, which implies lower cycling degradation. However, the main disadvantage of the latter control is that, as the sign of the first fluctuation is unknown, a double capacity battery was required to absorb both the upwards and downwards fluctuation setting the SOC reference at 50% (section 3.4.2). Considering the fact that this increased capacity involves high PV plant overheads, it therefore follows that a second control, making it possible not to double the storage system capacity, would be extremely useful. In this way, this new control would take advantage of both the less use of ESS capacity and the lower cycling degradation.

upna Universidad Pública de Navarra Nafarroako Unibertsitate Publikoa

In this chapter, two new strategies are proposed to make it possible to resolve this issue by improving the state of the art and halving the ESS requirements for the ramp-rate control strategy. For the first strategy, all the inverters are involved in the PV plant control, limiting their output in order to comply with a certain variation per minute during upward fluctuations. For the second strategy, the control is based on the two PV plant production limits: the maximum PV plant power which occurs under clear sky conditions ($P_{PV,Max}(t)$) and the minimum PV plant power which occurs with complete cloud cover ($P_{PV,Min}(t)$). Therefore, as a function of the instantaneous PV power, it is then possible to obtain the SOC needed to smooth out any potential fluctuations. These strategies have been successfully validated through real operational one year, 5 second PV power data at the 38.5 MW PV power plant at Moura (Portugal) (section 2.2). Finally, a comparison of all the strategies proposed in both this chapter and the previous one is made in terms of the performance and cyclability of the ESS.

4.2 RAMP-RATE CONTROL USING THE PV INVERTERS: $RR_{INVERTER}$

Let me refer to the ramp-rate control strategy already presented in section 3.4 as the classical ramp-rate control, $RR_{classical}$. One option to avoid doubling the battery required in $RR_{classical}$ is to limit the ramping-up events with the inverters. Although nothing can be done with the inverters during downward fluctuations, it is possible to limit the inverter operation at a point other than the maximum power point (MPP) making it possible to comply with a certain variation per minute during upward fluctuations. An implementation example can be found in Ruifeng and Saha, 2010. It is worth mentioning that despite the fact that the limitation is for the entire PV power of the plant under consideration, the upward ramp variation is going to be limited locally in each inverter because this is required by the PV plant architecture. In this way, the total PV power increase will be either less than or equal (in the worst case scenario), to the maximum variation per minute permitted in each inverter. In this case, the ESS is only needed during ramping down events and, consequently, the capacity needed will be half that required in Eq.(3.11). That is Eq.(4.1).

upna Universidad Pública de Navarra Nafarroako Unibertsitate Publikoa

$$C_{BAT,ramp,advanced} = \frac{0.9P_n}{3600}\left[\frac{90}{2 \cdot r_{MAX}} - \tau\right] \qquad (4.1)$$

Figure 4.1 shows the control scheme implemented for this technique. Although it is similar to the generic model used in the **Figure 3.8**, it does have some modifications. Firstly, the upward ramp variation of each inverter is limited to the desired value, r_{MAX}. In this way, the sum of the output power of all the inverters ($P_{PV,lim\ inverter}(t)$) is certain to ensure that the total power always complies with the desired maximum power variation during upward fluctuations. This means that it is only necessary to use a downhill limiter that is enabled in case of, Eq.(4.2).

$$\left[\frac{P_{PV}(t-\Delta t)}{P_N} - \Delta t \cdot r_{MAX}\right] > P_{PV}(t) \qquad (4.2)$$

where r_{MAX} is expressed in [%/min]. Again, the control scheme also includes a SOC control but in this case $E_{BAT,ref}$ will be the value corresponding to SOC =100%. Again, the control action is applied prior to the ramp-rate limiter to ensure that condition r_{MAX} is met at all times. To sum up, the upward fluctuations are limited at the inverters level whilst the downward fluctuations are limited by the ESS at the entire PV plant level. To evaluate this strategy, it will be taken K=1 which is the best relationship between speed and system stability for this case.

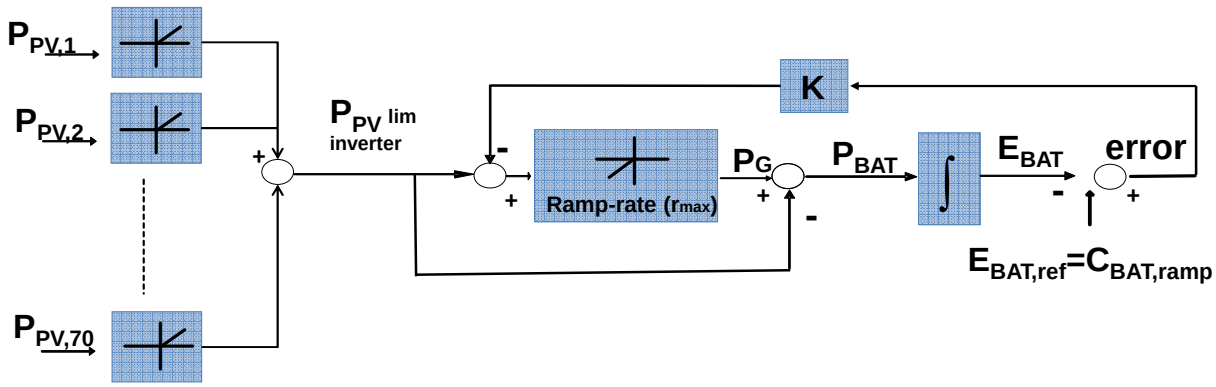

***Figure 4.1**: Ramp-rate control model modified with inverter SOC control.*

Figure 4.2 shows the response of the PV plant against an upward and downward fluctuation for r_{MAX}=2%/min. It should be noted that the SOC is calculated on the basis of Eq.(4.1) in this case. The blue line represents the total PV power available at MPP ($P_{PV,MPP}(t)$) whilst the green line represents the sum of the PV output power of the inverters, $P_{PV,lim\ inverter}(t)$, whose ramping-up variations have been limited. As can be seen, $P_{PV,lim\ inverter}(t)$ directly complies with the permitted variation (r_{MAX}=2%/min in this case) during the upward fluctuation. The black line is the power injected into the grid ($P_G(t)$) and the red line is the SOC of the ESS. Again, during the downward fluctuation, $P_G(t)$ complies with the limited value but with the back-up of the ESS. In this way, the ESS provides the energy necessary and its SOC decreases from 100% to almost 40%. It is worth noting that the differences between the blue line, $P_{PV,MPP}(t)$, and the green line, $P_{PV,lim\ inverter}(t)$, correspond to the energy losses due to the inverters limitations.

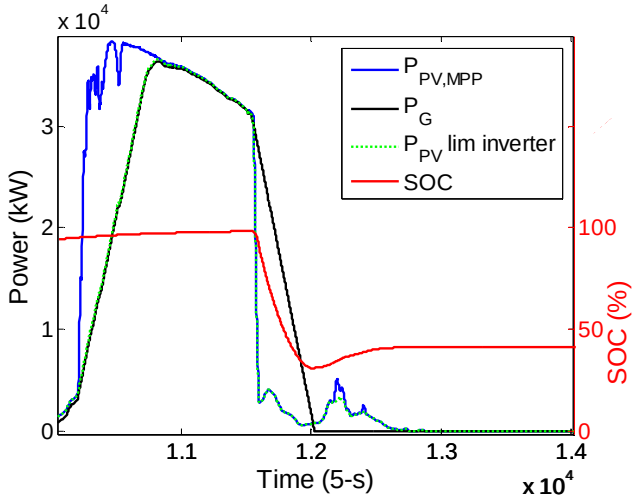

***Figure 4.2**: Response against an upward and downward fluctuation at the end of the day, 29th January 2012.*

Figure 4.3 shows the evolution of this new control during a day with extreme fluctuations (21st November 2012) with a maximum allowable ramp-rate value of 2%/min. In this figure, it can be seen that despite the strong fluctuations in $P_{PV}(t)$, the control response adequately complies with the ramp-rate value. According to Eq.(4.1), the minimum theoretical effective battery required is C_{BAT}=12279 kWh. For this particular day, SOC_{MAX} = 100% and SOC_{MIN}=39.30%. Thus, $C_{BAT,used} = E_{BAT,MAX}-E_{BAT,MIN}$ = 7453 kWh.

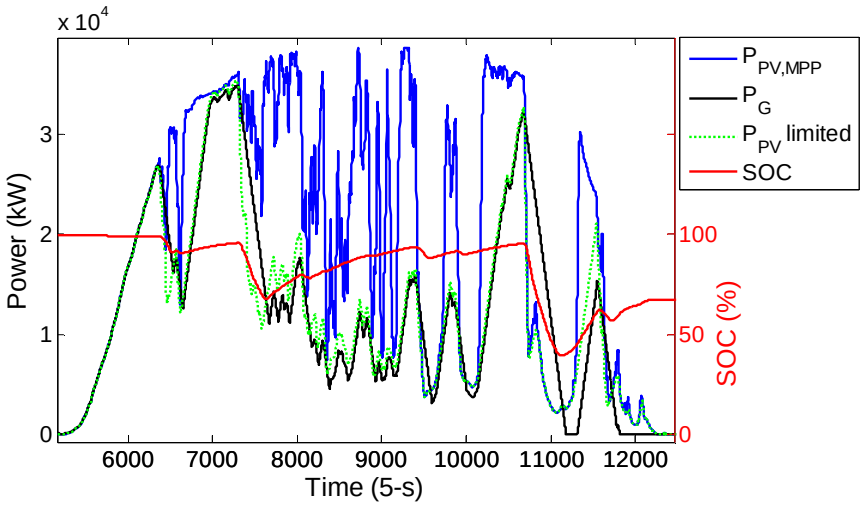

***Figure 4.3**: SOC control during 21st November 2012*

Note that this strategy halves the C_{BAT} required in $RR_{classical}$. On the other hand, the energy losses due to inverter limitation reach 36% of the total production of this day, quite a high value. Obviously, any other day with fewer fluctuations in the available power would have fewer losses caused by inverters limitations. The total losses for an entire operating year will be discussed later on.

4.3 RAMP-RATE CONTROL BASED ON THE PV POWER PLANT MODEL: $RR_{CLEAR-SKY}$

The second method proposed is to implement a SOC control based on the actual power given by the PV plant and its production limits. Despite the variable nature of solar radiation, it can be taken advantage of the fact that its limits are well known.

The instantaneous PV plant power generated, $P_{PV}(t)$, for specific values of irradiance, $G(t)$, and cell temperature, $T_c(t)$, can be easily estimated with a parametric model of the PV plant under consideration. It is possible to estimate at each moment, the PV plant production limits: the PV plant power under clear sky conditions, $P_{PV,Max}(t)$, and the PV plant power under totally cloudy sky conditions in which only the diffuse light reaches the PV arrays, $P_{PV,Min}(t)$. These powers represent both the maximum and minimum power that can occur at the PV plant at that moment in time. In this way, it is possible to calculate the maximum power variation that can take place, either positive or negative, from the instant power generated by the PV plant, $P_{PV}(t)$. So, as a function of

upna Universidad Pública de Navarra Nafarroako Unibertsitate Publikoa

the actual PV power, it is then possible to obtain the state of charge needed in order to either absorb or provide the necessary energy depending on the nature of the fluctuation, either upward or downward respectively. **Figure 4.4** shows the control diagram which is very similar to the one already used in section 3.4 and shown in **Figure 3.8** and **Figure 4.1**. The only difference is that, in this case, there is a new block that is able to calculate, through the measured cell temperature (T_c), the SOC value ($E_{BAT,ref}$) to allow the battery to provide sufficient power to cover a decrease in radiation or otherwise to absorb excess power.

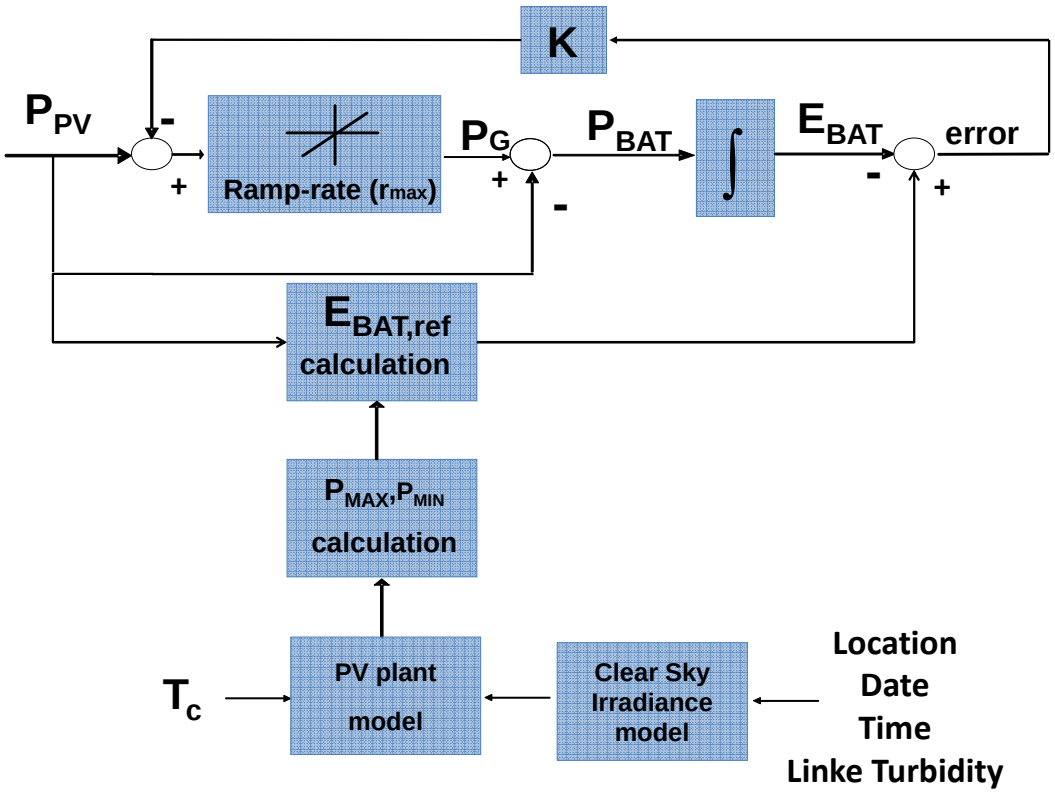

***Figure 4.4**: Ramp-rate control model for $RR_{clear\text{-}sky}$*

4.3.1 PV plant power production limits

The calculation of $P_{PV,Max}(t)$ corresponds to the calculation of the PV power under clear sky conditions. This power can be obtained through the following steps:

4.3.1.1 Clear sky irradiation model

The knowledge of the clear sky irradiance reaching the ground has been a key parameter in the field of solar radiation modelling and evaluation. As a result, many

empirical and physical models can be found in the literature (Bird and Hulstrom, 1980; Geiger et al., 2002; Gueymard, 1989; Kasten, 1980; Molineaux et al., 1998; Rigollier et al., 2000). Although, as will be seen later on, high accuracy is not required for the modelling of clear sky days for the goodness of the control, these models have been well validated and their performance on very clear condition measurements are within 4% in terms of standard deviation (Ineichen, 2006). For the purpose of this study, the model selection criteria must be based on both implementation simplicity and input parameter availability (Linke turbidity or aerosol optical depth). In this way, the clear sky model of the European Solar Radiation Atlas (ESRA) which only needs the Linke turbidity as an input parameter has been implemented (Rigollier et al., 2000). Monthly values of the Linke turbidity factor are sufficient for the purpose of this study and can be obtained from (SODA, n.d.)

In this model, the global horizontal irradiance for clear sky, $G_c(0)$, is split into the direct component, $B_c(0)$ and given by Eq.(4.3):

$$B_c(0) = B_0 \varepsilon_0 \sin\gamma_s \exp(-0.8662 T_L m \delta_R) \qquad \textbf{(4.3)}$$

where B_0 is the solar constant (1367 W·m^{-2}), ε_0 is the eccentricity correction; γ_s is the solar altitude angle (0° at sunrise and sunset); T_L is the Linke turbidity factor for an air mass equal to 2; m is the relative optical air mass; $\delta_R$is the integral Rayleigh optical thickness that depends on the precise optical path and hence on relative optical air mass, m, and its parameterization can be obtained in Kasten, 1996.

And the diffuse component, $Dc(0)$, given by Eq.(4.4):

$$D_c(0) = B_0 \varepsilon_0 T_{rd}(T_L) F_d(\gamma_s, T_L) \qquad \textbf{(4.4)}$$

In this equation, the diffuse radiation is expressed as the product of the diffuse transmission function at zenith (i.e. sun elevation 90°),T_{rd}, and diffuse angular function, F_d. Further information about the calculation of these parameters can be found in Rigollier et al., 2000.

upna Universidad Pública de Navarra Nafarroako Unibertsitate Publikoa

4.3.1.2 PV plant model

First of all, cell temperature, T_c, is required to calculate the PV module overheating losses. In this study, several temperature sensors have been recording data every 5 s. In case cell temperature sensors are not available, T_c can be calculated on the basis of ambient temperature (T_a), using the well-known Eq.(4.5):

$$T_C = T_A + \frac{NOCT - 20}{800} \cdot G_m \qquad \textbf{(4.5)}$$

where $NOCT$ is the nominal operation cell temperature obtained from the manufacturer datasheet, in °C, and G_m is the irradiance measured in the plane of the array, in $W \cdot m^{-2}$. Notice that in this case both an irradiance sensor and ambient temperature sensor are required.

Once both components of the global horizontal irradiance have been obtained, the radiation that reaches the PV generators must be calculated. To do so, the angle of incidence, β, and the PV generator orientation, α, at every instant in time must be calculated. All the expressions which allow these parameters for the main kinds of tracking systems can be found in Narvarte and Lorenzo, 2008.

Subsequently, based on the position of the PV generator, the radiation can be calculated in the plane of the generator, $G_c(\beta, \alpha)$. In order to obtain the value of the irradiance over an inclined plane, several models have been proposed (Hay and Mckay, 1985; Hay, J. E., Davis, 1980; Klucher, 1979; Lorenzo, 2011; Muneer, 1990; Perez et al., 1987; Reindl et al., 1990) which typically split the solar radiation in beam radiation, $B_c(\beta, \alpha)$; diffuse radiation, $D_c(\beta, \alpha)$; and reflected radiation, $R_c(\beta, \alpha)$. As was mentioned above, for the purpose of this application, as a great deal of precision is not required, any of the models proposed in the literature will be valid. In this case, the Hay-Davies model (Hay, J. E., Davis, 1980) was chosen. Further information about the parameters and equations implemented can be found in Hay, J. E., Davis, 1980; Lorenzo, 2011.

upna Universidad Pública de Navarra Nafarroako Unibertsitate Publikoa

Although the method is sufficiently accurate for the purpose of this study, it is worth noting that in order to improve the accuracy of the calculation, it is possible to take into account the deduction of power losses caused by shading (Martínez-Moreno et al., 2010), dirt and incidence (Martin and Ruiz, 2001) and spectrum (Ruiz, 1999).

The next step is to obtain the maximum output power ($P_{DC}(t)$) which is calculated using Eq.(4.6):

$$P_{DC}(t) = P^* \frac{G_c(t)}{G^*} \frac{\eta(t)}{\eta^*} \qquad \textbf{(4.6)}$$

where P^* is the maximum power under standard test conditions (STC, defined by a normal irradiance of G^*=1000W.m^{-2}, a cell temperature of T_C^*=25 °C, and AM1.5 spectrum), $\eta(t)$ is the efficiency as a function of the irradiance and cell temperature, T_c, and η^* is the efficiency under STC, $\eta^* = {P^*}/{A \cdot G^*}$ where A is the active area of the PV generator.

The simple implemented model, but with sufficient accuracy for the purpose of the study, only takes into account the dependence of efficiency with temperature (Eq.(4.7)):

$$\frac{\eta(t)}{\eta^*} = 1 + \gamma(T_C(t) - T_c^*) \qquad \textbf{(4.7)}$$

Finally, the inverter is characterized by its nominal output power (P_I) and three experimental parameters, (k_0, k_1 and k_2) used to calculate its power efficiency ($\eta_I(t)$) as it is shown in Jantsch et al., 1992 through Eq.(4.8):

$$\eta_I(t) = \frac{P_{AC}(t)}{P_{DC}(t)} = \frac{p_{ac}(t)}{p_{ac}(t) + (k_0 + k_1 p_{ac}(t) + k_2 p_{ac}^2(t))} \qquad \textbf{(4.8)}$$

where $p_{ac}(t)=P_{AC}(t)/P_I$ being P_{AC} the output AC power of the inverter and the mentioned parameters k_0, k_1 and k_2, which must be fitted either from the power efficiency curve

upna Universidad Pública de Navarra Nafarroako Unibertsitate Publikoa

provided by the inverter manufacturer or from experimental measurements (Muñoz et al., 2011).

4.3.1.3 $P_{PV,Max}(t)$ and $P_{PV,Min}(t)$ calculation

Once these parameters are known $P_{PV,Max}(t)$ is given by Eq.(4.9).

$$P_{PV,Max}(t) = P_{AC}(t) = P^* \frac{G_c(t)}{G^*}\left(1 + \gamma(T_C(t) - T_C^*)\right) \cdot \eta_I(t) \qquad \textbf{(4.9)}$$

And $P_{PV,Min}(t)$ corresponds to the power under maximum cloudiness conditions. A rough approach to define the cloudy day but good enough for the purpose of the control is to consider it as 10% of a clear day, which corresponds with the minimum diffuse radiation observed. In this way $P_{PV,Min}(t)$ is given by Eq.(4.10).

$$P_{PV,Min}(t) = 0.1 \cdot P_{PV,Max}(t) \qquad \textbf{(4.10)}$$

Note that any other losses, such as transformer and wiring losses, can be implemented to improve the accuracy of the calculation of $P_{PV,Max}(t)$ and $P_{PV,Min}(t)$. By way of example, **Figure 4.5** shows these limits and the real PV power, $P_{PV}(t)$, for the 21st November 2012.

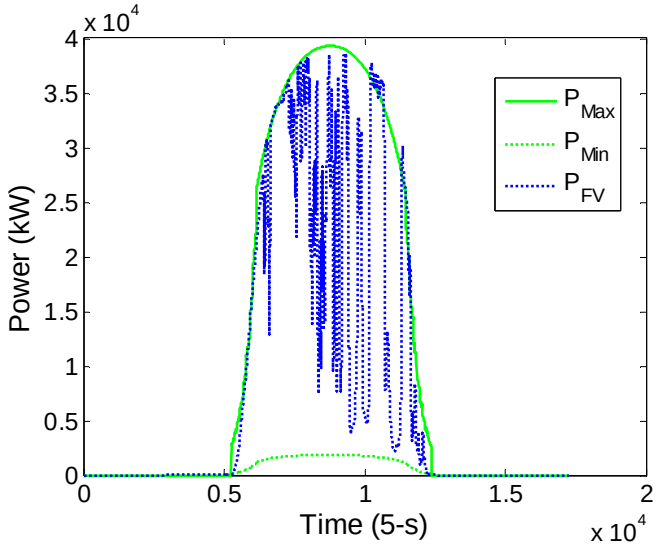

***Figure 4.5**: P Max and P Min limits for the 21st November 2012*

Note that there are some points in which $P_{PV}(t)$ exceeds the $P_{PV,Max}(t)$ limit modelled. This is because, on a day with scattered clouds, there may be some reflections between the radiation that reaches the ground and the clouds that cause these values to be slightly above normal. In any case, these are individual cases that do not affect the proper functioning of the application. On the other hand, it can be seen that $P_{PV,Max}(t)$ at the beginning and end of the day does not behave as a perfect bell curve as was to be expected. This is because the model is taking into account the shade losses of the PV plant in order to get a more precise result, although this is not necessary.

4.3.2 SOC reference calculation

Considering the fact that both the maximum and minimum power limits are well-known, it makes sense to implement a SOC control which takes into account these two limits. It is possible to control the SOC reference of the ESS depending on the nature of the day under consideration. In other words, it is possible to control the SOC of the battery close to 100% on a clear day and with the PV plant in full operation, given the fact that the only event that could possibly occur is a downward fluctuation, which will be mitigated by providing energy from the ESS. Whilst, on a cloudy day with the PV plant operating under diffuse irradiance with low power the ESS will be at a low state of charge in order to absorb the only possible upward fluctuation that could occur. Any other intermediate state of production will imply a SOC reference that will be variable as a function of the actual weather conditions. To evaluate this strategy, it will be taken K=6.

Figure 4.6 shows the capacity required at a time close to midday on the 21st November 2012 in order to correctly absorb both any potential upward and downward fluctuations. Note that, on one hand, the available capacity required for discharging in the event of the maximum possible downward fluctuation ($C_{BAT,d}$) is the energy storage that needs to be injected into the grid in order to mitigate this fluctuation. On the other hand, the capacity required to charge in the event of the maximum upward fluctuation ($C_{BAT,c}$) is the difference required in the ESS to absorb this fluctuation. $C_{BAT,d}$ and $C_{BAT,c}$ requirements are determined according to Eq.(4.1) and are expressed by Eq.(4.11) and Eq.(4.12).

upna Universidad Pública de Navarra Nafarroako Unibertsitate Publikoa

$$C_{BAT,d}(t) = \frac{0.9 \cdot \left(P_{PV}(t) - P_{Min}(t)\right)}{3600}\left[\frac{90}{2 \cdot r_{MAX}} - \tau\right] \qquad \textbf{(4.11)}$$

$$C_{BAT,c}(t) = \frac{0.9 \cdot \left(P_{Max}(t) - P_{PV}(t)\right)}{3600}\left[\frac{90}{2 \cdot r_{MAX}} - \tau\right] \qquad \textbf{(4.12)}$$

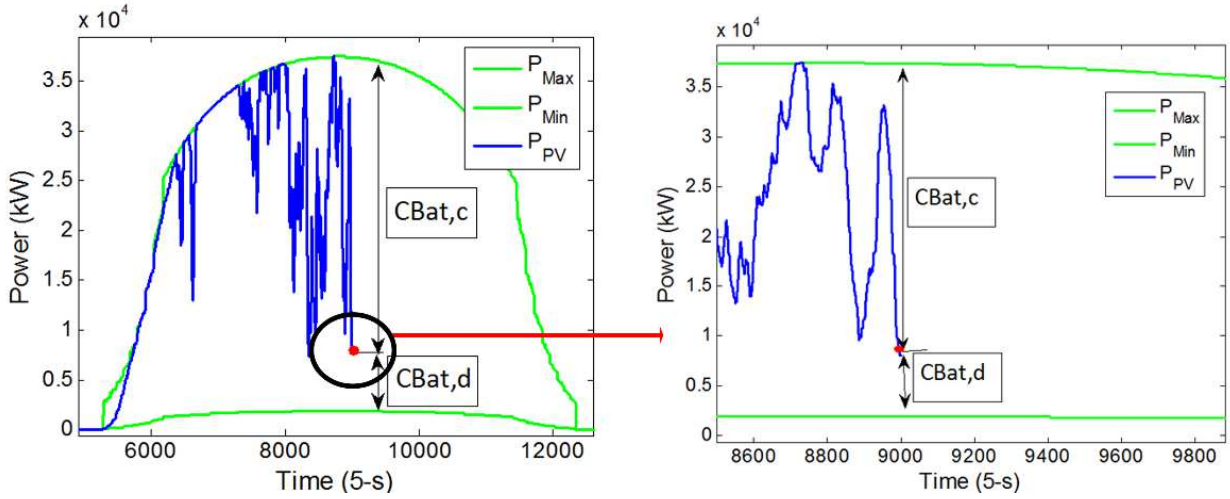

***Figure 4.6**: SOC control during an instant on 21st November 2012*

It is worth noting that when the PV plant is operating at any point close to midday, when $P_{PV,Max}(t) = P_N$, the sum $C_{BAT,d} + C_{BAT,c} = C_{BAT,ramp}$. This means there is only one SOC point which complies with the ramp limitation imposed. However, at any other time of day, the sum $C_{BAT,d} + C_{BAT,c} < C_{BAT,ramp}$, which means that not only is there a single point that meets the ramp limitation but an entire zone. If the SOC is within this zone, no modification will be required, a fact that makes it possible to reduce the ESS cycling degradation should this be necessary. This translates into the following control logic (Eq.(***4.13***)):

$$
\begin{aligned}
&if \quad E_{BAT}(t) < C_{BAT,d}(t) \\
&\quad E_{BAT,ref}(t) = C_{BAT,d}(t) \\
&elseif \quad C_{BAT,ramp,advanced} - E_{BAT}(t) < C_{BAT,c}(t) \\
&\quad E_{BAT,ref}(t) = C_{BAT,c}(t) \\
&else \\
&\quad E_{BAT,ref}(t) = E_{BAT,ref}(t-1) \\
&end
\end{aligned}
\qquad \textbf{(4.13)}
$$

As an example, **Figure 4.7** shows the evolution of the SOC control proposed during the fluctuations on the 21st November 2012. Despite the fluctuations recorded during the day, the strategy worked successfully. The SOC of the ESS was continuously adjusted to comply with both the ramp rate limitation implemented and any possible fluctuations that could take place. Furthermore, as mentioned above, at the beginning and end of the day when $E_{BAT}(t)$ values comply with the ramp rate limitation, so the SOC remains constant according to Eq.(4.13). As happened in $RR_{inverter}$, according to Eq.(4.1), the minimum theoretical effective battery required is C_{BAT}=12279 kWh. In this particular day, SOC_{MAX} = 88.84% and SOC_{MIN} = 21.43%. Thus, the effective capacity used in this day is $C_{BAT,used} = E_{BAT,MAX} - E_{BAT,MIN}$ = 8276 kWh. Again, this strategy allows to halve the C_{BAT} required in $RR_{classical}$.

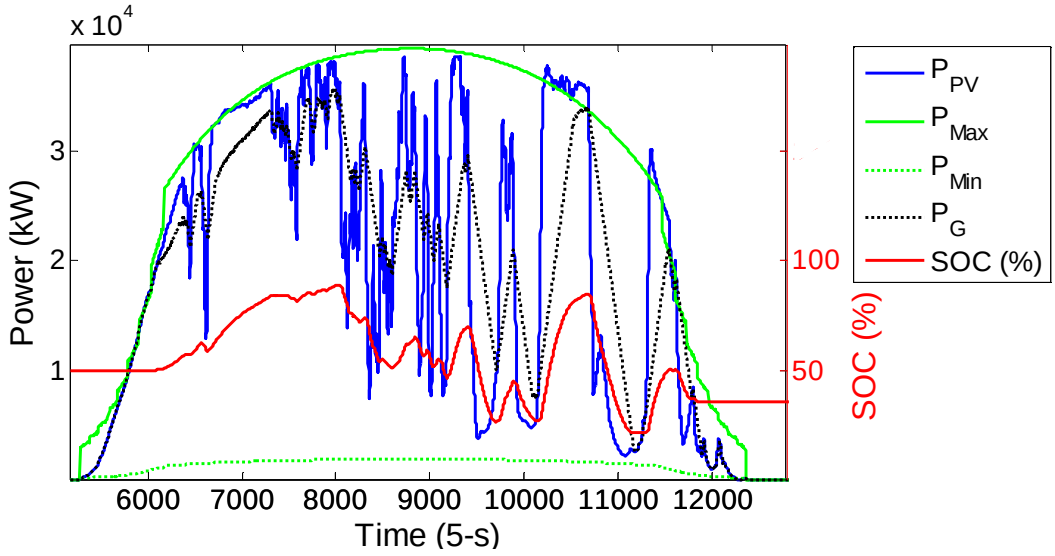

***Figure 4.7**: SOC control on the 21st November 2012*

Furthermore, **Figure 4.8** shows the evolution of the SOC during a clear day (26th August 2012) and a cloudy day (23rd November 2012). As was to be expected, during the clear day when $P_{PV}(t)$ is close to the $P_{PV,Max}(t)$ limit, once the SOC level of the ESS can provide enough energy to mitigate the only possible downward fluctuation, it remains constant. On the other hand, on a cloudy day, when the SOC level of the ESS is low enough to absorb the energy required to mitigate the only possible upward fluctuation, it also remains constant. Obviously, the lower the use of the ESS the lower the losses and the lower the ESS cycling degradation.

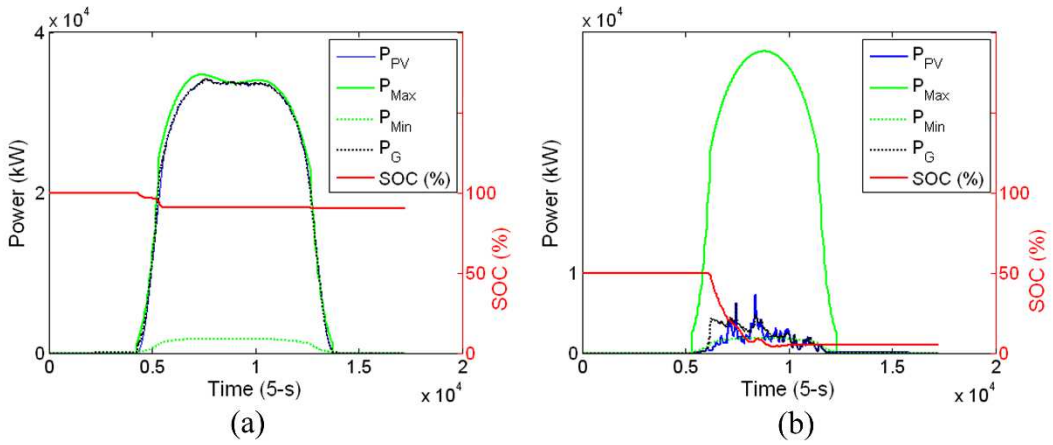

***Figure 4.8**: SOC control during (a) a clear day (26th August 2012) and (b) a cloudy day (23rd November 2012)*

4.4 EVALUATION OF RAMP-RATE CONTROLS OVER A ONE-YEAR SIMULATION PERIOD

The first ramp-rate control already proposed in section 3.4 and called $RR_{classical}$, and the two new strategies proposed in this chapter have been simulated for 5 s power outputs over the course of one year (2012) at the 38.5 MW Moura PV plant for a maximum allowable ramp-rate limitation of r_{MAX}=2%/min which is a similar restriction to that imposed by CRE, 2014. It is worth noticing that the SOC of the ESS has been calculated based on the theoretical effective capacity $C_{BAT,ramp}$, thereby allowing 100% variation in the SOC (effective SOC). **Table 4.1** shows the indexes of merit selected to compare the strategies after the simulation.

***Table 4.1**: Results after 1 year simulation of real power output data at 38.5 MW Moura PV plant.*

Results	$RR_{classical}$	$RR_{inverter}$	$RR_{clear\text{-}sky}$
Theoretical Capacity $C_{BAT,ramp}$ (kWh)	24558 [Eq.(3.11)]	12279 [Eq.(4.1)]	12279 [Eq.(4.1)]
Effective Capacity Used $C_{BAT,ramp,used}$ (kWh)	23678	8711	11703
Energy through the ESS (% Total Production)	6.39	2.26	6.15
Inverter Limitation Losses (% Total Production)	-	9.09	-

Theoretical effective capacity, $C_{BAT,ramp}$, has been calculated on the basis of Eq.(3.11 ***)*** for $RR_{classical}$ and on the basis of Eq.(4.1) for $RR_{inverter}$ and $RR_{clear\text{-}sky}$ alike. On the one hand, taking **Table 4.1** into account, $C_{BAT,ramp}$ for the two new proposed strategies ($RR_{inverter}$ and $RR_{clear\text{-}sky}$) is half the capacity required in $RR_{classical}$. On the other hand, the effective capacity used, $C_{BAT,ramp,used}$, which is just $C_{BAT,ramp,used} = E_{BAT,MAX}\text{-}E_{BAT,MIN}$ throughout the whole year, in $RR_{classical}$ and $RR_{clear\text{-}sky}$ alike, is close to the theoretical value(<5%). However, $C_{BAT,ramp,used}$ in $RR_{inverter}$ is 30% lower than the theoretical value. This is because in this strategy $P_{PV,lim\ inverter}(t)$ is always equal or lower than $P_{PV}(t)$ due to the inverter limitation. In this way, the inverter limitation mainly acts during days with fluctuations and, as a result, $P_{PV,lim\ inverter}(t)$ never reaches $P_{PV}(t)$ as can be seen in **Figure 4.9**. Consequently, the effective capacity used, $C_{BAT,ramp,used}$, is lower than the theoretical. However, it could occur that being in a clear day close to the midday, a front of clouds appear and convert the clear day in a complete cloudy day instantaneously. In this case, the whole theoretical effective capacity will be needed.

upna Universidad Pública de Navarra Nafarroako Unibertsitate Publikoa

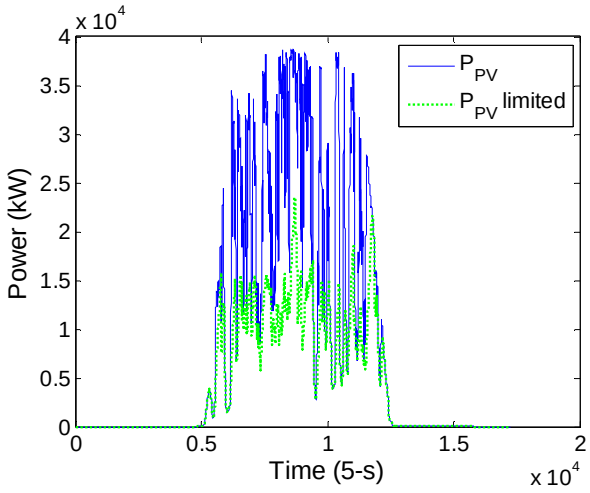

***Figure 4.9**: $P_{PV}(t)$ and $P_{PV,lim\ inverter}(t)$ limited for a very fluctuations day (31st October 2012). PV power at the output of the inverters, $P_{PV,lim\ inverter}(t)$, never reaches the original PV power, $P_{PV}(t)$.*

Figure 4.10 shows the effective SOC evolution for the whole year and for the three strategies analysed. In **Figure 4.10 (a)** it can be seen how for the $RR_{classical}$, the ESS is regulated by the SOC=50% with rises and falls throughout the year. The ESS is only used for a few days and the SOC is close to the limits 0% and 100%. In **Figure 4.10 (b)** the required theoretical effective capacity for $RR_{inverter}$ is half the required in $RR_{classical}$ and the SOC is regulated to the 100% of the charge because the ramping up events are limited by the inverters. There are few days in which the battery is discharged and SOC_{MIN} never get off below 30% because the inverter limitation makes that $P_{PV,lim\ inverter}(t)$ never reaches $P_{PV}(t)$ and the ramping down events that have to be smoothed are smaller than in the other strategies. In **Figure 4.10 (c)**, the required theoretical effective capacity for $RR_{clear\text{-}sky}$ is half the required in $RR_{classical}$ again. In addition, the SOC evolution shows that the ESS is much more used because it is continuously adjusting throughout the year depending on the climate conditions. There is not a constant SOC reference value.

upna Universidad Pública de Navarra Nafarroako Unibertsitate Publikoa

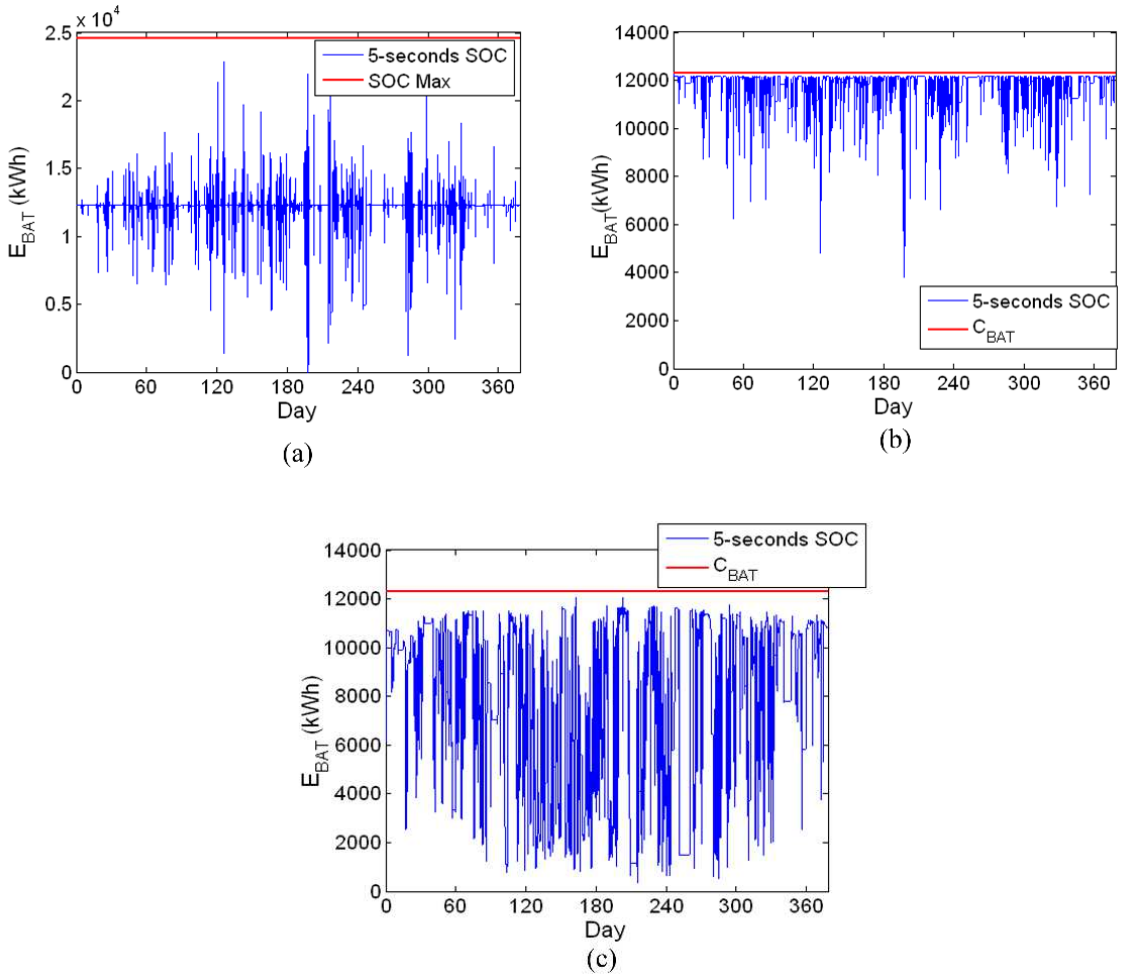

***Figure 4.10**: Annual effective 5-second SOC profile for the three strategies simulated: (a) $RR_{classical}$, (b) $RR_{inverter}$ and (c) $RR_{clear\text{-}sky}$. Note that the capacity required in $RR_{classical}$ is double the capacity required in $RR_{inverter}$ and $RR_{clear\text{-}sky}$.*

With regard to the energy supplied by the ESS, **Table 4.1** shows that, on the one hand, $RR_{classical}$ and $RR_{clear\text{-}sky}$ both make a similar use of the storage system at around 6%, whilst, on the other hand, the energy through the ESS in $RR_{inverter}$ is only 2.26%. In principle, this energy should be half the energy for $RR_{classical}$ and $RR_{clear\text{-}sky}$ because the ESS is only used for the ramping down events. However, as the inverter limitation makes that $P_{PV,lim\ inverter}(t)$ never reaches $P_{PV}(t)$, the ESS during the ramping down events is less used than in the other strategies and, consequently, the energy through the ESS is lower. In any case, it must be highlighted that this amount of energy for $RR_{classical}$ and $RR_{clear\text{-}sky}$ is relatively small in all cases (≈6%).

In spite of the fact that all the strategies work correctly based on the theoretical effective capacity, one of the main differences between them is that $RR_{inverter}$ entails

losses due to the inverter limitation. Taking **Table 4.1** into account, these losses reach 9% of the total production which is, a priori, an extremely high value in comparison with the other strategies which have no inverter losses. However, it is worth noting that the capacity required is half that needed in $RR_{classical}$.

4.5 CONCLUSIONS

The strategies presented in this chapter go far beyond the state of the art of the classical ramp-rate control and both the moving average and step control presented in chapter 3. By way of a summary, **Table 4.2** shows the main merit indexes seen throughout chapters 3 and 4 for all the strategies simulated for 5 s data over one year (2012) and for the 38.5 MW Amareleja PV plant section, with a ramp restriction of r_{MAX} = 2%/min (20%/10 min for the step-control), a similar restriction imposed by CRE, 2014. It is worth mentioning that for the two strategies proposed in this chapter, $RR_{inverter}$ and $RR_{clear\text{-}sky}$, in the same way as it was done in section 3.3, PEC losses are calculated through a real curve obtained from the Ingecon Sun Powermax® 1 MW (INGETEAM, 2014) connected to a 1MW transformer whose curve is shown in **Figure 3.3**; the ESS is supposed to be a lithium ion battery whose round-trip efficiency can be considered constant and equal to 95% (SAFT SA, 2008); and cycling degradation for this technology is calculated through a life cycle curve similar to that shown in **Figure 3.28** (SAFT SA, 2008).

***Table 4.2**: Summary results of all the strategies presented after 1 year simulation of real power output data at 38.5 MW Moura PV plant.*

Results	MA	$RR_{classical}$	Step	$RR_{inverter}$	$RR_{clear\text{-}sky}$
Capacity Required C_{BAT} (h)	0.36 [Eq.(3.16)]	0.64 [Eq.(3.11)]	0.56 [Eq.(3.11),(3.18)]	0.32 [Eq.(4.1)]	0.32 [Eq.(4.1)]
ESS Losses (% Total Production)	1.16	0.42	0.23	0.17	0.47
Inverter Limitation Losses (% Total Production)	-	-	-	9.09	-
Cycling Degradation (%)	9.94	0.78	0.44	1.36	2.56

The great advantage of $RR_{classical}$ already presented in the state of the art was that only acted when the fluctuation exceeded the maximum allowable ramp-rate value, a fact that implied low ESS losses (<0.5%) and cycling degradation (<1%). However, the main disadvantage was that, as the sign of the first fluctuation was unknown, a double capacity

upna Universidad Pública de Navarra Nafarroako Unibertsitate Publikoa

battery was required to absorb both the upwards and downwards fluctuation setting the SOC reference at 50%. The second strategy also analyzed in the state of the art is the moving average control, a strategy which is able to correctly operate with almost half the capacity (56%) required in $RR_{classical}$ but at the expense of an energy increase through the ESS which implied higher ESS losses (>1%) and cycling degradation (≈ 10%). Trying to reduce the capacity of the $RR_{classical}$ while maintaining the low ESS losses and cycling degradation rate, it was proposed the step control strategy (chapter 3) which was able to reduce the capacity based on the strictly compliance with the maximum ramp constraint r_{max} for the defined time window. The saving in the required capacity is 11.76% but with the sticking point of worsening the quality of the power injected into the grid.

Moreover, in order to reduce the capacity required, it was proposed the $RR_{inverter}$. Herein, the ramping-up events are limited with the inverters by making them to operate at a point other than the MPP making it possible to comply with a certain variation per minute during upward fluctuations. In this case, the ESS is only needed during ramping down events and, consequently, the capacity needed is half that required in $RR_{classical}$ whilst maintaining similar orders of magnitude regarding with ESS losses (<0.2%) and cycling degradation (<1.4%). The small increase in cycling degradation with respect to $RR_{classical}$ is due to the fact that the depth of discharges produced can reach the 100% while in $RR_{classical}$ the discharges only reach the 50%. The main disadvantage of this control is that it involves inverter limitation losses that reach to the 9.09% of the total production. Finally, the last strategy proposed was the $RR_{clear\text{-}sky}$ which as with $RR_{inverter}$ makes it possible to work with half the capacity required in $RR_{classical}$ but without any losses due to inverter limitation. It also has low ESS losses (<0.5%) but, as the ESS is used for both the upward and downward fluctuations, the ESS is more used, a fact that implies the inconvenience of doubling the cycling degradation (2.56%) of $RR_{inverter}$ but still remaining far from the moving average control value. In short, it is clear that both $RR_{inverter}$ and $RR_{clear\text{-}sky}$ are the best options when implementing a control strategy to comply with a maximum allowable ramp-rate limitation. However, the decision of choosing one strategy or another will be made depending on the ESS technology used. In this study, the ESS is supposed to be a lithium-ion battery which involves cycling degradation rates that make it necessary to do a cost analysis in order to choose the most cost-effective strategy. In case of installing a vanadium redox battery, which have

upna Universidad Pública de Navarra Nafarroako Unibertsitate Publikoa

an extremely large cycle life (Leadbetter and Swan, 2012), or ultra-capacitors (Luo et al., 2014), clearly the best strategy to implement would be $RR_{clear\text{-}sky}$.

Finally, it is worth mentioning that the step-control strategy has been only studied implementing it in the same way as the $RR_{classical}$. However, in a grid code framework which lets not to comply with the maximum ramp constraint r_{max} below the defined time window, this strategy could be implemented in a similar way as both the $RR_{inverter}$ and $RR_{clear\text{-}sky}$ using even less battery at the expense of worsening the quality of the power injected into the grid.

upna Universidad Pública de Navarra Nafarroako Unibertsitate Publikoa

5

GRID INTEGRATION OF A PV FLEET

"Coming together is a beginning; keeping together is progress; working together is success."
Henry Ford (1863-1947)

5.1 INTRODUCTION

Previous chapters 3 and 4 dealt with the problem of smoothing out PV power fluctuations at a PV plant level. It was shown that the higher the surface area considered, the smaller the fluctuations taking place and the lower the ESS capacity required. However, not only does the size of the PV plant serve as a natural means of smoothing fluctuations but different studies have also revealed that the geographical dispersion of PV plants produces a much smoother effect on the output power (Curtright and Apt, 2008; Hossain and Ali, 2014; Lave et al., 2012, 2011; Marcos et al., 2012; Murata and Otani, 1997; Otani et al., 1997; Perez et al., 2012; Sengupta and Keller, 2011; Wiemken et al., 2001). Taking advantage of this phenomenon, this chapter provides two tools in order to facilitate the grid integration of an aggregation of PV plants.

On the one hand, it is developed a first tool that enables transmission and distribution system operators to simulate the fluctuations of distributed PV power in electricity networks based on irradiance measurements. These simulated PV production profiles could prove extremely useful for the TSO and DSO, and even more so today when PV technology is gaining strength in distributed generation. Specifically, it would make it possible to determine the reserves required to offset fluctuations and the robustness of the grid against maximum fluctuations.

upna Universidad Pública de Navarra Nafarroako Unibertsitate Publikoa

On the other hand, the second tool is focused on the smoothing of PV power fluctuations at a PV fleet. Due to geographic smoothing it would also make sense to allocate an ESS in a network node in which a number of PV plants converge, expecting some savings in terms of the ESS capacity required to limit the total ramp-rate fluctuations. On the base of the worst fluctuation model for a PV plant, already explained in section 3.4.2, it is investigated the possible maximum fluctuation that could take place at a PV fleet i.e. the worst case fluctuation for a PV fleet in order to present a novel method which makes it possible, just by knowing the geometric shape of the surface occupied by any regularly distributed PV plant fleet combination and maximum allowable ramp-rate, to determine the maximum power and minimum energy storage requirements alike.

5.2 SIMULATING THE VARIABILITY OF DISPERSED LARGE PV PLANTS

5.2.1 Introduction

There are two natural factors known to smooth short-term irradiance fluctuations in relation to PV power fluctuations. The first is smoothing due to size: the fluctuations from incident irradiance on a PV plant are smoothed in proportion to $\sqrt{S}$, where S is the plant size (Marcos et al., 2011a). Therefore, the greater the plant size, the lower the fluctuations for the same time window. The second is geographical dispersion: for the same power output of inverter P_n to be installed, the fluctuations are lower if this power is divided between N PV plants that are at a sufficient distance apart to ensure that the short-term fluctuations are independent of each other. Therefore, for windows of just a few minutes, the additional smoothing effect achieved is proportional to $\sqrt{N}$ as demonstrated theoretically (Marcos et al., 2012; Mills et al., 2010) and experimentally (Marcos et al., 2012; Mills et al., 2010) in a number of studies. A more thorough and extensive study of both phenomena can be found in Hoff and Perez, 2010.

Although the mechanisms are well-known, at present there are few practical tools that enable TSO and DSO to simulate the fluctuations of distributed PV power in electricity networks based on irradiance measurements. As a preliminary approach, Kuszamaul et al., 2010 proposes creating networks of multiple synchronised sensors and averaging their readings. However, this is an expensive system that is difficult and

upna Universidad Pública de Navarra Nafarroako Unibertsitate Publikoa

impractical to implement in the field (all the more so if there are a number of dispersed PV plants). For a single plant, the proposal is to simulate the smoothing effect of the plant size by filtering the irradiance measurements: either by a window filter (Longhetto et al., 1989), or a low pass filter (Marcos et al., 2011b), where the cut-off frequency of both is adjusted according to the PV plant size. Although both methods are valid, they are only applicable to a single PV plant. As a more advanced method, (Lave et al., 2013) proposes the Wavelet Variability Model in order to simulate the reduction in fluctuations of a plant or a fleet of dispersed plants. It should firstly be pointed out that the model not only requires irradiance data measured at a single point, but also daily parameters such as the correlation scaling coefficient, whose value cannot be calculated immediately due to the fact that it depends on geographical and meteorological parameters such as cloud speed.

Making use of the size and dispersion smoothing factors, this section proposes a simple model to simulate the power that would be generated by a fleet of geographically dispersed plants based on incident irradiance measurements taken at a single location. Specifically, the model comprises two transfer functions: firstly a low pass filter already proposed in Marcos et al., 2011b to convert the irradiance time series into power generated by a PV plant. This model solely requires the mean size of the fleet of plants considered. Secondly, and as the main contribution of this section, a transfer function applies the reduction in variability due to dispersion, simply by providing the number of plants *N*. This model makes it possible to simulate the power fluctuations in any power grid with a distributed PV fleet, based solely on single point incident irradiance measurements. This work is based on experimental 1-s data collected in the course of 2013 from the six Ribera PV plants (section 2.3), with a total of 18 MWp, separated by a distance ranging from 6 to 60 km and dispersed over 1100 km^2.

5.2.2 PV plant model: smoothing effect of the size

The analysis conducted on the Fourier irradiance and power spectra at the power plants indicated in **Table 2.1** and conducted in Marcos et al., 2011b makes it possible to consider a PV plant as a low pass filter for irradiance (**Figure 5.1**). The cut-off frequency for this filter directly depends on the square root of the plant size: the larger the plant size, the fewer the power fluctuations for the same time window. As an example, **Figure**

upna Universidad Pública de Navarra Nafarroako Unibertsitate Publikoa

5.2 shows the results from 11:05 to 15:00 on 1 April 2013 at the Milagro (52 Ha) site. The left plot shows the irradiance measured during that period. The right plot compares the simulated and the real power data. The similarity is clearly observed.

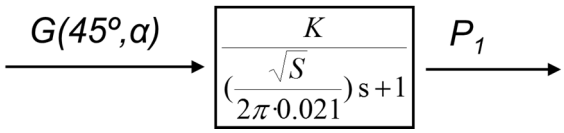

***Figure 5.1**. The PV plant power output is described as the signal output of a low pass filter where the input signal is the incident irradiance. Note that its pole value is a function of the PV plant area. Parameter K corresponds to ratio P_n /G* [m^2] for the PV plant.*

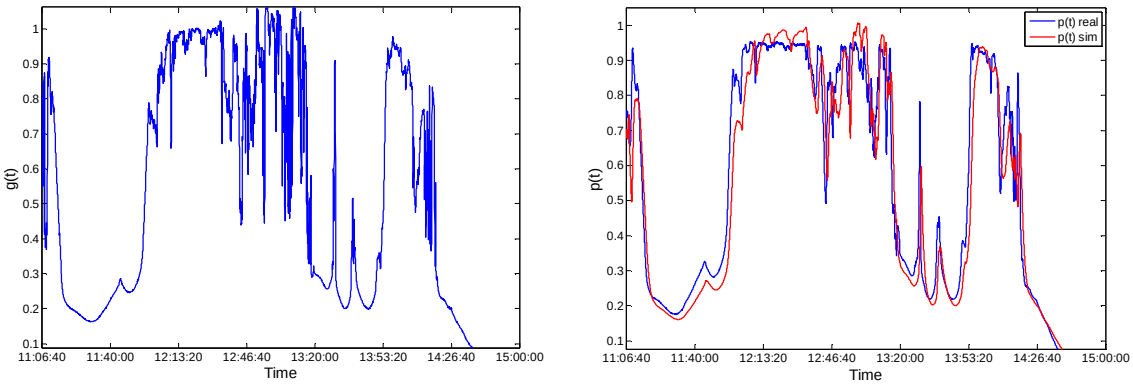

(a) (b)

***Figure 5.2**: (a) Irradiance G(45º,α) recorded from 12:30 h to 15:00 h on 25th October at the Milagro site, (b) real PV power output, p_{real}, (blue line) recorded during the same period at Milagro and the simulated power output p_{sim}, (red line) by the transfer function shown in **Figure 5.1**.*

5.2.3 Fleet model: smoothing due to dispersion

5.2.3.1 Definitions

In accordance with Marcos et al., 2012, the entire study was conducted with normalized PV plant output in order to avoid inaccurate results. When a single plant is significantly larger than the others, as it is in the case of the Milagro PV plant, then the smoothing effect of the geographic dispersion is masked by the predominance of the largest PV plant. This is a drawback when the goal is precisely to analyse geographical smoothing. Hence, the normalized power output at instant *t* of an aggregation of *N* PV plants, $p_N(t)$, is given by Eq.(5.1).

upna Universidad Pública de Navarra Nafarroako Unibertsitate Publikoa

$$p_N(t) = \frac{1}{N}\sum_{i=1}^{N}\frac{P^i(t)}{P_n^{\ i}} \qquad \textbf{(5.1)}$$

where $P^i(t)$ is the power output at instant t and P_n^i is the transformer power at the common coupling point of the i-th PV plant. It can be argued that because the power fluctuation is also smoothed by the PV plant size, Eq.(5.1) presents some drawbacks. Mainly, all the PV plants are assumed to have the same peak power, because they receive the same weight in Eq.(5.1); however their intrinsic fluctuation behaviour is considered to be different due to the fact that the rate is not affected by power normalization. However, as has been shown in Hoff and Perez, 2010; Marcos et al., 2012, smoothing by geographical dispersion is significantly more important than smoothing by size and, therefore, this drawback is in fact irrelevant. Likewise, this definition can also be applied to irradiance measurements Eq.(5.2):

$$g_N(t) = \frac{1}{N}\sum_{i=1}^{N}\frac{G^i(t)}{G^*} \qquad \textbf{(5.2)}$$

where G^*= 1000 W/m^2. It is now possible to define the magnitude of a power fluctuation, $\Delta P_{\Delta t,N}(t)$ for a given number, N, of PV plants grouped at an instant t, and for a given sampling period Δt, as the difference between two normalized power outputs, Eq.(5.3). That is:

$$\Delta P_{\Delta t,N}(t) = [p_N(t+\Delta t) - p_N(t)]\times 100 \qquad \textbf{(5.3)}$$

As an example, **Figure 5.3 (a)** shows the normalized output power $p_1(t)$, recorded at the Cintruénigo PV plant and the fleet of six PV plants located in Navarra, $p_6(t)$, on March 5th 2013. **Figure 5.3 (b)** shows the corresponding power fluctuation for Δt = 60 seconds. It can be observed that the fluctuations of the fleet are considerably lower than those of a single system.

upna Universidad Pública de Navarra Nafarroako Unibertsitate Publikoa

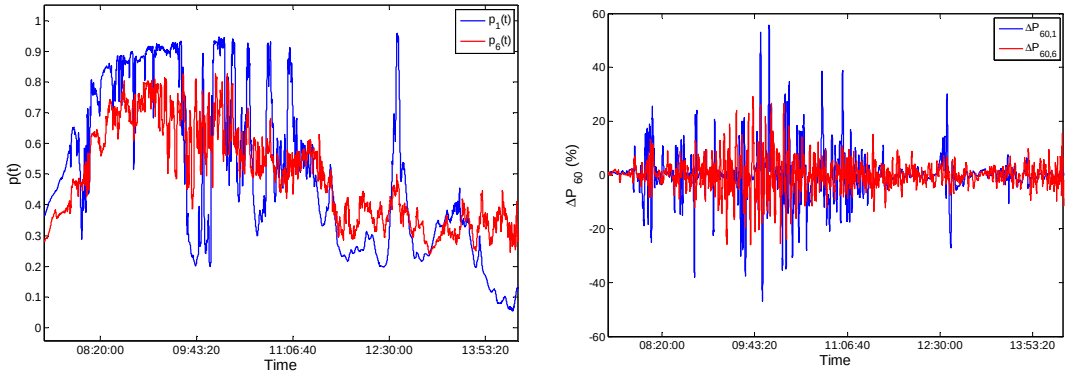

(a) (b)

***Figure 5.3**. (a) Normalized power output $p_1(t)$ (blue line) recorded on 5th March 2013 at Milagro and at the fleet of six plants located in Navarra, $p_6(t)$ (red line). (b) Power fluctuation trends at the Milagro PV plant $\Delta P_{\Delta t,1}$ (blue line) and at the fleet of six PV plants $\Delta P_{\Delta t,6}$ (red line) on 5th March 2013.*

5.2.3.2 Irradiance spectrum: influence of N

Figure 5.4 (a) presents the Discrete Fourier Transform (DFT) of the normalized irradiance signals, g_N, recorded in the course of a full year (2013) at the Milagro site, g_1, at the combination of Milagro and Castejón, g_2, and at the combination of Arguedas, Castejón, Milagro, Cintruénigo and Rada, g_5. DFT is computed through a Fast Fourier Transform (FFT) algorithm. In general terms, for a time series of a measured variable, $x=x_1 \ldots x_T$, the value at each point x_t in the frequency domain, X_k, is obtained by Eq.(5.4)

$$X_k = \sum_{t=1}^{T} x_t \ \omega_T^{(t-1)(k-1)} \qquad k = 1 \ldots (T-1) \qquad \textbf{(5.4)}$$

where T is the signal length and ω_T is calculated according to Eq.(5.5)

$$\omega_T = e^{(-2\pi i)/T} \qquad \textbf{(5.5)}$$

Following the suggestions made in Woyte et al., 2007 and in order to reduce the variance in coefficients X_k, the original signal is divided into a number of segments, 32 in this case. Coefficients X_k, are calculated for each segment and then averaged at each frequency. Despite the fact that the Nyquist theorem states that DFT can be calculated

upna Universidad Pública de Navarra Nafarroako Unibertsitate Publikoa

up to a maximum frequency that is double the sampling period, 0.5 Hz in this case, the analysis have been limited to 0.1 Hz, which is large enough for the present objectives.

Figure 5.4 (a) shows how the annual spectral irradiance values g_1, g_2 and g_5 are similar for very low frequencies, coinciding with the cyclic daily availability of the solar resource, as can be seen by a peak at 24h ($1.15 \cdot 10^{-5}$ Hz). However, at slightly larger frequencies of around $4 \cdot 10^{-4}$ Hz, a greater smoothing effect of the signals is evident, as more sites are taken into account. Specifically, the linear region of each spectrum fits function $a \cdot f^{-0.7}$, where parameter a establishes the smoothing magnitude and f the frequency. Trend $f^{-0.7}$ coincides with observations made by other authors (A. Curtright and Apt, 2008; Marcos et al., 2011b). This exercise was extended to the remaining site combinations in La Ribera in southern Navarra, N=1..6. **Figure 5.4 (b)** shows the value of parameter a based on N. The curve is well fitted (R^2=0.99) by a function of the form, Eq.(5.6):

$$a = m \cdot N^b \qquad \textbf{(5.6)}$$

where m = 1.003x10^{-5} and b = - 0.46. In other words, yet again it can be seen that the smoothing effect is practically given by a $1/\sqrt{N}$ law, which is in line with findings by other authors (Hoff and Perez, 2010; Kuszamaul et al., 2010; Marcos et al., 2012). As can be seen, a good dispersion smoothing effect can be achieved by aggregating just a few sites.

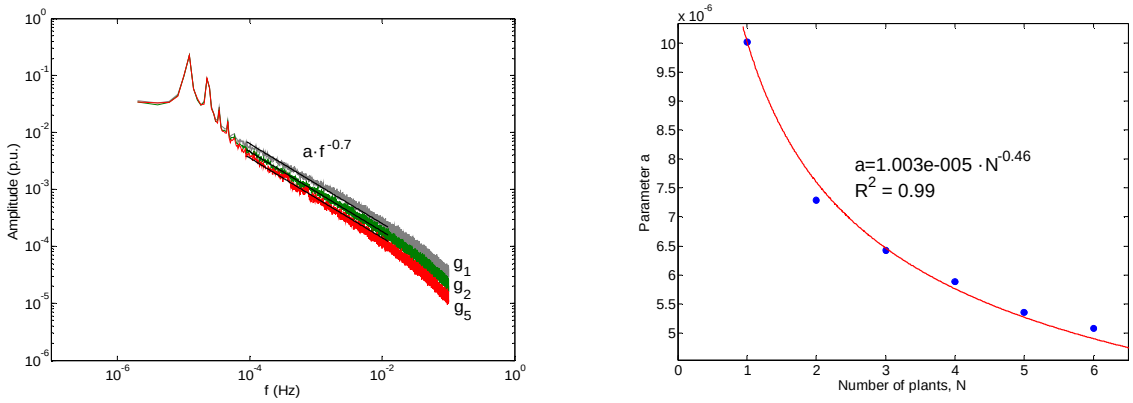

(a) (b)

***Figure 5.4**. (a) Spectrum of the normalized irradiance signals, g_N, recorded in the course of a full year (2013) for N=1, 2 and 5 (g_1, g_2 and g_5 respectvely). The linear region for the larger frequencies of the*

power spectra can be well fitted by a function of the form $a \cdot f^{-0.7}$. (b) Parameter a as a function of N. The trend can be correctly fitted (R^2=0.99) by function $a = m \cdot N^b$, where m = 1.0E-5 and b = - 0.46.

5.2.3.3 Power spectrum: influence of N

The same frequency domain analysis is also applied to power signals p_N recorded in the course of 2013. **Figure 5.5 (a)** shows the power spectra calculated for the same combinations indicated above: Milagro site p_1, Milagro and Castejón p_2, and Arguedas, Castejón, Milagro, Cintruénigo and Rada, p_6. The normalized power output at instant *t* of an aggregation of *N* was calculated based on Eq.(5.1). As was to be expected, it can yet again be seen that the smoothing of the various spectra is proportional to $1/\sqrt{N}$ ($m = 1.007 \cdot 10^{-5}$ and $b = -0.41$, R^2=0.97). The reason for a poorer fit is due to the fact that the power plant sizes are different and therefore the higher frequencies are smoothed differently.

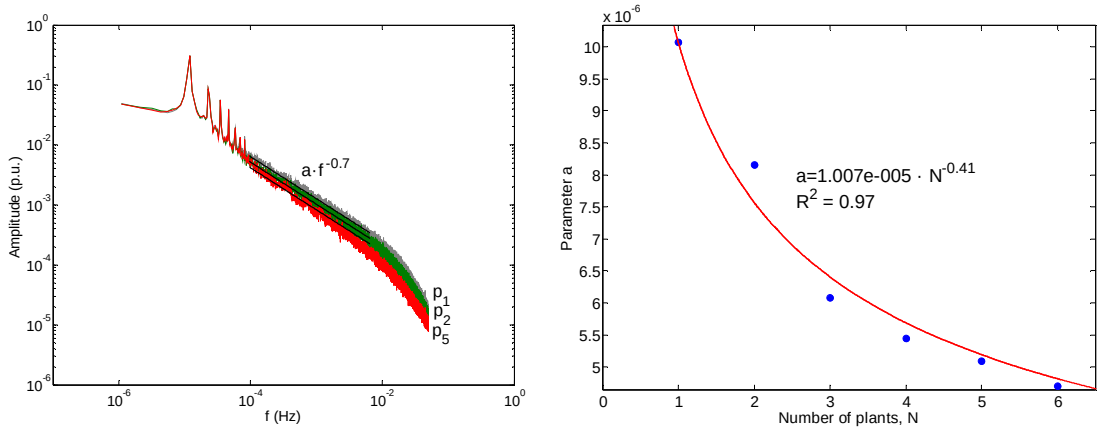

(a) (b)

***Figure 5.5**. (a) Spectrum of the normalized power signals, p_N, recorded in the course of a full year (2013) for N=1, 2 and 5 (p_1, p_2 and p_5 respectvely). (b) Parameter a as a function of N. The trend can be properly fitted (R^2=0.97) by function $a = m \cdot N^b$, where m = 1.0E-5 and b = - 0.41.*

5.2.3.4 Obtaining the fleet model

Given the power signal for a single plant, p_1, the aim is to obtain the power signal that would correspond to the aggregation of *N* similar plants, p_N. Therefore, the transfer function $TF_{PV,fleet}$ to be obtained is Eq.(5.7):

upna Universidad Pública de Navarra Nafarroako Unibertsitate Publikoa

$$TF_{PV,\,fleet} = \frac{p_N}{p_1} \qquad \textbf{(5.7)}$$

For example, for the case of N=2 and N=5, the experimental $TF_{PV,fleet}$ is obtained from ratios p_2/p_1 and p_5/p_1 respectively, as shown in **Figure 5.6**. As can be seen, these transfer functions can be approximated by a *pole* at a frequency close to 4 x 10^{-4} Hz (2400 seconds) and a *zero* the frequency of which depends on the number of plants considered. Taking into account the fact that the smoothing obtained at high frequencies is proportional to $\sqrt{N}$, the transfer function in the Lapace domain must be Eq.(5.8). The Bode diagram for the proposed model is also shown in **Figure 5.6** (solid black line), easily demonstrating its consistency with real spectra.

$$TF_{PV,\,fleet} = \frac{p_N(s)}{p_1(s)} = \frac{\left(2400\ /\sqrt{N}\right)s+1}{2400\ s+1} \qquad \textbf{(5.8)}$$

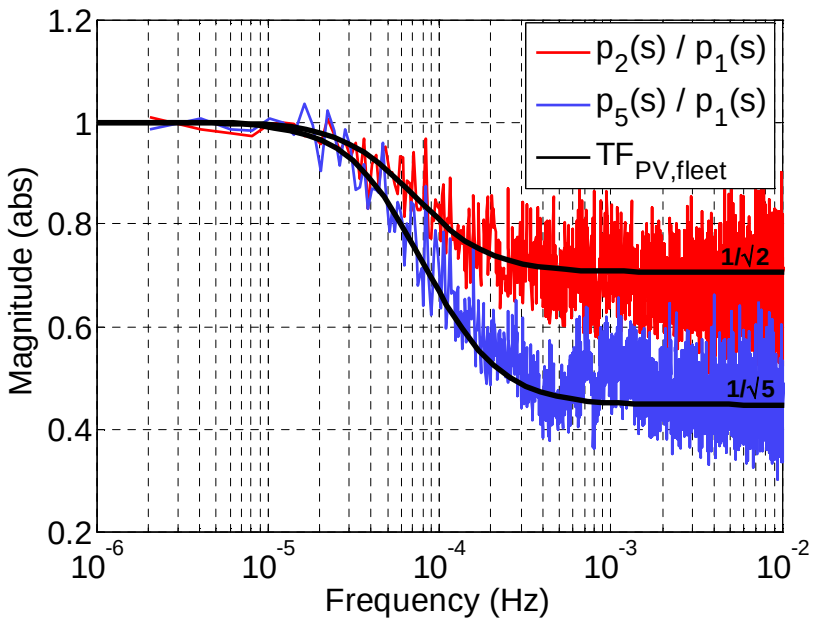

***Figure 5.6**. Spectra resulting from ratio p_2/p_1 (red line) and p_5/p_1 (blue line). The superimposed black line corresponds to the Bode diagram of the model proposed in Eq.(5.8). It can be seen how the high frequencies tend to smooth out due to $\sqrt{N}$.*

5.2.4 Simulation of the fluctuations for an N fleet of PV plants

For the measurements of a given irradiance time series, the power output of a PV fleet could now be obtained by simulation, using the combination of one PV plant model and the PV fleet model, that is, **Figure 5.7**. In this study, the model was simulated with MATLAB® Simulink. The simplicity of the model should be highlighted, which only requires the number of plants in the fleet *N* and the size *S* as input parameters. The selection of the *S* value for a PV fleet with plants of differing sizes, is debatable. However, as has been demonstrated in other works (Hoff and Perez, 2010; Marcos et al., 2012) the smoothing effect of size has scarcely any influence in relation to the smoothing effect of dispersion. For this reason, more than satisfactory results can be obtained by estimating *S* as the mean value of the size of all the plants, $\bar{S}$ (15.0 Ha in this case). **Figure 5.8 (b)** shows the evolution of the real power generated on the 26th March 2013 by the fleet of six PV plants $p_{6,real}(t)$ compared to that obtained by simulation $p_{6,sim}(t)$, applying the model proposed in Eq.(5.8) to the irradiance measured in Milagro, **Figure 5.8 (a)**, with $\bar{S}$=15 Ha and *N*=6. For this specific day, profiles $p_{6,real}(t)$ and $p_{6,sim}(t)$ are very similar except at the beginning and end of the day. In principle, this good correlation may appear surprising, considering that it is being simulated the performance of six PV plants dispersed over an area of 1100 km^2 yet with the irradiance measured at one single point. Logically, there are moments in which the irradiance conditions at the point measured are not exactly the same as those at the other plants. By way of example, **Figure 5.8 (c)** and **(d)** shows one of the days (7th May 2013) recording the greatest deviation, between $p_{6,real}(t)$ and $p_{6,sim}(t)$. It can be seen how the fluctuations at the place of measurement (Milagro) were less frequent than at other PV plants. In order to quantify the accuracy and, therefore, the validity of the proposed model, an analysis was made of the results obtained following the annual simulation with 1s data for $g(t)$, calculating three indices of merit: DFT error, maximum daily fluctuation and daily aggregate ramp rate.

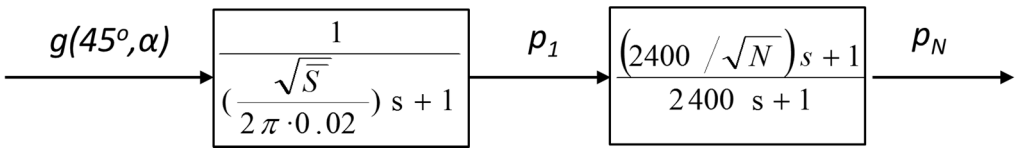

Figure 5.7: *Proposed transfer function for a PV fleet, consisting of N PV plants with a mean size equal to* $\bar{S}$.

upna Universidad Pública de Navarra Nafarroako Unibertsitate Publikoa

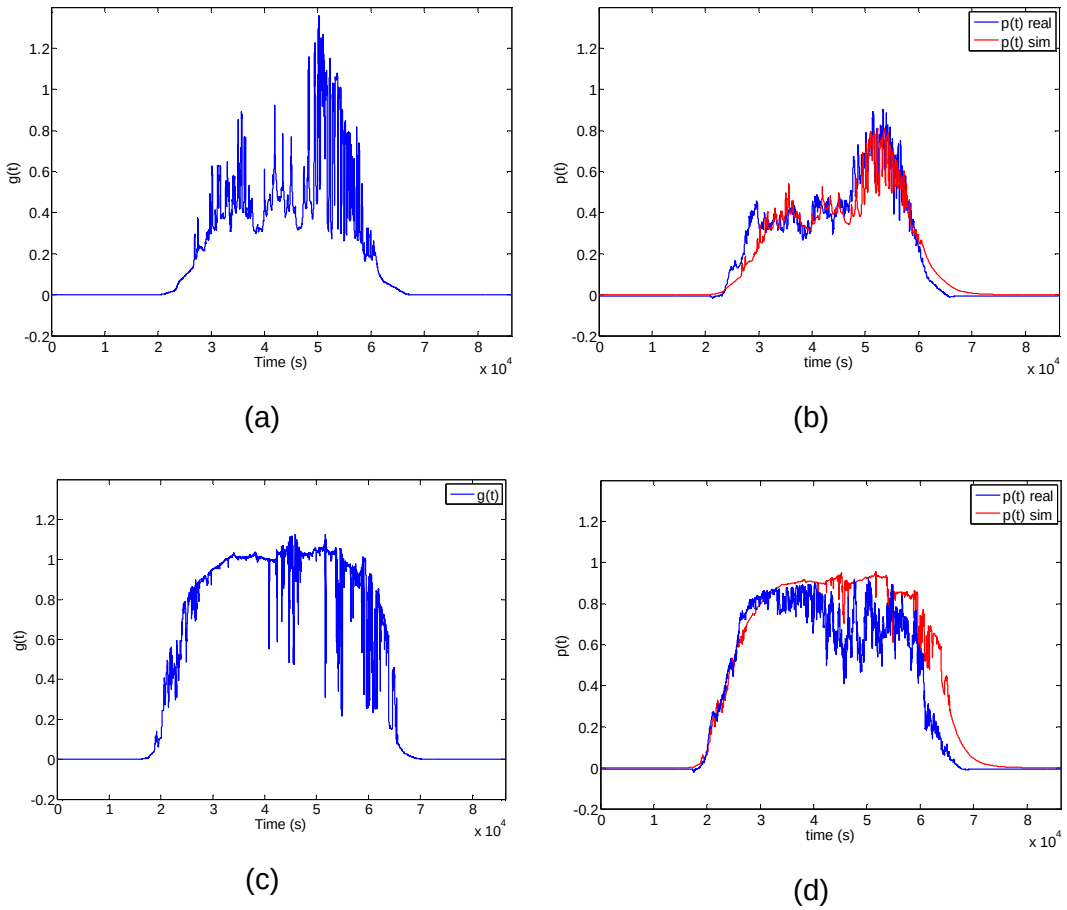

***Figure 5.8**. (a) Normalized irradiance g(t) recorded on 26th March 2013 at the Milagro site, (b) real output power, $p_{6,real}$, (blue line) recorded during the same day at the fleet of six PV plants located in Navarra, and output power simulated, $p_{6,sim}$, (red line) by the transfer function showed in **Figure 5.7**, with N = 6 and $\bar{S}$ = 15 Ha. Figures (c) and (d) show the same variables for the 7th May 2013. Both are shown, respectively, as an example of days with a larger or smaller deviation between $p_{6,real}$ and $p_{6,sim}$.*

5.2.4.1 DFT error

As an initial step, the validity of this simulation exercise was also checked in the frequency domain. **Figure 5.9 (a)** shows the annual power spectrum for $p_{6,real}$ (redline) and $p_{6,sim}$ (blue line) while **Figure 5.9 (b)** shows that the DFT error is under 1.5% for all frequencies. This same analysis was performed for different combination of N = 2…6 PV plants, obtaining similar results.

upna Universidad Pública de Navarra Nafarroako Unibertsitate Publikoa

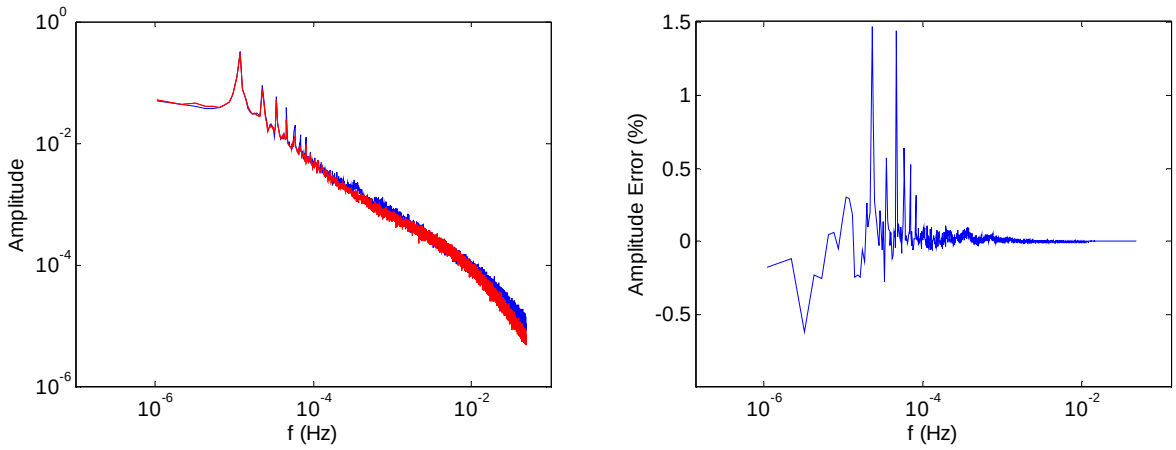

(a) (b)

***Figure 5.9**. (a) Annual power spectrum for $p_{6,real}$ (redline) and $p_{6,sim}$ (blue line) (b) DFT error between $p_{6,real}$ and $p_{6,sim}$ output power one year data (2013).*

5.2.4.2 Maximum daily power fluctuation in one minute

The maximum power fluctuation in the course of a day $Max(\Delta P_{\Delta t,N})$ is of particular interest from the grid operator's point of view. Specifically, the new grid codes specify the limitations in time windows Δt equal to 1 minute. For example, according to PREPA, 2012 the maximum permitted ramp for a PV plant is 10% per minute, whilst in Mexico it is 1 - 5% per minute (CRE, 2014). Therefore, **Figure 5.10** shows the real 365 daily maximum power fluctuations $Max(\Delta P_{1min,6,real})$ compared to the simulated values, $Max(\Delta P_{1min,6,sim})$ where fluctuations have been calculated by Eq.(5.3). Highlighting the goodness-of-fit (RMSE < 4.7%), whilst taking into consideration the fact that the maximum fluctuation of the 1s data responds to very particular situations (see **Figure 5.3 (b)**) and the simplicity of the model (just two well-known parameters, $\bar{S}$ = 15.0 Ha and N=6).

upna Universidad Pública de Navarra Nafarroako Unibertsitate Publikoa

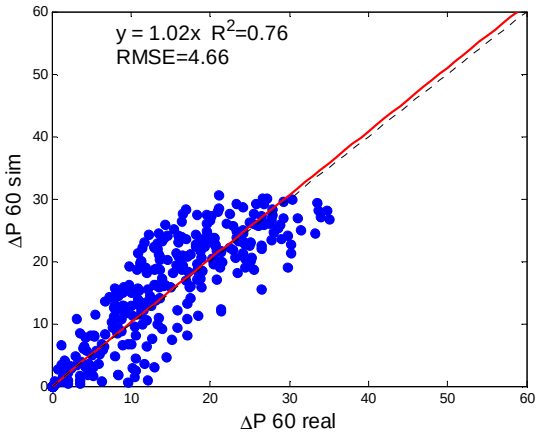

***Figure 5.10**: Daily maximum simulated power fluctuations Max($\Delta P_{1min,6,sim}$) versus the real values, Max($\Delta P_{1min,6,real}$) for one year data (365 values).*

5.2.4.3 Daily aggregate ramp rate

Likewise, it is of interest to quantify the variability of a daily production profile, as it is directly related to the spinning reserve levels required to offset fluctuations. To do so, in this work it has been used the *Daily aggregate ramp rate* (*DARR*) parameter proposed by (van Haaren et al., 2014) and which makes it possible to categorise the days according to the fluctuation level, based on the observed minute-averaged variability. In other words, Eq.(5.9):

$$DARR = \sum_{t=1}^{1440} \frac{\left| x(t) - x(t-1) \right|}{X^*} \qquad \textbf{(5.9)}$$

where $x(t)$ is a time series of minute-averaged records and X^* the nominal value of x. For the specific case of this study, it is considered $DARR_{N,sim}$ if $x(t)$ to be equal to $p_{N,sim}(t)$ and $DARR_{N,real}$ in the case of if $x(t)$ is equal to $p_{N,real}(t)$. And as both are normalised power outputs, X^*=1. **Figure 5.11** shows the 365 real values for $DARR_{6,real}$ compared to the simulated values, $DARR_{6,sim}$. The regression coefficients yet again confirm the goodness of fit of the model (RMSE < 2%). By way of example, the figure shows one of the days with the worst results (7th May 2013), previously presented in **Figure 5.8 (c)** and **(d)**.

upna Universidad Pública de Navarra Nafarroako Unibertsitate Publikoa

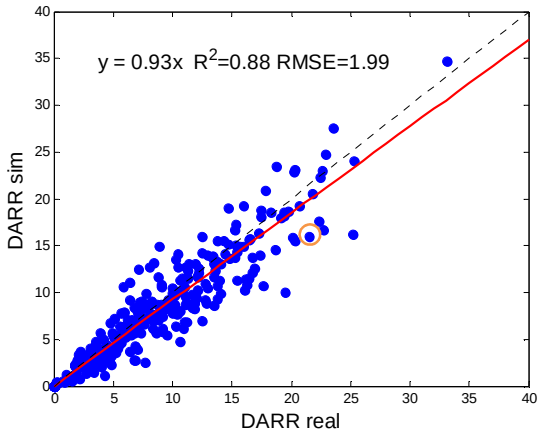

***Figure 5.11**. Daily aggregate ramp rate simulated values for the fleet of six plants $DARR_{6,sim}$ compared to the real values, $DARR_{6,real}$ for one year data (365 values). One of the days with the worst results (7th May 2013), has been circled, previously presented in **Figure 5.8** **(c)** and **(d)**.*

As indicated in van Haaren et al., 2014, one of the advantages of the *DARR* is that is makes it possible to classify the days based on the risk of fluctuations and, therefore, it makes it easier for the TSO to plan future projects. Days can be classified into five categories, ranging from very stable days (Category 1) to highly variable days (Category 5), based on arbitrary suggestions:

- Category 1: $DARR < 3$
- Category 2: $3 \leq DARR < 13$
- Category 3: $13 \leq DARR < 23$
- Category 4: $23 \leq DARR < 33$
- Category 5: $33 \leq DARR$

Therefore, **Figure 5.12** shows the classification of all the simulated and real values for $DARR_6$ as already shown in **Figure 5.11**, revealing how the real and simulated data show very similar daily distributions.

upna Universidad Pública de Navarra Nafarroako Unibertsitate Publikoa

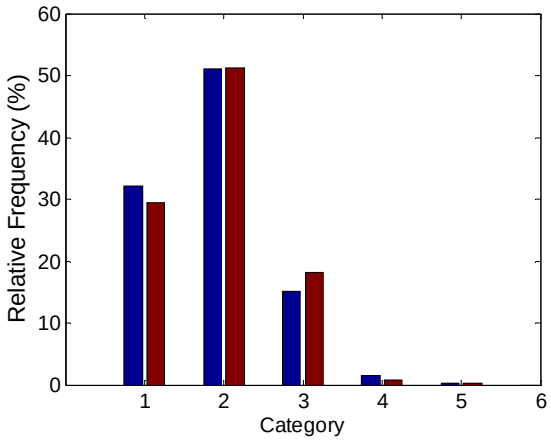

***Figure 5.12**. Histograms of $DARR_{6,real}$ observed over a year and the simulated ones, $DARR_{6,sim}$*

This regression exercise made for $Max(\Delta P_{1min,N})$ and $DARR_{,N}$ was completed for the remaining cases, N=2..5, (**Table 5.1**). The slight improvement in the regression residuals (particularly for $Max(\Delta P_{1min,N})$) suggests that the model accuracy is strengthened as the number of PV plants increases, at least for PV plants located in the same climatic region, as in this experiment. More PV systems would be needed to confirm this trend.

***Table 5.1**: RMSE error evolution as a function of N.*

N	RMSE $Max(\Delta P_{1min,N})$	RMSE $DARR_N$
2	7.1	2.75
3	7.0	2.36
4	5.9	2.35
5	5.2	2.15
6	4.6	1.99

5.2.5 Conclusions

In this section it has been presented a model to simulate the fluctuations generated by a fleet of dispersed PV plants, solely based on irradiance data measured at one single location. The model was obtained from 1-year data with a 1 s resolution from six PV plants (up to 18MWp) dispersed over an area of 1100 km^2, within the same climatic region. This simple model has been satisfactorily used to quantify the power variability of the PV fleet, just by defining two parameters: mean plant size $\bar{S}$ and the number of plants

upna Universidad Pública de Navarra Nafarroako Unibertsitate Publikoa

in the PV fleet. Specifically, the model reliably reproduces the critical parameters for the grid operator, such as maximum fluctuation or the reserves required to offset these fluctuations. Therefore, the model proposed could prove to be an extremely useful tool for studying the grid integration of distributed PV generation, by providing a series of simulated power outputs that may be used in the grid operator simulation programs.

5.3 STORAGE REQUIREMENTS FOR PV POWER RAMP-RATE CONTROL IN A PV FLEET

5.3.1 Introduction

As it has been previously commented, taking advantage of the smoothing effect of geographical dispersion, it makes sense to allocate an ESS in a network node in which a number of PV plants converge, expecting some savings in terms of the ESS capacity required to limit the total ramp-rate fluctuations due to geographic smoothing. This is of particular interest in islands with stand-alone power grids. A previous study Perez and Hoff, 2013 analysed the economic cost of the installation of an ESS to smooth out short-term PV output variability as a function of the maximum allowable ramp-rate, the intermittency time scale and the geographic dispersion of the PV resource. It is shown that the use of geographic dispersion as a means of smoothing out PV fluctuations enables considerable savings in the ESS. However, nowadays no methodology is available to size the ESS required to smooth out short-term PV output variability to r_{MAX} in the case of an aggregation of PV plants or a PV fleet.

This section firstly examines and models the maximum fluctuation observed at several aggregation cases of 5 PV plants in the course of a year. Once the main features of the fluctuations are modelled and well known, it is then investigated the possible maximum fluctuation that could take place at a PV fleet i.e. the worst case fluctuation. It is presented a novel method which makes it possible, simply by knowing the geometric shape of the surface occupied by any regularly distributed PV plant fleet combination and maximum allowable ramp-rate, to determine the maximum power and minimum energy storage requirements alike. The general validity of the method has been successfully validated through real operational PV power data taken every 1 s in the course of one year from five PV plants already presented in Section 2.3 (Arguedas, Castejón,

upna Universidad Pública de Navarra Nafarroako Unibertsitate Publikoa

Cintruénigo, Milagro and Rada) with powers ranging from 1 to 9.5 MWp located in Navarre (Spain). It is worth noticing that in this study the Sesma PV plant is not used because a regularly distributed PV fleet was necessary. **Figure 5.13** shows the geographic distribution of the PV plants for this study. Finally, a comparison is made of the energy storage requirement savings for smoothing short-term PV power fluctuations in a regularly distributed PV fleet using a centralized instead of a distributed ESS.

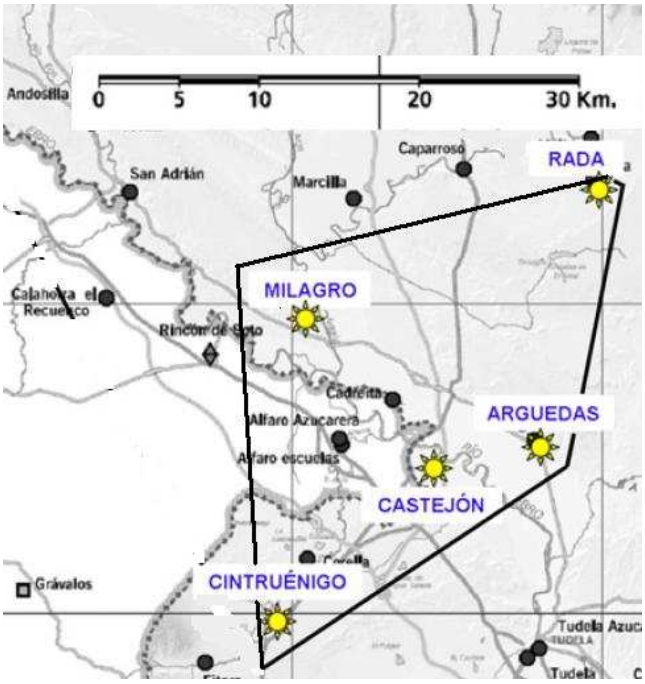

***Figure 5.13**: Geographic distribution of the PV plants under study.*

Again, the entire study was conducted with normalized PV plant output in order to avoid inaccurate results.

5.3.2 Extrapolation of the worst fluctuation model from a PV plant to a PV fleet

5.3.2.1 The worst fluctuation model for a single PV plant

Section 3.4.2 described an effective method to calculate, for any PV plant size and maximum allowable ramp-rate (r_{MAX}), the maximum power and the minimum energy storage requirements alike. This method, called the *worst fluctuation model,* is based on the worst fluctuation that can take place at a PV plant and is a function of the shortest measurement for the PV plant perimeter. This is duly described in **Figure 3.10**.

A careful study of the worst case fluctuations observed at the 38.5 MW of Amareleja (Portugal) made it possible to assert that the worst fluctuation that can appear at a PV plant is described in Eq.(3.6) as a power exponential decay from P_n to 0.1 P_n (or an exponential rise from 0.1 P_n to P_n). In this case, as the study is made with the normalized power, the decay will be from 1 (normalized nameplate power, p_n) to 0.1p_n (or an exponential increase from 0.1p_n to p_n) which means that the beam irradiance disappears and only the diffuse light remains. That is Eq.(5.10):

$$p_{PV}(t) = [90 \cdot (\exp(-t/\tau)) + 10] \qquad \textbf{(5.10)}$$

In this equation, τ *[s]* is a time constant which is empirically correlated with the shortest measurement of the PV plant perimeter, *l [m]*, by the Eq.(5.11) (section 4.4.2):

$$\tau = a \cdot l + b \qquad \textbf{(5.11)}$$

where a = 0.042 [s/m] and b = -0.5 s.

Battery requirements for ramp-rate limitations in the case of a worst fluctuation event are easily derived from **Figure 3.10**. The normalized power demanded to the battery $p_{BAT}(t)$ corresponds to the difference between the PV power injected into the grid, $p_G(t)$, and the generated PV power, $p_{PV}(t)$. Therefore, the normalized battery power, $p_{BAT}(t)$, for the worst fluctuation time is given by Eq.(5.12):

$$p_{BAT}(t) = \frac{1}{100}[90\,(1 - \exp(-t/\tau)) - t \cdot r_{\max}] \qquad \textbf{(5.12)}$$

where r_{MAX} is expressed as [%/min]. Specifically, the minimum theoretical effective normalized battery required (C_{BAT}) is obtained by simply integrating Eq.(5.12) and is given in Eq.(5.13) (with the control proposed in sections 4.2 and 4.3):

upna Universidad Pública de Navarra Nafarroako Unibertsitate Publikoa

$$C_{BAT} = \frac{0.9}{3600}\left[\frac{90}{2 \cdot r_{MAX}} - \tau\right] \qquad \textbf{(5.13)}$$

where C_{BAT} is expressed in [h] based on the nameplate power of the PV plant. An ESS that is able to smooth out the worst case fluctuation, means that it will operate correctly under any other circumstances simply by implementing the right control.

Another important issue is the maximum power that must be absorbed or provided by the ESS and the associated power electronic converter. This is calculated as the maximum of the expression given in Eq.(5.12). Hence, the required normalized battery power is given by Eq.(5.14):

$$p_{BAT,MAX} = \frac{1}{100}\left[90 - \tau \cdot r_{MAX}\left(1 + \ln\frac{90}{\tau \cdot r_{MAX}}\right)\right] \qquad \textbf{(5.14)}$$

5.3.2.2 Maximum fluctuations observed in a PV fleet

A full study was conducted of the maximum fluctuations observed for different combinations of the PV plants under consideration. By way of example, **Figure 5.14 (a)** and **(b)** shows the normalized PV power evolution during a day with one of the most extreme fluctuations (16th April 2013) for the combination of Arguedas, Castejón, Milagro and Rada (N = 4), $p_{PV,4}(t)$. It can be seen that this is a day with many breaks in the cloud cover, with a huge front of clouds in the afternoon that almost caused all the PV plants to stop generating. The plants gradually dropped, one after the other: Castejón was the first, followed by, Arguedas and Milagro at almost at the same time and, finally, Rada.

upna Universidad Pública de Navarra Nafarroako Unibertsitate Publikoa

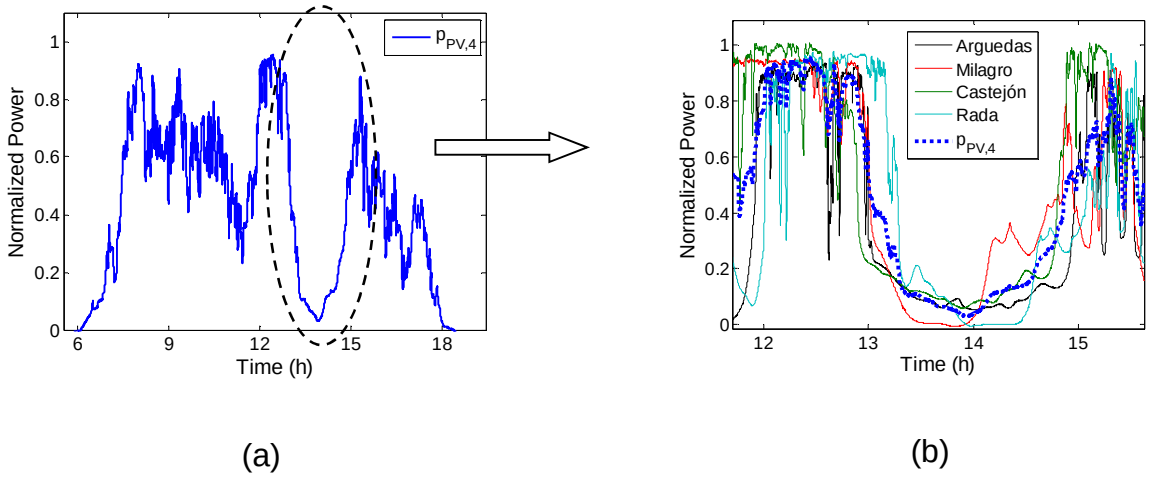

***Figure 5.14**: Evolution of the power of one case of N=4 combination on 16th April 2013. (a) Power evolution of the N = 4 combination, $p_{PV,4}$ (t). (b) Zoom of the power evolution of the combination, $p_{PV,4}$ (t), and each PV plant individually.*

Figure 5.15 shows the evolution of the front of clouds through satellite images during the day studied, as the front advances in a north-easterly direction. As was to be expected, these images confirm how the clouds cover the PV plants. At 12 hours, the PV fleet is uncovered, whilst the first PV plant is covered at 13 hours approximately. At 14 hours, the PV fleet is completely covered commensurate with **Figure 5.14**. Finally, at 16 hours, the front has passed over and the PV fleet is uncovered again. From these images and the fact that the Arguedas and Milagro PV plants drop at the same time, it is to be assumed that the front is in a perpendicular direction to the imaginary line joining these two PV plants.

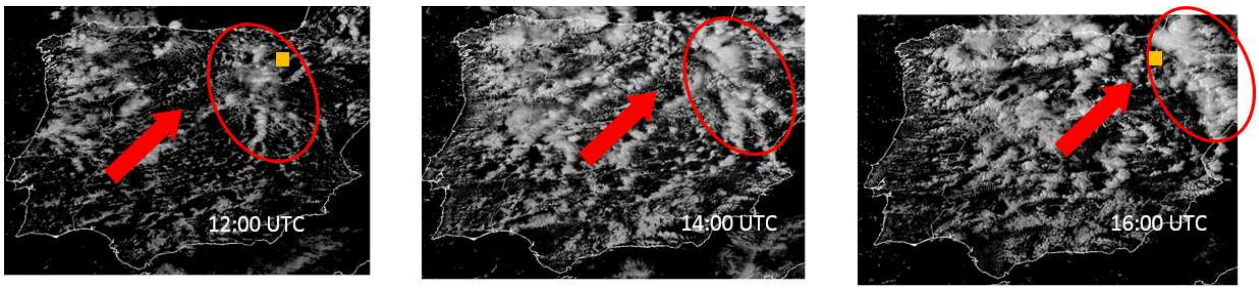

***Figure 5.15**: Evolution of the front of clouds crossing the PV plants under study on the 16th April 2013. Source: EUMETSAT.*

The previously presented Eq.(5.10) models the drop in the PV power at a PV plant due to cloud passage as an exponential function that only depends on time constant τ.

This τ is given by Eq.(5.11) and it is correlated with the inverse value of the cloud speed and the distance that the cloud needs to travel in order to completely cover the PV plant. Now, it would make sense to fit Eq.(5.11) to model the fall in the total power generated by a PV fleet which is being covered by a front of clouds travelling at a specific speed. On the one hand, the observed distance, l_{obs}, to be travelled by the front of clouds in order to cover all the PV plants under consideration in this case is 20 km (**Figure 5.16**). On the other hand, parameter *a* would be the inverse of the speed of the cloud front. According to **Figure 5.14 (b)**, Castejón drops at 13 hours and Rada, which is the last one to drop, 950 seconds later, which is almost 16 minutes. In this way, the cloud front travels 20 km in 16 minutes. Hence, the front speed is 75 km/h, which is 20.83 m/s and, consequently, the observed parameter *a,* a_{obs} = 0.048 s/m. Therefore, it is now possible to model the normalized power of the fluctuation observed in the PV fleet by Eq.(5.15):

$$P_{PV,f,obs}(t) = \left[90 \cdot \left(exp\left(\frac{-t}{\tau_{obs}}\right)\right) + 10\right] \qquad \textbf{(5.15)}$$

where the observed, $\tau_{obs,}$ is given by Eq.(5.16):

$$\tau_{obs} = a_{obs} \cdot l_{obs} = 0.048 \cdot 20000 = 960\ s \qquad \textbf{(5.16)}$$

Note that in this case parameter *b* shown in Eq.(5.11) has now been omitted because it was used in order to fit the correlation for the smallest values of *l,* a fact that is not necessary for PV fleets due to the fact that distances, l_{obs}, are far greater than for a single PV plant.

upna Universidad Pública de Navarra Nafarroako Unibertsitate Publikoa

***Figure 5.16**: Calculation of τ_{obs} for the for the PV fleet formed by Arguedas, Castejón Milagro and Rada (N = 4) during the fluctuation on 16th April 2013.*

Figure 5.17 shows both the real normalized PV power, $p_{PV,4}(t)$, and the modelled, $p_{PV,f,obs}(t)$. The model has been rescaled to fit with the start of the downward fluctuation occurring that day. In other words, as the downward fluctuation starts at $p = 0.87$, $p_{PV,f,obs}(t)$ is multiplied by this factor. The model and the real normalized PV power of the PV fleet under consideration can be seen to be in a very good agreement.

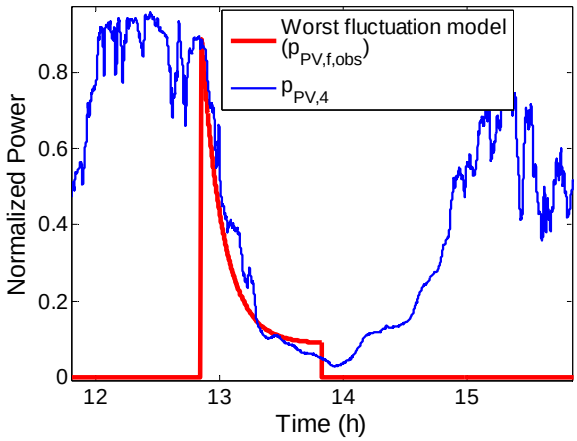

***Figure 5.17**: PV power modelled through the observed τ_{obs} ($p_{PV,f,obs}$), and real normalized PV power, $p_{PV,4}$, of the PV fleet formed by Arguedas, Castejón Milagro and Rada (N = 4) during the fluctuation on 16th April 2013.*

Another example with very high fluctuations but for the five PV plants combination took place on the 1st August 2013. This is a mostly clear day in which a huge downward

fluctuation occurred near midday. **Figure 5.18 (a)** shows the coupled normalized power for the five PV plants, $p_{PV,5}(t)$, and **(b)** individually and again the normalized sum of all the plants. An analysis clearly shows that Cintruénigo is the first PV plant to drop, closely followed by Milagro, then Castejón, Arguedas and, finally, Rada. In this case, the front is heading in an easterly direction with a slight northern component. The front takes 950 seconds to cover all the PV plants, approximately 15.84 minutes. **Figure 5.18 (c)** shows the direction of the advancing cloud front, deduced from the way in which the PV plants drop in **Figure 5.18 (b)**, and the calculation of the l_{obs} = 21 km. Then, the front speed is 79.55 km/h or 22.10 m/s and a_{obs} = 0.045. **Figure 5.18 (d)** shows the actual normalized PV power of the PV fleet, $p_{PV,5}(t)$, and the modelled PV power drop, $p_{PV,f,obs}(t)$. Again, there is a good agreement between both power outputs.

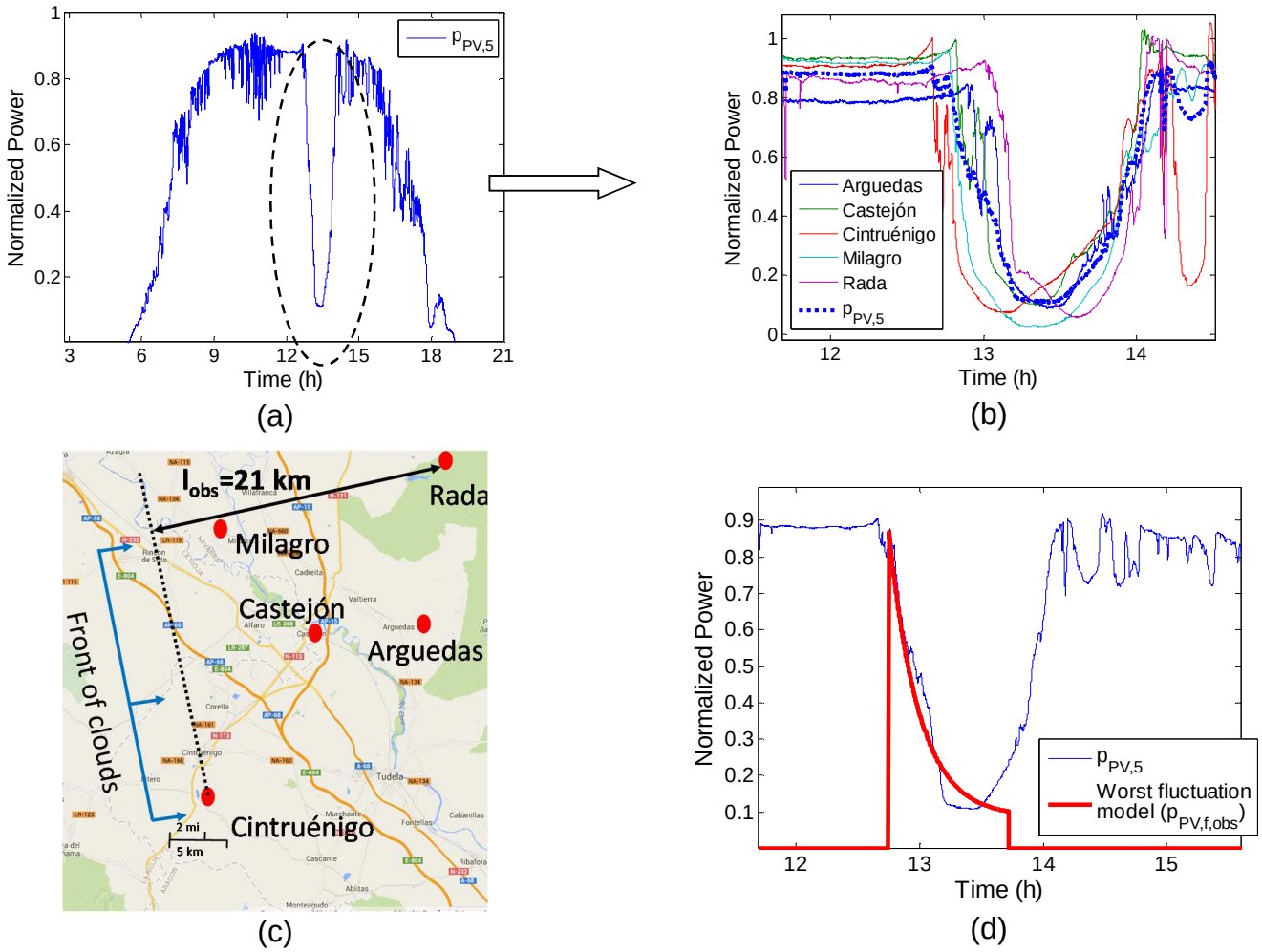

***Figure 5.18**: Results of the model for the five PV plant fleet (N = 5) during a fluctuation on 1st August 2013. (a) Normalized PV power of the PV fleet, $p_{PV,5}$. (b) Normalized PV power of the individual PV plants and the PV fleet. (c) Calculation of l_{obs}. (d) PV power modelled through the observed, T_{obs} ($p_{PV,f,obs}$) and real normalized PV power, $p_{PV,5}$, of the PV fleet.*

Once both cases have been correctly modelled, it is possible to calculate the minimum ESS capacity required for these two extreme fluctuations observed in the PV fleet, $C_{BAT,f,obs}$, by Eq.(5.17):

$$C_{BAT,f,obs} = \frac{0.9}{3600}\left[\frac{90}{2 \cdot r_{MAX}} - \tau_{obs}\right] \qquad \textbf{(5.17)}$$

where r_{MAX} is expressed in [%/s] and τ_{obs} in [s].

And, the required maximum normalized battery power for the fluctuation observed is given by Eq.(5.18):

$$p_{BAT,f,obs} = \frac{1}{100}\left[90 - \tau_{obs} \cdot r_{MAX}\left(1 + \ln\frac{90}{\tau_{obs} \cdot r_{MAX}}\right)\right] \qquad \textbf{(5.18)}$$

The corresponding battery requirements for the observed fluctuations $C_{BAT,f,obs}$ = 0.101 h and $p_{BAT,f,obs}$ = 0.254 for N = 4 combination and $C_{BAT,f,obs}$ = 0.097 h and $p_{BAT,f,obs}$ = 0.249 for N = 5 combination. The next step is to design the control strategy of the system. From now on, the strategy used will be the $RR_{clear\text{-}sky}$*: ramp-rate control based on the PV power plant model* proposed in section 4.3. According to this strategy, it is possible to estimate at each moment the PV plant production limits. These are the PV plant under clear sky conditions, $p_{PV,Max}(t)$, and the PV power under totally cloudy sky conditions in which only the diffuse light reaches the PV arrays, $p_{PV,Min}(t)$. In this way, just calculating these powers at each PV plant and adding them, it is possible to calculate the maximum power variation that can take place from the instant power generated by the PV fleet, $p_{PV,N}(t)$. So, as a function of the actual PV power, it is then possible to obtain the SOC needed (SOC_{ref}) to absorb or provide the necessary energy depending on the nature of the fluctuation. **Figure 5.19** shows the control diagram for this strategy. The sum of the PV plants power, $p_{PV,TOTAL}(t)$, enters into a ramp-rate limiter that is enabled if the $p_{PV,TOTAL}(t)$ dynamics exceed the ramp-rate limitation, that is Eq.(5.19):

upna Universidad Pública de Navarra Nafarroako Unibertsitate Publikoa

$$\frac{\left|\Delta p_{PV,TOTAL,1\min}(t)\right|}{p_n}\cdot 100 > r_{MAX} \qquad \textbf{(5.19)}$$

where r_{MAX} is expressed in [%/min]. The ramp-rate limiter output is the power that must be injected into the grid for the centralized solution, $p_{G,C}(t)$. This $p_{G,C}(t)$ will be similar to $p_{PV,TOTAL}(t)$ but with the ramps limited. The difference between $p_{G,C}(t)$ and $p_{PV,TOTAL}(t)$ will be the power through the battery, $p_{BAT}(t)$. Simply by integrating $p_{BAT}(t)$, the SOC of the ESS is obtained and it is compared to the corresponding SOC_{ref} and the error is multiplied by constant k to obtain the necessary power for the SOC control. This power is subtracted from $p_{PV,TOTAL}(t)$. Note that the control action is applied prior to the ramp-rate limiter to ensure that condition r_{MAX} is met at all times.

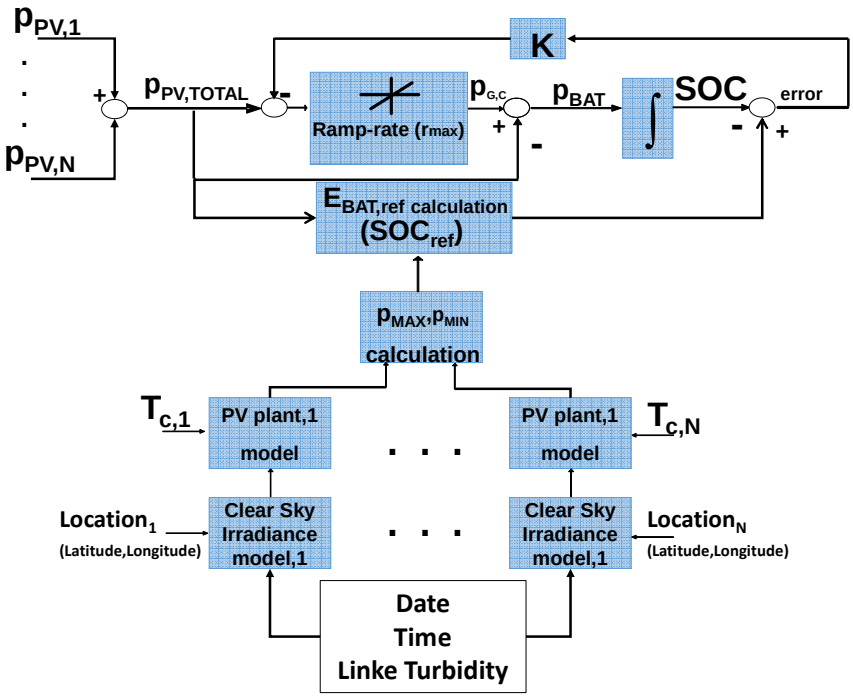

***Figure 5.19**: Ramp-rate control strategy algorithm.*

It should be noted that the PV power from each PV plant cannot be read at the ESS level, given the fact that a communication system between the PV plants and the ESS system is needed. In the same way as section 4.3, to evaluate this strategy, it will be taken k = 6, a value which allows a good trade-off between speed and system stability. Further information about the implementation of the strategy can be found in section 4.3.

upna Universidad Pública de Navarra Nafarroako Unibertsitate Publikoa

Figure 5.20 (a) and **(b)** shows the PV power, $p_{PV,N}(t)$, the limited power injected into the grid, $p_{PV,N,limited}(t)$, and the evolution of the SOC as a [%] according to the values calculated for $C_{BAT,f,obs}$ after applying the control strategy for the two cases analysed. In addition, **Figure 5.20 (c)** and **(d)** show the ESS normalized power, $p_{BAT}(t)$, for both cases analysed. As expected, in all the cases the actual values are almost equal to or less than the theoretical limits calculated by Eq.(5.17) and Eq.(5.18). The same exercise was made for different combinations with similar results, confirming the validity of the extrapolation of the model from a single PV plant to a PV fleet.

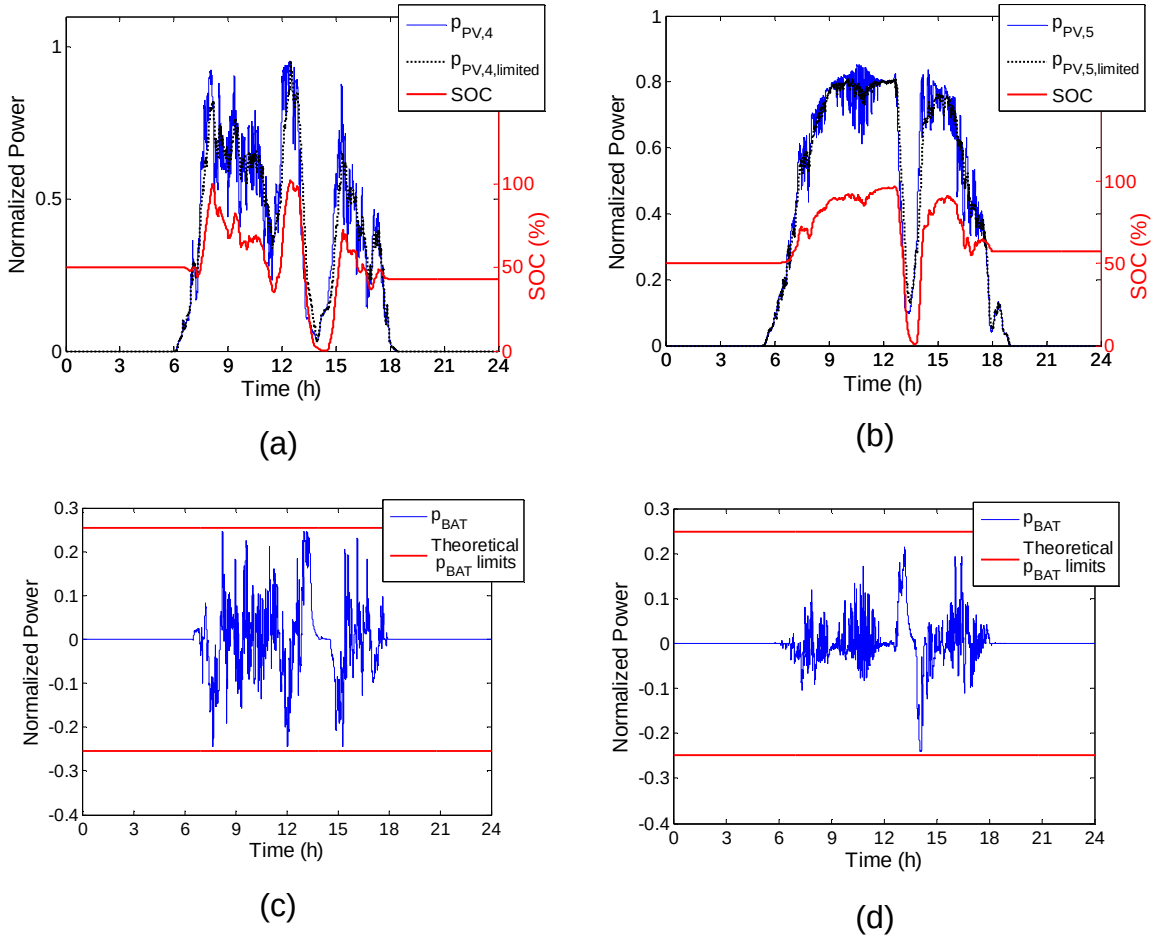

***Figure 5.20**: PV power, $p_{PV,N}$, limited power injected into the grid, $p_{PV,N,limited}$, and the evolution of the SOC as a [%] according to the values calculated for $C_{BAT,f,obs}$ for (a) N=4 combination on the 16th April 2013 and (b) the 1st August 2013 for the N=5 combination. Normalized ESS power evolution for (c) N=4 on 16th April 2013 and (b) N=5 on 1st August 2013.*

5.3.2.3 The worst fluctuation model for a PV fleet

Given the fact that the purpose of this study is to calculate the capacity required to smooth out any potential fluctuations, then the capacity required for the worst case fluctuation for a PV fleet needs to be calculated. This would occur when the PV fleet is being covered by a front of clouds travelling at maximum speed, which depends on the location, and the direction in which all the PV plants can be covered in a minimum space of time. On the one hand, the maximum clouds speed recorded during the highest fluctuations days analysed was 79.55 km/h. However, for the worst case fluctuation, it will be taken 85 km/h, a value which is in line with values proposed in other studies such as Lave and Kleissl, 2013 and section 3.4.2. Thus, the parameter a given in Eq.(5.11) particularized for the worst fluctuation case, a_w, will be a_w = 0.042 s/m. On the other hand, the shortest distance, l_w, would take place when the cloud front covers the PV fleet in the direction of the smallest height of the polygon formed by the external PV plants that contain all the PV plants within the least number of sides. Hence, the time constant of the PV fleet for the worst fluctuation case, τ_w, is given by Eq.(5.20):

$$\tau_w = a_w \cdot l_w \qquad \textbf{(5.20)}$$

where l_w is expressed in (m). Therefore, the normalized PV power for a PV fleet during the worst fluctuation case is given by Eq.(5.21):

$$p_{PV,f,w}(t) = \lfloor 90\,(\exp(-t/\tau_f)) + 10 \rfloor \qquad \textbf{(5.21)}$$

By way of example, **Figure 5.21** shows graphically how to calculate l_f for the two combinations analysed above. For the analysed cases, l_w = 14.8 km for the N = 4 combination and l_w = 16 km for the N = 5 combination.

upna Universidad Pública de Navarra Nafarroako Unibertsitate Publikoa

(a) (b)

***Figure 5.21**: Calculation of l_w for (a) the N = 4 combination and (b) the N = 5 combination.*

It is worth explaining the calculation of l_w when N = 2, which may not be so clear. In this case, l_w would be the largest dimension of the two PV plants under consideration measured in a straight line at right angles to the imaginary line that connects the two PV plants. **Figure 5.22** graphically shows an example of how to calculate l_w for Arguedas and Castejón, which gives a value of l_w = 490 m.

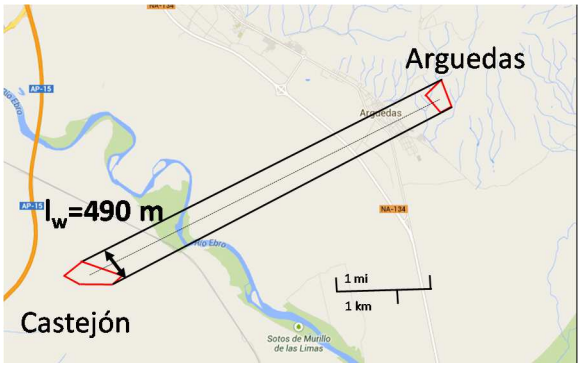

***Figure 5.22**: Calculation of the shortest measurement for a PV fleet comprising two PV plants.*

Taking all this into account, the minimum ESS capacity required for a PV fleet, $C_{BAT,f}$, can be calculated by Eq.(5.22):

$$C_{BAT,f} = \frac{0.9}{3600}\left[\frac{90}{2 \cdot r_{MAX}} - \tau_W\right] \qquad \textbf{(5.22)}$$

where r_{MAX} is expressed in [%/s] and τ_W in [s].

And, according to the worst fluctuation model, the required maximum normalized battery power for a PV fleet that is covered by a front of clouds travelling at maximum speed and in the direction of the minimum distance, l_w, is given by Eq.(5.23):

$$p_{BAT,f,W} = \frac{1}{100}\left[90 - \tau_W \cdot r_{MAX}\left(1 + \ln\frac{90}{\tau_W \cdot r_{MAX}}\right)\right] \qquad \textbf{(5.23)}$$

Applying these two equations, the corresponding battery requirements for the cases under study are $C_{BAT,f}$ = 0.17 h and $p_{BAT,f,W}$ = 0.36 for the N = 5 combination and $C_{BAT,f}$ = 0.18 h and $p_{BAT,f,W}$ = 0.39 for the N = 4 combination.

Figure 5.23 (a) and **(b)** shows the evolution of the SOC as a [%] according to the calculated values of $C_{BAT,f}$ in each case during the days of extreme fluctuations analysed in the previous subsection, 16th April 2013 for the N = 4 combination and 1st August 2013 for the N = 5 combination. As expected, in both cases the decline in SOC during these downward fluctuations does not use the whole theoretical capacity, $C_{BAT,f}$, of the ESS as there was no cloud front travelling in the l_w direction at the maximum speed considered. The corresponding effective battery used, $C_{BAT,used}$, for the N = 4 and N = 5 combinations for these days was, respectively, 67% and 63% of the theoretical capacity. With regard to the battery power, **Figure 5.23 (c)** and **(d)** shows the ESS normalized power for both cases analysed. It can be observed that the power used is also lower than the theoretical, $p_{BAT,f,W}$, for the same reasons discussed above.

upna Universidad Pública de Navarra Nafarroako Unibertsitate Publikoa

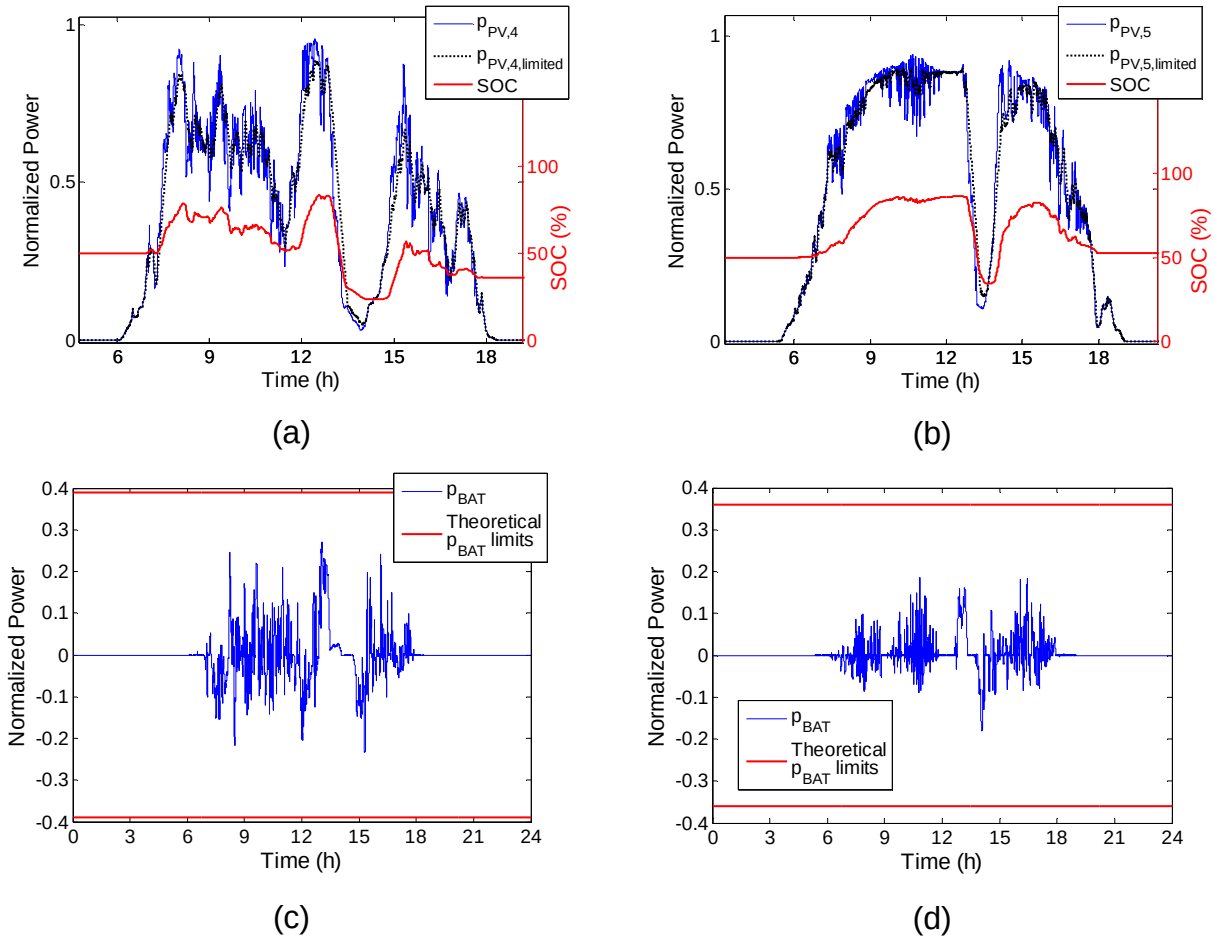

***Figure 5.23**: SOC evolution according to the calculated values of $C_{BAT,f}$ on (a) 16th April 2013 for the N=4 combination and (b) 1st August 2013 for the N=5 combination. Normalized ESS power evolution for (c) N=4 on 16th April 2013 and (d) N=5 on 1st August 2013.*

The same analysis was conducted for the whole year under study for all the possible combinations: 5 PV plants individually, 10 combinations of $N = 2$, 10 combinations of $N = 3$, 5 combinations of $N = 4$ and 1 combination of $N = 5$. As can be seen in **Figure 5.24**, the effective capacity used to mitigate the worst case fluctuation to take place that year, $C_{BAT,used}$, for all the possible combinations simulated is less than the $C_{BAT,f}$ calculated on the basis on the worst fluctuation model for a PV fleet due to the mentioned reasons.

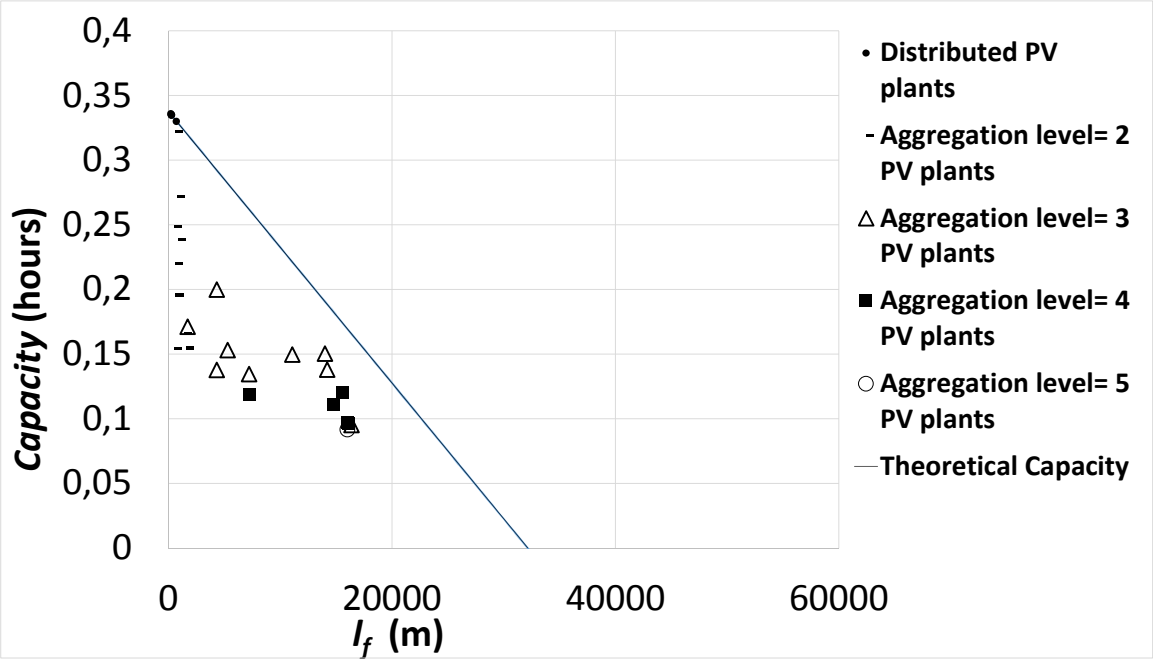

***Figure 5.24**; $C_{BAT,f}$ and $C_{BAT,used}$ for all possible combinations for N = 1…5 PV plants.*

Finally, **Figure 5.25 (a)** and **(b)** shows the SOC evolution for the whole year analysed for both combinations, $N = 4$ and $N = 5$ respectively. As can be observed, the implemented strategy works successfully with $C_{BAT,f}$. Note that in **Figure 5.25 (a)** and **(b)** all the theoretical $C_{BAT,f}$ is used due to the way the control strategy implemented operates and not because this was necessary. In other words, the strategy would have worked successfully with a smaller ESS calculated by Eq.(5.22) but using the minimum distance and maximum speed observed during the year under study. Moreover, **Figure 5.25 (c)** and **(d)** shows the normalized ESS power for the whole year for the cases analysed, showing that there are some days, in both cases, in which the normalized ESS power exceeds the theoretical limits.

upna Universidad Pública de Navarra Nafarroako Unibertsitate Publikoa

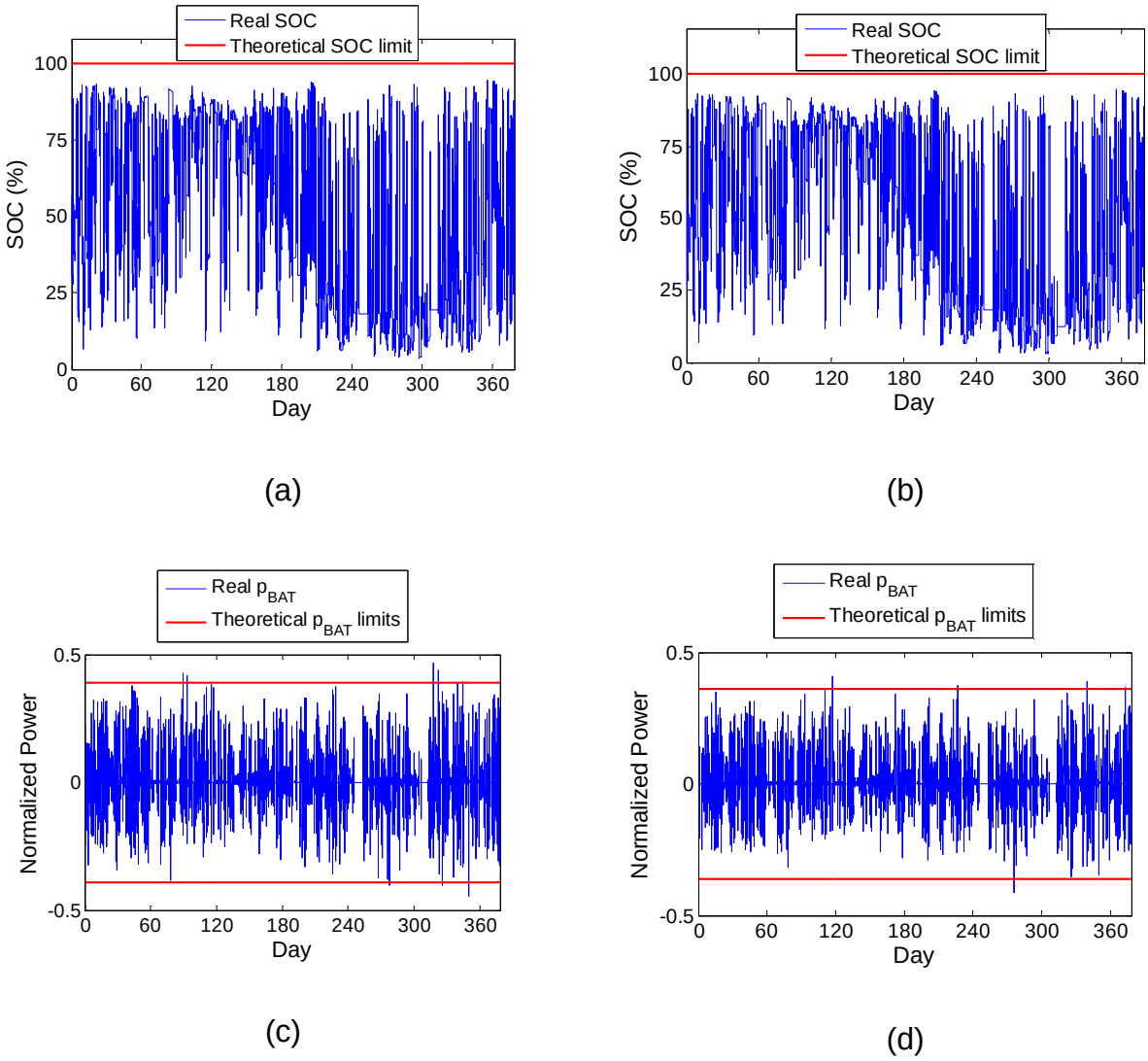

***Figure 5.25**: ESS SOC evolution during the whole year studied for (a) the N=4 combination and (b) the N=5 combination. ESS power evolution during the whole year studied for (c) N=4 and (d) N=5.*

Figure 5.26 (a) and **(b)** show the PV power of both the PV fleet and the individual PV plants for one of these days (23rd December 2013) for the *N* = 5 combination. In this figure, it can be observed that the maximum battery power takes place with continuously moving cumulus clouds which affect all the PV plants. **Figure 5.26 (c)** shows that these kind of days give rise to high battery power values but small SOC variations. This is due to the fact that there are very fast irradiance changes that strongly affect the power but not very much the SOC, which is linked with the integral of the battery power.

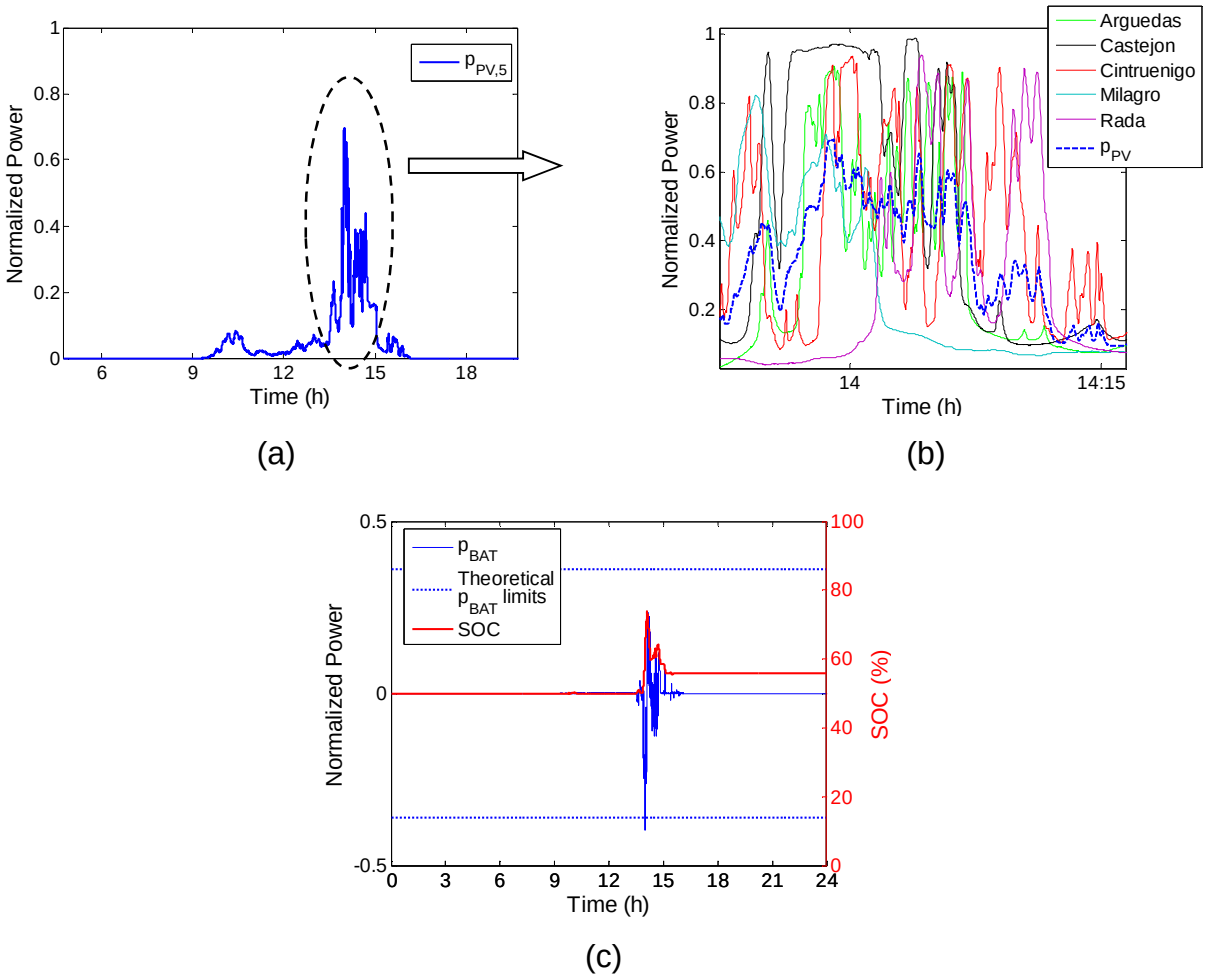

***Figure 5.26**: Specific analysis of the 23rd December 2013. (a) Normalized PV power of the PV fleet. (b) Normalized PV power of the individual PV plants and the PV fleet. (c) ESS SOC and power evolution.*

Logically, when this last power fluctuation takes place, the battery will either have to absorb or provide this power, something that also needs to be taken into account in the ESS power sizing. In this way, the battery will be able to operate with the maximum power fluctuation that can take place in the PV fleet. This value has been subject to study by other authors (Hoff and Perez, 2010; Marcos et al., 2012) showing that the maximum fluctuations that can take place in an aggregation of regularly distributed PV plants spaced sufficiently far apart, is equal to the inverse of the square root of the number of PV plants. Therefore, in order to size the battery power for a PV fleet, two criteria must be taken into account. On the one hand, the battery power based on the worst fluctuation model, $p_{BAT,f,W}$, Eq.(5.23) and, on the other hand, the maximum potential power fluctuations in a PV plant aggregation. Hence, the maximum required normalized battery power for a PV fleet is given by Eq.(5.24):

$$p_{BAT,f} = \max\left(p_{BAT,f,W}, 1/\sqrt{N} \right) = \max\left(\frac{1}{100}\left[90 - \tau_W \cdot r_{MAX}\,(1 + \ln \frac{90}{\tau W \cdot r_{MAX}}) \right], 1/\sqrt{N} \right) \quad (5.24)$$

Figure 5.27 shows both the maximum battery power used, $p_{BAT,used}$, and the maximum required normalized battery power, $p_{BAT,f}$, for the whole year under study and for all the combinations analysed. It can be observed that in all cases $p_{BAT,used}$ is below or equal the limits established by $p_{BAT,f}$. Note that, for single PV plants, the battery power required is around 0.8, while for the N = 5 combination the battery power required drops to 0.465 resulting in a battery power saving of around 50%.

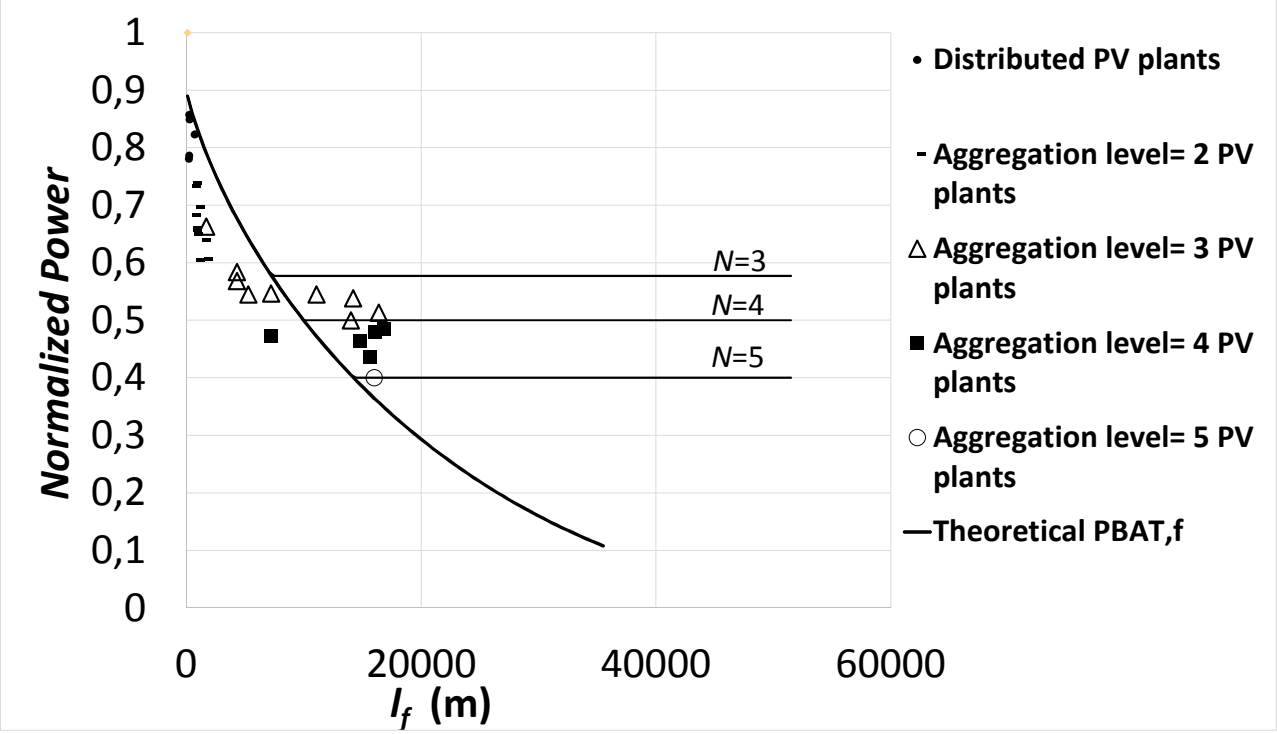

***Figure 5.27**: (a) Theoretical limit for the battery power, $p_{BAT,f}$, and maximum battery power used, $p_{BAT,used}$, for all possible combinations for N = 1…5 PV plants.*

As was mentioned earlier, the study was conducted with normalized PV powers. In this way, $C_{BAT,f}$ is expressed in [hours] and $p_{BAT,f}$ per unit. It is easy to calculate $C_{BAT,f}$ in [Wh] and $p_{BAT,f}$ in [W] by simply multiplying the result by $\sum_{i=1}^{N} P_{n,i}$.

upna Universidad Pública de Navarra Nafarroako Unibertsitate Publikoa

5.3.3 A comparison of storage requirements: distributed versus centralized solutions

Now that a model has been developed to size the ESS for both a single PV plant and a PV fleet as a function of the allowable r_{MAX}, this section carries out a study of the storage requirements savings when advantage is taken of the smoothing effect on PV power by geographical dispersion by allocating a centralized instead of a distributed ESS. **Figure 5.28** shows the comparison of the results for r_{MAX} = 2%/min and for the two solutions for the 1st August 2013 for the N = 5 combination. Both solutions comply with the r_{MAX} imposed but it can be seen how the power injected into the grid in the distributed solution ($p_{G,D}(t)$) has a smoother power output than the centralized solution, $p_{G,C}(t)$. This is due to the fact that $p_{G,C}(t)$ has been exactly limited to r_{MAX} while $p_{G,D}(t)$ has been limited to r_{MAX} at each PV plant individually, considered to be an over-limiting of the PV power output. This is good in principle but what happens is that the differences between the total PV power generated, $p_{PV,5}(t)$, and $p_{G,D}(t)$ and the differences between $p_{PV,5}(t)$ and $p_{G,}(t)$ must be either absorbed or provided by the ESS in each option. It is clear that at any given time $p_{G,C}(t)$ is closer to $p_{PV,5}(t)$, a fact that makes it possible to save on the ESS capacity requirement. ESS capacity requirements for the N = 5 combination analysed are $C_{BAT,f}$ = 0.17 h (Eq.(5.22)) for the centralized solution and $\sum_{i=1}^{N=5} C_{BAT,i} = 0.34$ h (with $l_{Arguedas}$ = 200m, $l_{Castejón}$ = 265m, $l_{Cintruénigo}$ = 245m, $l_{Milagro}$ = 700m and l_{Rada} = 230m) for the distributed solution. In this way, the centralized solution saves half the required capacity needed in the distributed solution. It is worth noting that the PV plants analysed occupy 315 km^2, an area which is similar to that of a small island with a stand-alone electricity network. This is where it is worthwhile taking advantage of the smoothing effect of geographical dispersion.

upna Universidad Pública de Navarra Nafarroako Unibertsitate Publikoa

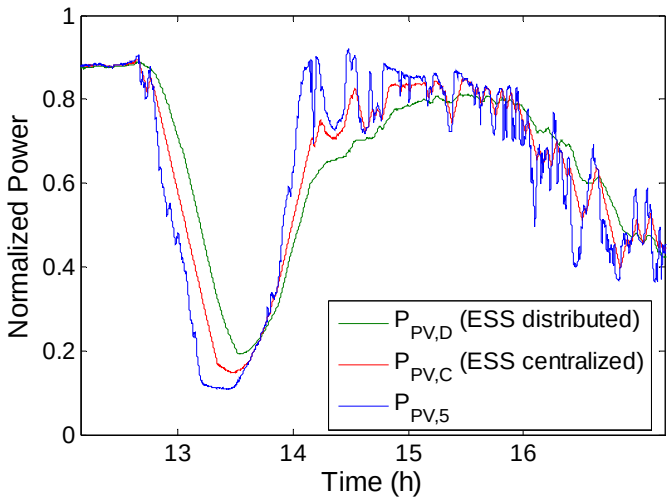

***Figure 5.28**: Comparison of the results for the two configurations analysed, centralized and distributed ESS, on the 1st August 2013 for the N=5 combination.*

Figure 5.29 (a) and **(b)** shows both the capacity and power savings as a function of the shortest dimension of the PV fleet under consideration for r_{MAX} = 2%/min. From a minimum l_f = 15000 m and N = 5, it is possible to appreciate considerably savings in the required capacity and power for the ESS of up to 45%. Moreover, from l_f = 25000 m it is possible to save up to 80% of the ESS capacity requirement. It must be remembered, that two criteria need to be taken into account when sizing the battery power: the worst fluctuation model for the PV fleet and the maximum fluctuations. For the N = 5 combination, regardless of the minimum l_f, the power savings cannot be greater than 50 %. In any case, these savings are considered to be a considerable cost saving, not only due to the lower capacity required but also due to the savings in the ESS converters.

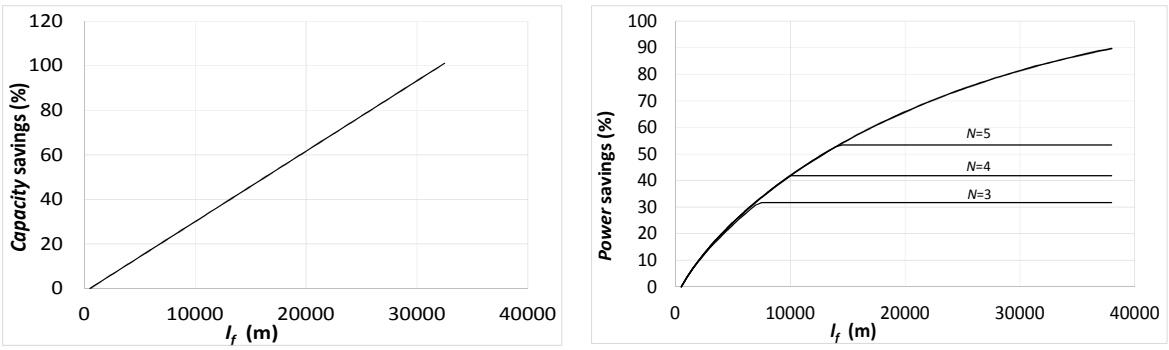

(a) (b)

***Figure 5.29**: (a) $C_{BAT,f}$ and (b) $p_{BAT,f}$ saving as a function of the shortest dimension of the PV fleet.*

Up to this point, the entire study has been focussed on r_{MAX} = 2%/min. However, Eq.(5.22) and Eq.(5.24) make it possible to calculate the ESS storage requirements, $C_{BAT,f}$ and $P_{BAT,f}$ for any l_f and r_{MAX}. **Figure 5.30 (a)** and **(b)** shows the results for both $C_{BAT,f}$ and $P_{BAT,f}$ for a regularly distributed PV fleet. In the case of $P_{BAT,f}$, the limit due to the maximum fluctuation that can occur in the PV fleet is not included. In this way, **Figure 5.30 (b)** is only valid for a large number of aggregated PV plants, when this last limit is almost negligible. Analysing both graphs, it can be observed how geographical dispersion is an important natural smoothing factor to mitigate short-term PV output variability even for r_{MAX} = 1%/min, where, for l_f >33 km, and for at least 5 aggregated, regularly distributed PV plants , the centralized solution enables further savings of up to 50% in capacity and power.

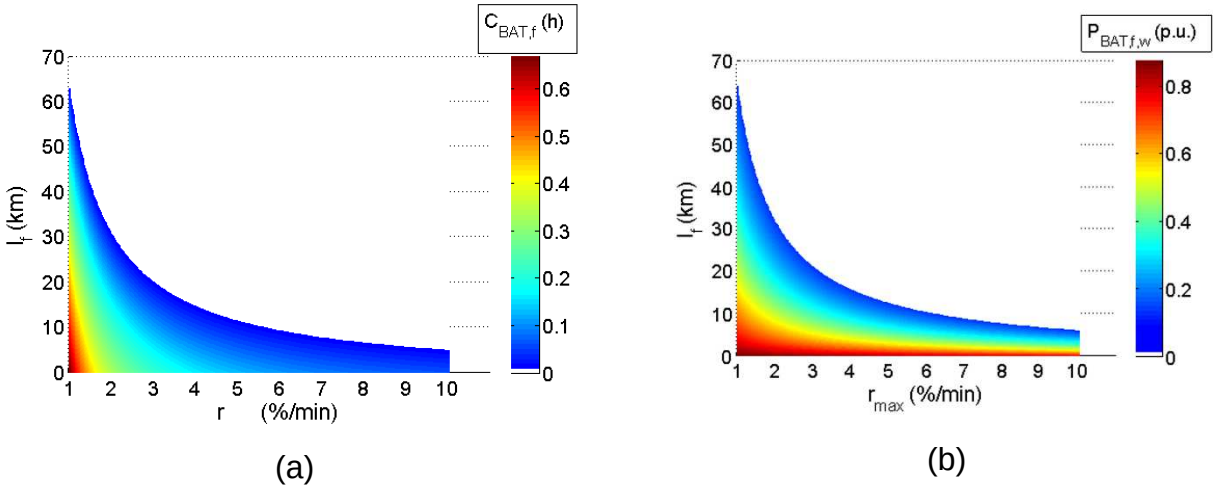

(a) (b)

***Figure 5.30**: ESS capacity requirements, $C_{BAT,f}$, and power requirements according to the worst fluctuation model for a PV fleet, $P_{BAT,f,W}$, for different l_f and r_{MAX}.*

5.3.4 Conclusions

The aim of this section was to analyse the savings in the energy storage requirements for smoothing short-term PV power fluctuations in a regularly distributed PV fleet using a centralized ESS instead of a distributed one. An analysis was made of the PV power fluctuations of a PV fleet when a front of clouds covers all the PV plants and the worst case fluctuation was calculated. An analytical theoretical model for this fluctuation has been proposed, providing information on the minimum energy storage requirements needed to comply with a maximum allowable ramp-rate value. In the case of the power required for the ESS, two criteria must be taken into account for this

upna Universidad Pública de Navarra Nafarroako Unibertsitate Publikoa

calculation: the worst case fluctuation for a PV fleet and the maximum potential fluctuations in an aggregation of regularly distributed PV plants spaced sufficiently far apart. The general validity of the model has been shown to work successfully with 1 s real data taken from five PV plants located in Navarre (Spain). It has been simulated all possible combinations in the course of a full year, for N = 1…5 plants. Regardless of the PV plant combination chosen, all the PV plants are able to operate correctly with the minimum theoretical effective requirements based on the proposed PV fleet model that complies with a maximum allowable ramp-rate given by a grid code regulation. The centralized solution for the five PV plants under study and for r_{MAX} = 2%/min, is able to correctly operate with half the storage requirements needed in the distributed solution, resulting in considerably cost savings.

upna Universidad Pública de Navarra Nafarroako Unibertsitate Publikoa

6

CONCLUSIONS, CONTRIBUTIONS AND FUTURE LINES

"Learn from yesterday, live for today, hope for tomorrow. The important thing is not to stop questioning."
Albert Einstein (1879-1955)

6.1 FINAL CONCLUSIONS

The huge growing of large-scale PV plants worldwide is leading to changes in the TSO's requirements in order to deliver PV power without creating reliability, stability and power quality problems in the main electrical grid. In that way, new restrictions in recent grid codes have appeared including new criteria to make it easier for the TSO to react appropriately against harmful irradiance fluctuations - i.e., PV power fluctuations - with a time scale of less than 10 minutes. This ensures that the power variation of PV generators does not exceed the dynamics with which conventional plants in the system may increase or reduce power, so that the production and consumption balance is not altered at any time. The compliance with these new requirements demands the incorporation of some kind of ESS. The installation of an ESS has a major impact on the energy/economic balance of the PV system, playing a key role in the viability of the future PV systems due to their high costs and reduced shelf life.

Among the first part of this thesis dissertation, particularly in chapter 3, it has been quantified the storage requirements needed to smooth short-term PV power fluctuations based on different control strategies for any PV plant size and ramp-rate limitation. Basically, battery requirements are essentially imposed by the worst fluctuation. An

upna Universidad Pública de Navarra Nafarroako Unibertsitate Publikoa

analytical-theoretical model for this fluctuation case has been proposed and validated, by comparing the corresponding battery requirements obtained through the model with the ones derived from detailed simulations based on real power data. Then, an equation based on the worst fluctuation model is given and it is applicable to any of the strategies analysed. The control strategy selected for the ESS is a crucial decision and storage requirements will depend on the strategy chosen. The first strategy that was studied is the classical ramp-rate control, $RR_{classical}$, whose great advantage is that only acts when the fluctuation exceeds the maximum allowable ramp-rate value, a fact that implies low ESS losses and cycling degradation. However, the main disadvantage was that as the sign of the first fluctuation was unknown, a double capacity battery was required to absorb both the upwards and downwards fluctuation setting the SOC reference at 50%. The second strategy studied is the moving average control, MA, which is able to correctly operate with almost half the capacity (56%) required in the classical ramp-rate control. At first instance, its great advantage is the use of less ESS capacity at the expense of an energy increase through the ESS which implied higher ESS losses (>1%) and cycling degradation when considering a lithium-ion system as the ESS (≈ 10%). Finally, trying to reduce the capacity of the classical ramp-rate control strategy while maintaining the low ESS losses and cycling degradation rate, the step control strategy was proposed. It was able to reduce the capacity based on the strictly compliance with the maximum ramp constraint for the defined time window and higher but not below. The saving in the required capacity reach 11.76%.

Moreover, in an attempt of reducing the capacity required and go beyond the state of the art, two novel strategies are proposed in chapter 4, the ramp-rate control strategy using the PV inverters, $RR_{inverter,}$ and the ramp-rate control strategy based on the PV plant model, $RR_{clear\text{-}sky}$. In the first strategy, the ramping-up events are limited with the inverters by making them to operate at a point other than the MPP which makes possible to comply with a certain variation per minute during upward fluctuations. In this case, the ESS is only needed during ramping down events and, consequently, the capacity needed is half that required in $RR_{classical}$ and both ESS losses (<0.2%) and cycling degradation (<1.4%) are very low. The main disadvantage of this control is that it involves inverter limitation losses that reach 9.09% of the total production. The second strategy proposed was the $RR_{clear\text{-}sky}$ which let to work with half the capacity required in $RR_{classical}$ but without

upna Universidad Pública de Navarra Nafarroako Unibertsitate Publikoa

any loss due to inverter limitation at the expense of doubling the cycling degradation (2.56%) of $RR_{inverter}$. In short, it is clear that both $RR_{inverter}$ and $RR_{clear-sky}$ are the best options when implementing a control strategy to comply with a maximum allowable ramp-rate limitation. However, depending on the ESS technology, the decision of choosing one strategy or another will be made. In this study, the ESS is supposed to be a lithium-ion battery which involves cycling degradation rates that make it necessary to do a detailed economic analysis of implementing one or another of these strategies.

With the aim of minimize even more the ESS requirements, chapter 5 try to take advantage of the well-known smoothing effect due to geographical dispersion by proposing a sizing method for an ESS allocated in a network node in which a number of PV plants converge.

To do so, the worst fluctuation model has been extrapolated from a PV plant to a PV fleet. Simply by knowing the geometric shape of the surface occupied by any regularly distributed PV plant fleet combination and maximum allowable ramp-rate, it is determined the maximum power and minimum energy storage requirements alike. Moreover, it has also been analysed the savings in the energy storage requirements for smoothing short-term PV power fluctuations in a regularly distributed PV fleet using a centralized ESS instead of a distributed one. The centralized solution for the five PV plants under study and for r_{MAX}=2%/min was able to correctly operate with half the energy and power storage requirements needed in the distributed solution resulting in considerably cost savings.

Finally, also regarding with the aggregation of PV plants, another issue motivated from the point of view of both TSO and DSO has come into light. A practical tool that enables to simulate the fluctuations generated in electricity networks by a fleet of dispersed PV plants, solely based on irradiance data measured at one single location is proposed. This is of particular interest for both TSO and DSO as they can simulate PV production profiles being proved to be extremely useful and even more nowadays when PV technology is gaining strength in distributed generation. This simple model has been satisfactorily used to quantify the power variability of the PV fleet, simply by defining two parameters: mean plant size and the number of plants in the PV fleet. Specifically, the model reliably reproduces the critical parameters for the grid operator, such as maximum fluctuation or the reserves required to offset these fluctuations. It is also helpful for the

upna Universidad Pública de Navarra Nafarroako Unibertsitate Publikoa

design of new PV projects studying its impact in the main electrical grid and even it could be integrated in the grid operator simulation tools.

6.2 CONTRIBUTIONS

The main results from this thesis dissertation are presented in this section:

Contribution to international journals

- De la Parra, I., Marcos, J., García, M., Marroyo, L., 2015. "Energy Storage Requirement for PV power ramp-rate control in a PV fleet," submitted.
- Marcos, J., de la Parra, I., García, M., Marroyo, L., 2015. "Simulating the variability of large PV plants," submitted.
- De la Parra, I., Marcos, J., García, M., Marroyo, L., 2015. "Control strategies to use the minimum energy storage requirement for PV power ramp-rate control," Sol. Energy 111, 332–343. doi:10.1016/j.solener.2014.10.038
- Marcos, J., de la Parra, I., García, M., Marroyo, L., 2014. "Control Strategies to Smooth Short-Term Power Fluctuations in Large Photovoltaic Plants Using Battery Storage Systems," Energies 7, 6593–6619. doi:10.3390/en7106593

- ***Contribution to international conferences***

- De la Parra, I., Marcos, J., García, M., Marroyo, L., 2014. "Minimizing Energy Storage Requirement for PV Power Ramp-Rate Limitation Controlling the Inverters MPPT," in: 29th European Photovoltaic Solar Energy Conference and Exhibition. Amsterdam, pp. 2376–2379.

- ***Participation in public R&D projects***

- Seventh Framework Programme of the European Commission with the project PVCROPS (Photovoltaic Cost R€duction, Reliability, Operational Performance, Prediction and Simulation), Grant Agreement no: 308468, November 2012-October 2015.

upna Universidad Pública de Navarra Nafarroako Unibertsitate Publikoa

- R&D national plan Project, “Technologies for the grid integration of renewable energies: power electronics, storage, energy management and interaction,” DPI2013-42853-R., Spanish Ministry of Economy and Competitiveness, Public University of Navarre (UPNA), 2014-2016.

- ***Participation in private R&D projects***

- Collaborative project between Acciona Energía and the Public University of Navarre in the framework of the ILIS Project. “Innovative Lithium-Ion System management design for MW solar plants.” March 2011 - December 2012. (OTRI number 2010-024-093).

- ***International presentations***

During the process of this investigation, different presentations were made in order to disseminate the important results.

- “Management of PV power generation: less variability and more predictability.” in 29th European Photovoltaic Solar Energy Conference and Exhibition PVCROPS Parallel Event, “Grid-connected PV systems: Field testing, performance monitoring and energy storage.” Amsterdam, 24th September 2014.

- “PV energy management and storage integration.” Intersolar Europe 2014, PVCROPS Side Event, Industry showcase. Munich, 4th June 2014.

- ***International seminar***

Furthermore, a seminar was also carried out to disseminate the more important results of this work.

- “Security in PV generation. Making PV fluctuation more predictable.” PVCROPS seminar at ELIA (Belgium’s electricity transmission system operator) offices. Brussels, 2nd April 2014.

- ***Final master degree projects***

In addition, two final master degree projects arose from this thesis, in which the author performed tutoring tasks:

upna Universidad Pública de Navarra Nafarroako Unibertsitate Publikoa

- Atarratze Rota Villanueva. “PV systems technology evolution for the compliance with new standards and grid codes.” Final project of the Master in renewable energies: electrical generation. June 2014.

- Josu Zamarbide Ducun. “Short and medium-term forecasting of solar radiation.” Final project of the Master in renewable energies: electrical generation. June 2014.

6.3 FUTURE WORK

The dramatically reduction in the costs of the PV technology (costs of 0.50$/Wp in the 2013) has led solar PV energy to be below retail electricity prices in several countries and particularly in a number of islands. This situation has supposed the appearance of new grid codes that impose a maximum allowable ramp-rate restriction with the main objective of the effective control of the PV power fluctuations. Although the first steps dealing with these new grid codes have been carried out in this thesis dissertation, the following lines of research are suggested below:

- The ramp-rate control strategy using the PV inverters proposed in chapter 4, supposes that there is no communication system between the inverters of the PV plant. In this way, all the inverters limit the ramping up events to the maximum allowable ramp rate restriction. The existence of communication between the inverters would let to fix the limit of the sum of the total PV power instead of the power at each inverter. On the other hand, if the ESS is not fully charged, it can take part together with the inverters in the limitation of the PV power ramping up events. The ESS can store part of the energy that was previously depreciated. In this way, a study of the reducing the inverter limitation losses should be carried out.

- The methodology proposed to calculate ESS requirements lets exhaustive cost-effective analysis about which ESS technology is better to smooth short term PV output variability.

upna Universidad Pública de Navarra Nafarroako Unibertsitate Publikoa

- Large PV fluctuations are unusual during the year and, consequently, ESS is scarcely used. This fact come into light the potential use of the ESS for ancillary services (frequency regulation or time shifting), in an endeavour to take full economical advantage of its installation. To do so, a fluctuation prediction tool would be necessary to determine the critical times in order to ensure the smart management of the energy stored.

- The calculation of the ESS energy storage requirements is based on the worst fluctuation model. This model has shown to correctly work within the PV technology. However, not only is this model valid for the solar energy but also for any other kind of renewable generation whose limits are well-known. In this way, it would be of particular interest to extrapolate this model to other kind of renewable energies, for instance, to wind energy.

upna Universidad Pública de Navarra Nafarroako Unibertsitate Publikoa

upna Universidad Pública de Navarra Nafarroako Unibertsitate Publikoa

NOMENCLATURE

Symbol	Description	Units
A	Active area of the PV generator	m^2
$A_{MA,ramp}$	Area between ramp-rate curve and moving-average curve	m^2
A_{tri}	Area of each triangle between the area of ramp-rate control strategy and step-rate control strategy	m^2
a	Slope of the adjusting line of τ (0.042 s/m) (chapter 4)	s/m
a	Adjusting coefficient (chapter 5)	-
a_{obs}	Observed slope of the adjusting line of τ_{obs}	s/m
a_w	Slope of the adjusting line of τ_w	s/m
b	Adjusting coefficient of τ (-0.5 s) (chapter 4)	s
b	Adjusting coefficient (chapter 5)	-
B_0	Solar constant (1367 W/m^2)	W/m^2
$B_c(0)$	Direct horizontal irradiance	W/m^2
$B_c(\beta,\alpha)$	Beam irradiance in the plane of the generator	W/m^2
C_{BAT}	ESS capacity	Wh
$C_{BAT,c}(t)$	ESS capacity required to charge in the event of the maximum upward fluctuation at instant *t*	Wh
$C_{BAT,d}(t)$	ESS capacity required to discharge in the event of the maximum downward fluctuation at instant *t*	Wh
$C_{BAT,f}$	ESS capacity for the PV fleet	h

upna Universidad Pública de Navarra Nafarroako Unibertsitate Publikoa

$C_{BAT,f,obs}$	Observed ESS capacity for the PV fleet	h
$C_{BAT,loss}$	ESS Annual degradation due to cycling	Wh
$C_{BAT,MA}$	ESS capacity for the moving-average control strategy	Wh
$C_{BAT,ramp}$	ESS capacity for the ramp-rate control strategy	Wh
$C_{BAT,ramp,advanced}$	ESS capacity for the advanced ramp-rate control strategies	Wh
$C_{BAT,used}$	Effective ESS capacity used	Wh
$D_c(0)$	Diffuse horizontal irradiance	W/m^2
$D_c(\beta,\alpha)$	Diffuse irradiance in the plane of the generator	W/m^2
$DARR$	Daily aggregate ramp rate for a generic power series data	-
$DARR_{N,real}$	Daily aggregate ramp rate for the power series generated by *N* PV plants	-
$DARR_{N,sim}$	Daily aggregate ramp rate for the power series simulated by *N* PV plants	-
$E_{BAT}(t)$	ESS energy at instant *t*	Wh
$E_{BAT,end\ day_{i-1}}$	ESS energy at the end of the previous day	Wh
$E_{BAT,beginning\ day_i}$	ESS energy at the beginning of the day	Wh
$E_{BAT,MAX}$	ESS Maximum energy	Wh
$E_{BAT,MIN}$	ESS Minimum energy	Wh
$E_{BAT,RAMP}$	ESS energy for the ramp-rate control strategy	Wh
$E_{BAT,REF}$	ESS energy reference	Wh
$E_{BAT,REF}(t)$	ESS energy reference at instant *t*	Wh
$E_{step-ramp}$	Energy saving for a PV power plant using the step-rate control strategy instead of the ramp-rate control strategy	Wh
F_d	Diffuse angular function	-
G^*	Irradiance under standard test conditions (1000W/m^2)	W/m^2

upna Universidad Pública de Navarra Nafarroako Unibertsitate Publikoa

$G(t)$	Irradiance at an instant *t*	W/m^2
$G^i(t)$	Irradiance of PV plant *i* at an instant *t*	W/m^2
$G_c(\alpha,\beta)$	Irradiance in the plane of the generator	W/m^2
$G_c(t)$	Irradiance in the plane of the generator at instant *t*	W/m^2
G_{eff}	Effective irradiance	W/m^2
$g_N(t)$	Normalized irradiance measured at instant *t* in the aggregation of *N* locations	p.u,
k_0, k_1, k_2	Experimental parameters to calculate inverters efficiency	-
K	Controller gain constant	h^{-1}
l	Shortest dimension of the perimeter of the PV plant	m
l_{obs}	Distance travelled by a front of clouds	m
l_w	Shortest distance that a front of clouds has to travel to cover all the PV fleet	m
$Max(\Delta P_{\Delta t,N})$	Maximum power fluctuation for a time interval, Δt, for a given number *N* of PV plants grouped	%
$Max(\Delta P_{\Delta t,N,real})$	Maximum power fluctuation measured for a time interval, Δt, for a given number *N* of PV plants grouped	%
$Max(\Delta P_{\Delta t,N,sim})$	Maximum power fluctuation simulated for a time interval, Δt, for a given number *N* of PV plants grouped	%
m	Adjusting coefficient (chapter 3)	S·%/min
m	Relative optical air mass (chapter 4)	-
m	Adjusting coefficient (chapter 5)	-
n	Number of times the duration of the sampling time Δt	-
N	Number of PV plants grouped	-
N_{cycl}	Number of cycles	-
$N_{cycl,\max}$	Number of maximum possible cycles	-
$N_{\max}$	Number of maximum cycles	-

upna Universidad Pública de Navarra Nafarroako Unibertsitate Publikoa

N_{tri}	Number of triangles between the area of ramp-rate control strategy and step-rate control strategy	-
$P*$	Maximum power under standard test conditions.	W
$P(t)$	Power generated at instant *t*	W
P_{AC}	AC power	W
P_{BAT}	ESS power	W
p_{BAT}	Normalized ESS power	p.u.
$P_{BAT}(t)$	ESS power at instant *t*	W
$P_{BAT,MAX}$	ESS maximum power	W
$p_{BAT,f}$	Maximum normalized ESS power in a PV fleet	p.u.
$p_{BAT,f,obs}$	Maximum normalized ESS power for the fluctuation observed in the PV fleet	p.u.
$p_{BAT,f,W}$	Maximum normalized ESS power in a PV fleet for the worst fluctuation case	p.u.
$p_{BAT,MAX}$	Normalized ESS maximum power	p.u.
$P_{BAT,ramp}(t)$	ESS power for the ramp-rate control strategy at instant *t*	W
P_{DC}	DC power	W
$P_{ESS}(t)$	ESS power at instant *t*	W
$P_G(t)$	Grid power at instant *t*	W
$P_{G,MA}(t)$	Grid power at instant *t* for the moving-average control strategy	W
$P_{G,ramp}(t)$	Grid power at instant *t* for the ramp-rate control strategy	W
$P_{G,STEP}(t)$	Grid power at instant *t* for the step control strategy	W
$P_{G,ramp}(t)$	Grid power at instant *t* for the moving-average control strategy	W
P_I	Inverter nominal power output	W
P_L	Power losses	W
$P_{PV,\lim,inverter}(t)$	Sum of the PV power output with the ramping-up variations limited by the inverters at instant *t*	W

upna Universidad Pública de Navarra Nafarroako Unibertsitate Publikoa

P_n	Nameplate power	W
P_N	Power of *N* PV plants	W
$P^i(t)$	Power output of PV plant *i* at instant *t*	W
$P_n^{\ i}$	Transformer power at the common coupling point of the *i*-th PV plant	W
$p_N(t)$	Normalized PV power output at instant *t of* an aggregation of *N* PV plants	p.u.
$p_{N,real}(t)$	Measured normalized PV power output at instant *t of* an aggregation of *N* PV plants	p.u.
$p_{N,sim}(t)$	Simulated normalized PV power output at instant *t of* an aggregation of *N* PV plants	p.u.
$P_{PV}(t)$	PV power at instant *t*	W
$p_{PV}(t)$	Normalized PV power at instant *t*	p.u.
$p_{PV,f,obs}(t)$	Normalized PV power of the fluctuation observed in the PV fleet at instant *t*	p.u.
$p_{PV,f,W}(t)$	Normalized PV power of the worst fluctuation case in a PV fleet at instant *t*	p.u.
$P_{PV,MPP}(t)$	PV power available with inverters working at MPP at instant *t*	W
$p_{PV,TOTAL}(t)$	Normalized sum of the PV power of all the PV plants at instant *t*	p.u.
$p_{real}(t)$	Real normalized PV power at instant *t*	p.u.
$p_{sim}(t)$	Simulated normalized PV power at instant *t*	p.u.
$\Delta P_{\Delta t}(t)$	Power fluctuation for a time interval, Δt, at instant *t*	%
$\Delta P_{PV,1\min}(t)$	Power fluctuation for 1 minute interval at instant *t*	%
$\Delta p_{PV,TOTAL,1\min}(t)$	Normalized power fluctuation for 1 minute interval at instant *t* for all the PV plants	%
$\Delta P_{\Delta t,N}(t)$	Power fluctuation for a time interval, Δt, at instant *t* for a given number *N* of PV plants grouped	%
r	Ramp-rate value	%/min
r_{max}	Maximum allowable ramp-rate limitation	%/min
$R_c(\beta,\alpha)$	Reflected irradiance in the plane of the generator	W/m^2

upna Universidad Pública de Navarra Nafarroako Unibertsitate Publikoa

s	Laplace operator	rad·s^{-1}
S	PV plant Surface	m^2
$\overline{S}$	Mean surface of *N* PV plants	m^2
SOC	ESS state of charge	%
$SOC\ (t)$	State of charge at instant *t*	%
SOC_{MAX}	ESS maximum state of charge	%
SOC_{MIN}	ESS minimum state of charge	%
t	Time	s
t_{bat}	Effective storage time	s
$t_{P_{BAT},MAX}$	Time when P_{BAT} gets a maximum	s
T	Time window (chapter 3)	s
T	Signal length (chapter 5)	-
T_C^*	Cell temperature under standard test conditions (25°C)	°C
$T_C(t)$	Cell temperature at instant *t*	°C
T_L	Linke turbidity	-
T_R	Time span	s
T_{rd}	Diffuse transmission function at zenith	-
X_k	Generic variable in the frequency domain	-
x_t	Generic variable in the time domain	-
α	Angle of incidence	deg
β	PV generator orientation	deg
Δt	Time interval between two measurements.	s
ε_0	Eccentricity correction	-
δ_R	Integral Rayleigh optical thickness	m
η^*	Efficiency under standard test conditions.	%
$\eta(t)$	PV module efficiency as a function of the irradiance and cell temperature	%

upna Universidad Pública de Navarra Nafarroako Unibertsitate Publikoa

η_I	Inverter efficiency	%
η_{PEC}	Power electronic converter performance	%
η_{BAT}	Battery performance	%
γ	Power temperature coefficient	%·ºC^{-1}
γ_s	Solar elevation angle	deg
τ	Time constant	s
τ_{obs}	Observed time constant	s
τ_w	Time constant for the worst fluctuation case in a PV fleet	s
ω_t	Angular frequency	rad·s^{-1}

upna Universidad Pública de Navarra Nafarroako Unibertsitate Publikoa

upna
Universidad Pública de Navarra
Nafarroako Unibertsitate Publikoa

REFERENCES

Alam, M.J.E., Muttaqi, K.M., Sutanto, D., 2014. A Novel Approach for Ramp-Rate Control of Solar PV Using Energy Storage to Mitigate Output Fluctuations Caused by Cloud Passing. IEEE Trans. Energy Convers. 1–12.

Apt, J., 2007. The spectrum of power from wind turbines. J. Power Sources 169, 369–374. doi:10.1016/j.jpowsour.2007.02.077

Arghandeh, R., Woyak, J., Onen, A., Jung, J., Broadwater, R.P., 2014. Economic optimal operation of Community Energy Storage systems in competitive energy markets. Appl. Energy 135, 71–80. doi:10.1016/j.apenergy.2014.08.066

Atwa, Y.M., El-Saadany, E.F., 2010. Optimal Allocation of ESS in Distribution Systems With a High Penetration of Wind Energy. IEEE Trans. Power Syst. 25, 1815–1822.

Beltran, H., Bilbao, E., Belenguer, E., Etxeberria-otadui, I., Rodriguez, P., 2013. Evaluation of Storage Energy Requirements for Constant Production in PV Power Plants. IEEE Trans. Ind. Electron. 60, 1225–1234.

Beltran, H., Swierczynski, M., Luna, a., Vazquez, G., Belenguer, E., 2011. Photovoltaic plants generation improvement using Li-ion batteries as energy buffer. 2011 IEEE Int. Symp. Ind. Electron. 2063–2069. doi:10.1109/ISIE.2011.5984478

Bird, R., Hulstrom, R.L., 1980. Direct insolation models. Trans. ASME J. Sol. Energy Eng. 103 182–192.

Boicea, V. a., 2014. Energy Storage Technologies: The Past and the Present. Proc. IEEE 102, 1777–1794. doi:10.1109/JPROC.2014.2359545

Bozchalui, M.C., Sharma, R., 2014. Optimal Operation of Energy Storage in Distribution Systems with Renewable Energy Resources, in: 2014 Clemson University Power Systems Conference (PSC).

Bradbury, K., Pratson, L., Patiño-Echeverri, D., 2014. Economic viability of energy storage systems based on price arbitrage potential in real-time U.S. electricity markets. Appl. Energy 114, 512–519. doi:10.1016/j.apenergy.2013.10.010

Byrne, R.H., Donnelly, M.K., Loose, V.W., Daniel, J., 2012. Methodology to Determine the Technical Performance and Value Proposition for Grid-Scale Energy Storage Systems A Study for the DOE Energy Storage Systems Program. A Study DOE Energy Storage Syst. Progr. (Nº. SAND2012-10639). Mont. Tech Univ. Mont. Butte, MT; Sandia Natl. Lab. (SNL-NM), Albuquerque, NM (United States), 2012.

Chanhom, P., Sirisukprasert, S., Hatti, N., 2013. A new mitigation strategy for photovoltaic power fluctuation using the hierarchical simple moving average, in: 2013 IEEE International Workshop on Inteligent Energy Systems (IWIES). Ieee, pp. 28–33. doi:10.1109/IWIES.2013.6698557

Cheng, F., Willard, S., Hawkins, J., Arellano, B., Lavrova, O., Mammoli, A., 2012. Applying battery energy storage to enhance the benefits of photovoltaics. 2012 IEEE Energytech 1–5. doi:10.1109/EnergyTech.2012.6304684

CRE, 2014. Reglas generales de interconexión al sistema eléctrico nacional [WWW Document]. URL http://www.cre.gob.mx/resolucion.aspx?id=7012

Curtright, A., Apt, J., 2008. The character of power output from utility scale photovoltaic systems. Prog. Photovoltaics Res. Appl. 16, 241–247. doi:10.1002/pip

Curtright, A.E., Apt, J., 2008. The character of power output from utility-scale photovoltaic systems. Prog. Photovoltaics Res. Appl. 16, 241–247. doi:10.1002/pip.786

Darras, C., Muselli, M., Poggi, P., Voyant, C., Hoguet, J.-C., Montignac, F., 2012. PV output power fluctuations smoothing: The MYRTE platform experience. Int. J. Hydrogen Energy 37, 14015–14025. doi:10.1016/j.ijhydene.2012.07.083

Datta, M., Senjyu, T., Yona, A., Funabashi, T., 2011. Photovoltaic Output Power Fluctuations Smoothing by Selecting Optimal Capacity of Battery for a Photovoltaic-Diesel Hybrid System. Electr. Power Components Syst. 39, 621–644. doi:10.1080/15325008.2010.536809

Datta, M., Senjyu, T., Yona, A., Funabashi, T., Kim, C.-H., 2010. Photovoltaic output power fluctuations smoothing methods for single and multiple PV generators. Curr. Appl. Phys. 10, S265–S270. doi:10.1016/j.cap.2009.11.027

Dufo-López, R., Bernal-Agustín, J.L., Contreras, J., 2007. Optimization of control strategies for stand-alone renewable energy systems with hydrogen storage. Renew. Energy 32, 1102–1126.

Dufo-López, R., Lujano-Rojas, J.M., Bernal-Agustín, J.L., 2014. Comparison of different lead–acid battery lifetime prediction models for use in simulation of stand-alone photovoltaic systems. Appl. Energy 115, 242–253.

Eclaeron, 2014. PV GRID PARITY MONITOR Commercial Sector 1st issue [WWW Document]. URL http://www.leonardo-energy.org/sites/leonardo-energy/files/documents-and-links/pv_gpm_3_commercial_2014.pdf (accessed 12.18.14).

upna Universidad Pública de Navarra Nafarroako Unibertsitate Publikoa

Ellis, A., Schoenwald, D., 2012. PV Output Smoothing with Energy Storage. Sandia Natl. Lab. Albuquerque, New Mex. 87185 Livermore, Calif. 94550 SAND2012-1.

Gee, A.M., Robinson, F.V.P., Dunn, R.W., 2013. Analysis of Battery Lifetime Extension in a Small-Scale Wind-Energy System Using Supercapacitors. IEEE Trans. Energy Convers. 28, 24–33. doi:10.1109/TEC.2012.2228195

Geiger, M., Diabate, L., Menard, L., Wald, L., 2002. A web service for controlling the quality of measurements of global solar irradiation. Sol. Energy 73, 475–480.

Gueymard, C., 1989. A two-band model for the calculation of clear sky solar irradiance, illuminance and photosynthetically active radiation at the earth surface. Sol. Energy 43, 252–265.

Han, X., Chen, F., Cui, X., Li, Y., Li, X., 2012. A Power Smoothing Control Strategy and Optimized Allocation of Battery Capacity Based on Hybrid Storage Energy Technology. Energies 5, 1593–1612. doi:10.3390/en5051593

Hansen, T., 2007. Utility Solar Generation Valuation Methods, USDOE Solar America Initiative Progress Report. Tucson Electr. Power, Tucson, AZ. doi:10.1002/tcr.201190008

Hay, J.E., Mckay, D.C., 1985. Estimating Solar Irradiance on Inclined Surfaces : A Review and Assessment of Methodologies. Int. J. Sol. Energy 3, 203–240.

Hay, J. E., Davis, J.A., 1980. Calculations of the solar radiation incident on an inclined surface, in: Proc. of First Canadian Solar Radiation Data Workshop, 59. Ministry of Supply and Services, Canada.

Hoff, T.E., Perez, R., 2010. Quantifying PV power Output Variability. Sol. Energy 84, 1782–1793. doi:10.1016/j.solener.2010.07.003

Hossain, K., Ali, M.H., 2014. Statistical Analysis of Ramp Rates of Solar Photovoltaic System Connected to Grid, in: Energy Conversion Congress and Exposition (ECCE), 2014 IEEE. pp. 2524–2531.

Hund, T.D., Gonzalez, S., Barrett, K., 2010. Grid-Tied PV system energy smoothing. 2010 35th IEEE Photovolt. Spec. Conf. 002762–002766. doi:10.1109/PVSC.2010.5616799

Ineichen, P., 2006. Comparison of eight clear sky broadband models against 16 independent data banks. Sol. Energy 80, 468–478. doi:10.1016/j.solener.2005.04.018

INGETEAM, 2014. INGECON SUN POWERMAX [WWW Document]. URL http://www.ingeteam.com/es-es/energia/energia-fotovoltaica/p15_24_36/ingecon-sun-powermax.aspx (accessed 1.30.14).

upna Universidad Pública de Navarra Nafarroako Unibertsitate Publikoa

Jantsch, M., Schmidt, H., Schmid, J., 1992. Results on the concerted action on power conditioning and control, in: 11th European Photovoltaic Solar Energy Conference. p. page 1589–1592.

Jewell, W.T., Ramakumar, R., 1987. The Effects of Moving Clouds on Electric Utilities with Dispersed Photovoltaic Generation. Energy Conversion, IEEE Trans. 2, 570–576. doi:10.1109/60.50805

Jewell, W.T., Unruh, T.D., 1990. Limits on cloud-induced fluctuation in photovoltaic generation. Energy Conversion, IEEE Trans. 5, 8–14. doi:10.1109/60.50805

Jolmson, J., Schenkman, B., Ellis, A., Quiroz, J., Lenox, C., 2012. Initial Operating Experience of the 1.2-MW La Ola Photovoltaic System. 38th IEE Photovolt. Spec. Conf. 2, 1–6.

Kakimoto, N., Satoh, H., Takayama, S., Nakamura, K., 2009. Ramp-Rate Control of Photovoltaic Generator With Electric Double-Layer Capacitor. IEEE Trans. Energy Convers. 24, 465–473. doi:10.1109/TEC.2008.2001580

Kasten, F., 1980. A simple parametrization of two pyrheliometric formulae for determining the Linke turbidity factor. Meteor. Rundsch. 33 124–127.

Kasten, F., 1996. The linke turbidity factor based on improved values of the integral Rayleigh optical thickness. Sol. Energy 56, 239–244. doi:10.1016/0038-092X(95)00114-7

Khanh, L.N., Seo, J., Kim, Y., Won, D., 2010. Power-Management Strategies for a Grid-Connected PV-FC Hybrid System. IEE Trans. Power Deliv. 25, 1874–1882.

Klucher, T.M., 1979. Evaluation of models to predict insolation on tilted surfaces. Sol. Energy 23, 111–114.

Kuszamaul, S., Ellis, A., Stein, J., Johnson, L., 2010. Lanai High-Density Irradiance Sensor Network for characterizing solar resource variability of MW-scale PV system. 2010 35th IEEE Photovolt. Spec. Conf. 000283–000288. doi:10.1109/PVSC.2010.5615868

Lave, M., Kleissl, J., 2013. Cloud speed impact on solar variability scaling – Application to the wavelet variability model. Sol. Energy 91, 11–21. doi:10.1016/j.solener.2013.01.023

Lave, M., Kleissl, J., Arias-Castro, E., 2012. High-frequency irradiance fluctuations and geographic smoothing. Sol. Energy 86, 2190–2199. doi:10.1016/j.solener.2011.06.031

Lave, M., Kleissl, J., Stein, J.S., 2013. A Wavelet-Based Variability Model (WVM) for Solar PV Power Plants. IEEE Trans. Sustain. Energy 4, 501–509. doi:10.1109/TSTE.2012.2205716

upna Universidad Pública de Navarra Nafarroako Unibertsitate Publikoa

Lave, M., Stein, J.S., Ellis, A., Hansen, C.W., Nakashima, E., 2011. Ota City : Characterizing Output Variability from 553 Homes with Residential PV Systems on a Distribution Feeder. Sandia Natl. Lab. Albuquerque, NM Livermore, Calif. SAND2011-9. doi:SAND2011-9011

Leadbetter, J., Swan, L.G., 2012. Selection of battery technology to support grid-integrated renewable electricity. J. Power Sources 216, 376–386.

Leitermann, O., 2012. Energy Storage for Frequency Regulation on the by. Energy storage Freq. Regul. Electr. grid, Massachusetts Inst. Technol.

Li, X., Hui, D., Lai, X., 2013. Battery Energy Storage Station (BESS) -Based Smoothing Control of Photovoltaic (PV) and Wind Power Generation Fluctuations. IEE Trans. Eustainable Energy 4, 464–473.

Longhetto, A., Elisei, G., Giraud, C., 1989. Effect of correlations in time and spatial extent on performance of very large solar conversion systems. Sol. Ener 43, 77–84.

Lorenzo, E., 2011. Energy collected and delivered by PV modules. Photovoltaics Sci. Eng. 984–1042.

Luo, X., Wang, J., Dooner, M., Clarke, J., 2014. Overview of current development in electrical energy storage technologies and the application potential in power system operation. Appl. Energy. doi:10.1016/j.apenergy.2014.09.081

Marcos, J., Marroyo, L., Lorenzo, E., Alvira, D., Izco, E., 2011a. Power output fluctuations in large scale pv plants: One year observations with one second resolution and a derived analytic model. Prog. Photovoltaics Res. Appl. 19, 218–227. doi:10.1002/pip.1016

Marcos, J., Marroyo, L., Lorenzo, E., Alvira, D., Izco, E., 2011b. From irradiance to output power fluctuations: the PV plant as a low pass filter. Prog. Photovoltaics Res. Appl. 19, 505–510. doi:10.1002/pip

Marcos, J., Marroyo, L., Lorenzo, E., García, M., 2012. Smoothing of PV power fl uctuations by geographical dispersion 226–237. doi:10.1002/pip

Martin, N., Ruiz, J.M., 2001. Calculation of the PV modules angular losses under " eld conditions by means of an analytical model. Sol. Energy Mater. Sol. Cells 70, 25–38.

Martínez-Moreno, F., Muñoz, J., Lorenzo, E., 2010. Experimental model to estimate shading losses on PV arrays. Sol. Energy Mater. Sol. Cells 94, 2298–2303. doi:10.1016/j.solmat.2010.07.029

Masson, G., Latour, M., Rekinger, M., Theologitis, L.-T., Papoutsi, M., 2013. Global market Outlook for photovoltaics 2013-2017 [WWW Document]. Eur. Photovolt. Ind. Assoc. URL http://www.epia.org/fileadmin/user_upload/Publications/GMO_2013_-_Final_PDF.pdf

upna Universidad Pública de Navarra Nafarroako Unibertsitate Publikoa

Matsuishi, M. & Endo, T., 1968. Fatigue of metals subjected to varying stress. Japan Soc. Mech. Eng.

Mills, A., Ahlstrom, M., Brower, M., Ellis, A., George, R., 2011. Dark shadows. IEEE Power Energy Mag. 33–41.

Mills, A., Ahlstrom, M., Brower, M., Ellis, A., George, R., Hoff, T., Kroposki, B., Lenox, C., Nicholas, M., Stein, J., Wan, Y.W., 2010. Understanding Variability and Uncertainty of Photovoltaics for Integration with the Electric Power System. Lawrence Berkeley Natl. Lab. on-line av.

Mills, A., Wiser, R., 2010. Implications of Wide-Area Geographic Diversity for Short- Term Variability of Solar Power. Lawrence Berkeley Natl. Lab. on-line av.

Molineaux, B., Ineichen, P., O'Neill, N., 1998. Equivalence of pyrheliometric and monochromatic aerosol optical depths at a single key wavelength. Appl. Opt. 37, 7008–18.

Muneer, T., 1990. Solar radiation model for Europe. Build. Serv. Eng. Res. Technol. 11, 153–163. doi:10.1177/014362449001100405

Muñoz, J., Martínez-Moreno, F., Lorenzo, E., 2011. On-site characterisation and energy efficiency of grid-connected PV inverters. Prog. Photovoltaics Res. Appl. 19, 192–201. doi:10.1002/pip.997

Murata, A., Otani, K., 1997. An analysis of time-dependent spatial distribution of output power from very many PV power systems installed on a nation-wide scale in Japan. Sol. Energy Mater. Sol. Cells 47, 197–202. doi:10.1016/S0927-0248(97)00040-8

Narvarte, L., Lorenzo, E., 2008. Tracking and Ground Cover Ratio. Prog. Photovoltaics Res. Appl. 703–714. doi:10.1002/pip

NERSA, 2012. Grid connection code for renewable power plants (RPPs) connected to the electricity transmission system (TS) or the distribution system (DS) in South Africa [WWW Document]. URL http://www.nersa.org.za/Admin/Document/Editor/file/Electricity/TechnicalStandards/South African Grid Code Requirements for Renewable Power Plants - Vesion 2 6.pdf.

Nuhic, A., Terzimehic, T., Soczka-Guth, T., Buchholz, M., Dietmayer, K., 2013. Health diagnosis and remaining useful life prognostics of lithium-ion batteries using data-driven methods. J. Power Sources 239, 680–688. doi:10.1016/j.jpowsour.2012.11.146

Otani, K., Minowa, J., Kurokawa, K., 1997. Study on areal solar irradiance for analyzing areally-totalized PV systems filshl Odod ~ Tsukulxl Uriluersily. Sol. Energy Mater. Sol. Cells 47.

Perez, R., Hoff, T.E., 2013. Mitigating Short-Term PV Output Intermittency. 28th Eur. Photovolt. Sol. Energy Conf. Exhib. 3719–3726.

upna Universidad Pública de Navarra Nafarroako Unibertsitate Publikoa

Perez, R., Kivalov, S., Schlemmer, J., Hemker, K., Hoff, T.E., 2012. Short-term irradiance variability: Preliminary estimation of station pair correlation as a function of distance. Sol. Energy 86, 2170–2176. doi:10.1016/j.solener.2012.02.027

Perez, R., Seals, R., Ineichen, P., Stewart, R., Menicucci, D., 1987. A New simplified version of the Perez diffuse irradiance model for tilted surfaces. Sol. Energy 39, 221–231.

Perpiñán, O., Marcos, J., Lorenzo, E., 2013. Electrical power fluctuations in a network of DC/AC inverters in a large PV plant: Relationship between correlation, distance and time scale. Sol. Energy 88, 227–241. doi:10.1016/j.solener.2012.12.004

PREPA, 2012. Puerto Rico Electric Power Authority Minimum Technical Requirements for Photovoltaic (PV) Generation Projects [WWW Document]. URL http://www.fpsadvisorygroup.com/rso_request_for_quals/PREPA_Appendix_E_PV_Minimum_Technical Requirements.pdf.

Rahman, S., Tam, K.S., 1988. A feasibility study of photovoltaic fuel cell hybrid energy system. IEEE Trans. Energy Convers. 3, 50–55.

Reindl, D.T., Beckman, W.A., Duffle, J.A., 1990. Diffuse fraction correlations. Sol. Energy 45, 1–7.

REN21, 2014. REN21. 2014. Renewables 2014 Global Status Report. doi:ISBN 978-3-9815934-2-6

Rigollier, C., Bauer, O., Wald, L., 2000. On the clear sky model of the ESRA — European Solar Radiation Atlas — with respect to the heliosat method. Sol. Energy 68, 33–48.

Ruifeng, Y., Saha, T.K., 2010. Power ramp rate control for grid connected photovoltaic system. 2010 IEE Conf. Proc. IPEC 83–88. doi:10.1109/IPECON.2010.5697135

Ruiz, J.M., 1999. A New Method for the Spectral Characterisation of PV modules. Prog. Photovoltaics Res. Appl. 310, 299–310.

SAFT SA, 2008. Intensium Flex ®, Product brochure http://www.saftbatteries.com/battery-search/intensium%C2%AE-flex accesed January 2014.

Schaltz, E., Khaligh, A., Rasmussen, P.O., 2009. Influence of Battery/Ultracapacitor Energy-Storage Sizing on Battery Lifetime in a Fuel Cell Hybrid Electric Vehicle. IEEE Trans. Veh. Technol. 58, 3882–3891. doi:10.1109/TVT.2009.2027909

Sengupta, M., Keller, J., 2011. PV Ramping in a Distributed Generation Environment : A Study Using Solar Measurements, in: IEE Photovoltaic Specialists Conference. pp. 586–589. doi:978-1-4673-0066-7/12

Seo, H., Kim, G., Kim, S., Kim, N., Lee, H., Hwang, C., Park, M., Yu, I., 2010. Power quality control strategy for grid-connected renewable energy sources using PV array and supercapacitor 2, 3–7.

upna Universidad Pública de Navarra Nafarroako Unibertsitate Publikoa

Shah, R., Mithulananthan, N., Bansal, R.C., Ramachandaramurthy, V.K., 2015. A review of key power system stability challenges for large-scale PV integration. Renew. Sustain. Energy Rev. 41, 1423–1436. doi:10.1016/j.rser.2014.09.027

SODA, n.d. Solar Energy Services for Professionals [WWW Document]. URL http://www.soda-is.com

Van Haaren, R., Morjaria, M., Fthenakis, V., 2014. Empirical assessment of short-term variability from utility-scale solar PV plants. Prog. Photovoltaics Res. Appl. 22, 548–559. doi:10.1002/pip

Wang, L., Ying-Hao, L., 2001. Random Fluctuations on Dynamic Stability of a Grid-Connected Photovoltaic Array, in: Power Engineering Society Winter Meeting, 2001. IEEE (Volume:3). pp. 985–989.

Wiemken, E., Beyer, H.G., Heydenreich, W., Kiefer, K., 2001. Power characteristics of PV ensembles: experiences from the combined power production of 100 grid connected PV systems distributed over the area of Germany 70, 513–518.

Woyte, A., Belmans, R., Nijs, J., 2007. Fluctuations in instantaneous clearness index: Analysis and statistics. Sol. Energy 81, 195–206. doi:10.1016/j.solener.2006.03.001

Zakeri, B., Syri, S., 2015. Electrical energy storage systems: A comparative life cycle cost analysis. Renew. Sustain. Energy Rev. 42, 569–596. doi:10.1016/j.rser.2014.10.011

upna Universidad Pública de Navarra Nafarroako Unibertsitate Publikoa